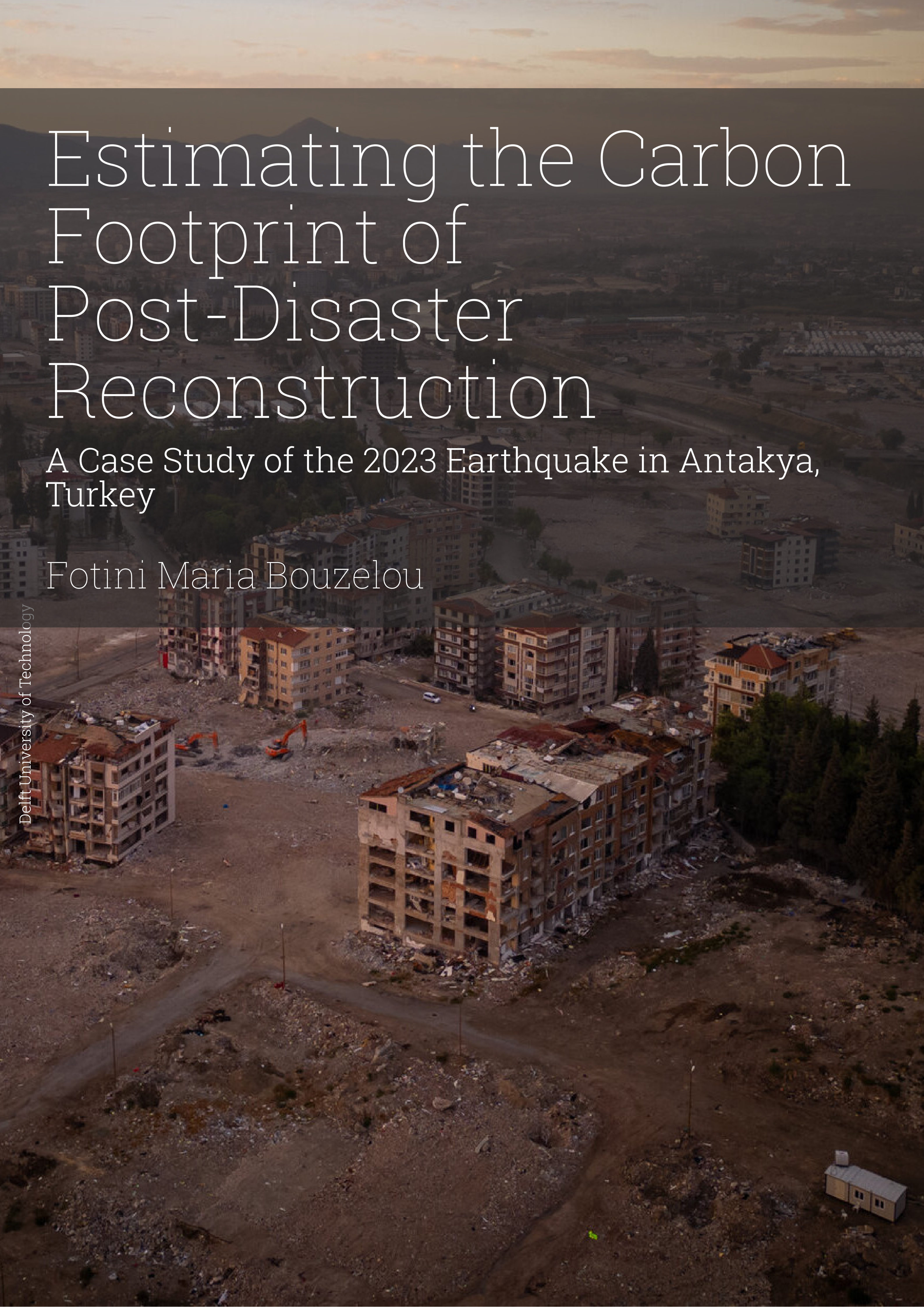

Estimating the Carbon Footprint of Post-Disaster Reconstruction

A Case Study of the 2023 Earthquake in Antakya, Turkey

Fotini Maria Bouzelou

Delft University of Technology

Estimating the Carbon Footprint of Post-Disaster Reconstruction

A Case Study of the 2023 Earthquake in Antakya, Turkey

by

Fotini Maria Bouzelou

Student Number 5865727

Chair and First Supervisor:	Nazli Aydin
Second Supervisor	Ming Yang
Advisor	Jasper Verschuur
Faculty:	Technology, Policy and Management

Cover: Nicole Tung
Style: TU Delft Report Style, with modifications by Daan Zwaneveld

Summary

This thesis addresses a critical and often overlooked challenge: quantifying the carbon emissions generated by large-scale post-disaster reconstruction efforts. In the wake of natural disasters, rapid rebuilding is essential to restore critical infrastructure and housing. However, this urgency leads to a pronounced carbon spike due to the energy-intensive production and transportation of materials such as concrete, steel, and other construction inputs. Such emissions not only intensify the greenhouse effect but also contribute to a reinforcing cycle, where increased emissions exacerbate climate change and, in turn, drive the frequency and severity of future disasters.

Using Antakya, Turkey -a city severely affected by the 2023 Turkey-Syria earthquake- as a case study, this research develops and a framework to estimate the carbon footprint of post-disaster reconstruction. By using Life Cycle Assessment (LCA) studies and employing Monte Carlo simulations, the research quantifies the carbon footprint of reconstructing approximately 38,000 buildings in Antakya while analyzing the sensitivity of the outcomes to variations in critical input parameters.

The analysis indicates that the reconstruction of the Antakya could result in emissions between 12.6 and 14.2 million tonnes of CO_2 *an amount comparable to the annual emissions of small countries like Slovenia or Lithuania, and roughly 3% of Turkey's total emissions. Preliminary estimates suggest that the societal costs of these emissions could reach up to $1 billion, underscoring a hidden burden that is rarely considered in disaster recovery planning.*

While the model provides a transparent and practical tool for preliminary decision-making in post-disaster contexts, several limitations warrant further investigation. Notably, the model simplifies complex construction processes by consolidating various emission sources into a single CO_2 *factor, and it does not yet account for the potential emission reductions from recycling construction waste.*

In conclusion, this thesis presents a methodological approach that can be adapted- but also further refined in the future- to quantify the emissions from post-disaster reconstruction, as demonstrated in the Antakya case study. By translating abstract assumptions about the environmental impact of reconstruction into tangible, measurable estimates, the study clarifies the significance of this phenomenon. This measurable basis facilitates a better understanding for policymakers and decision-makers, making it easier to incorporate environmental cost considerations into disaster management strategies and planning.

Contents

List of Figures

List of Tables

1

Introduction

Natural disasters leave behind more than just immediate devastation. Beyond the tragic loss of life and widespread displacement, they destroy infrastructure on a massive scale, triggering urgent reconstruction efforts. These rebuilding activities, while essential for recovery, come with steep environmental costs, ranging from pollution and deforestation to a marked increase in carbon emissions.

Even under normal circumstances, the construction industry is a major contributor to global carbon emissions. In post-disaster scenarios, however, the environmental impact of rebuilding is greatly amplified. Reconstruction projects require vast amounts of natural resources and rely heavily on energy-intensive materials like steel and cement, which are notorious for their high emission levels. In the rush to restore communities, environmental concerns are often sidelined, resulting in a pronounced carbon spike during the initial phase of rebuilding. This surge not only exacerbates climate change but also perpetuates a feedback loop, where escalating emissions contribute to the increasing severity and frequency of disasters. Despite its critical importance, the carbon footprint of large-scale reconstruction remains under-explored.

This thesis addresses this gap by developing a method to estimate the carbon emissions associated with post-disaster reconstruction under uncertainty. It applies this method to the case of Antakya, Turkey -a city severely affected by the 2023 Kahramanmaras earthquake - to quantify the emissions impact of rebuilding. The case of Antakya presents a timely and critical opportunity to study these impacts. With more than 38,000 buildings already underway to be constructed, it offers real -world relevance and data to support this analysis.

1.1. Carbon Cost of Post-Disaster Recovery

Understanding the carbon cost of reconstruction requires more than tracking operational emissions. It demands attention to construction-phase emissions -especially embodied carbon- released during the urgent and large-scale use of materials. This is being supported by recent research that increasingly highlights the significance of embodied emissions-those resulting from material extraction, transportation, and manufacturing-which predominantly occur during the construction phase.

This concern is amplified in post-disaster scenarios, where reconstruction efforts trigger a concentrated release of emissions over a relatively short period (typically one to five years). The duration depends on factors such as the disasters severity, the accessibility of the affected area, available resources, and the efficiency of coordination among stakeholders. For example, the reconstruction following the 2008 Wenchuan Earthquake in China saw the completion of most efforts within three years, including nearly 2 million rural housing units, 290,000 urban housing units, and numerous repairs (Johnson and Olshansky 2016). Similarly, substantial progress was achieved within five years after the 2011 Great East Japan Earthquake, despite the extensive damage caused by the tsunami across 216 square miles (Cho 2014). In the case of the 2001 Gujarat Earthquake in India, over 70% of reconstruction and repair work was completed within two years, with more than 911,000 houses repaired and 201,000 newly built by 2006 (Johnson and Olshansky 2016).

The release of vast amount of emissions in the relative short duration of construction is often referred to as the "carbon spike". To evaluate these emissions, it is essential to estimate the carbon footprint of reconstruction activities. The standard method for assessing the carbon emissions of construction projects is through Life Cycle Assessment (LCA). While LCA is not specifically designed for post-disaster reconstruction, it remains the most widely accepted framework for quantifying the environmental impact of buildings, including emissions generated during the initial (re)-construction stage.

Methods for Estimating Carbon Emissions Life Cycle Assessment (LCA) is the most commonly used method for estimating the carbon emissions generated from construction activities, particularly in the context of building reconstruction (Bastos et al. 2014). LCA offers a comprehensive evaluation of a building's environmental impact throughout its entire lifecycle, from raw material extraction to its end-of-life phase (Cai et al. 2022). In the context of post-disaster reconstruction, LCA focuses on the emissions released up to the point when construction materials arrive at the construction site, encompassing stages A1 to A5. These stages include raw material extraction, manufacturing, transportation, and on-site construction processes.
The main types of Life Cycle Assessment (LCA) are process-based LCA, input-output (IO) LCA, and hybrid LCA. Process-based LCA focuses on specific processes and materials, providing detailed assessments of a products life cycle but can be data-intensive and may overlook broader economic interactions (Bastos et al. 2014). IO-LCA uses economic input-output tables to estimate environmental impacts across industries, offering a more macro-level perspective but often with less specificity. Hybrid LCA combines both methods, leveraging the detailed analysis of process-based LCA and the comprehensive scope of IO-LCA to provide a more accurate and complete assessment of environmental impacts Syngros et al. 2017.
By applying LCA in this context, researchers can gain a more holistic understanding of the carbon cost associated with reconstruction activities, thereby informing more sustainable recovery strategies.

1.2. Knowledge Gap

While significant progress has been made in addressing operational emissions, there is a growing realization of the urgent need to tackle construction emissions (Röck et al. 2020; Pomponi and Moncaster 2016; Pöyry et al. 2015). Unlike operational emissions, which accumulate gradually over a buildings 50-100 year lifespan, construction emissions are released in a short time-frame, contributing immediately and significantly to atmospheric CO_2 levels.

Reconstruction efforts following natural disasters exacerbate this issue due to their scale and urgency. Vast amounts of materials, energy, and labor are required within compressed time-frames, leading to a pronounced "carbon spike" (Bastos et al. 2014). It is expected that events that show this carbon spike are gonna be increased as the increasing frequency and intensity of natural disasters, driven by climate change, are expected to further compound these challenges (on Climate Change IPCC). Not only natural disaster but also rebuilding after conflicts can also play a significant role. For instance, the reconstruction of Gaza is projected to generate emissions comparable to the annual carbon footprints of Sweden or Portugal, amounting to around 60 million tonnes (Benjamin Neimark 2024). While, the increasing frequency and intensity of natural disasters, driven by climate change, are expected to further compound these challenges (on Climate Change IPCC).

This has sparked a growing importance of post-disaster reconstruction (PDR) research, but most of the literature has focused on areas such as waste management od PDR (Habib 2019), stakeholder analysis (Xiaodong et al. 2014), and the "build back better" framework (Ismail et al. 2014). Studies directly investigating the carbon footprint of reconstruction are limited and usually concentrate on emissions associated with temporary structures and shelters, like in the work of Ali and Mourshed 2021 and Ogo 2018) where they looked to the carbon footprint of constructing temporary shelters in for Syrian refugees and to the seekers of shelters after the Great East Japan earthquake, respectively.

An exception is the work of Pan et al. 2014, which estimated the carbon emissions of permanent housing reconstruction after the Great East Japan Earthquake by multiplying the reconstruction area by a fixed CO_2 factor per square meter. Similarly, Benjamin Neimark 2024 applied a standardized CO_2 factor to calculate emissions from rebuilding destroyed structures in Gaza. While these studies provide straightforward methodologies, they fail to account for the inherent uncertainties in reconstruction activities, such as variations in CO_2 factors across materials, regional practices, the final number of housing units or square meters.

This underscores a significant gap in understanding and quantifying the carbon footprint of post-disaster reconstruction-particularly when accounting for the inherent uncertainties that reconstruction projects inevitably entail. Without this measurement, we remain in the dark about the true magnitude of the problem, unable to make fully informed decisions or hold accountable those overseeing reconstruction activities. As climate change exacerbates the frequency and severity of natural disasters, and with ongoing conflicts leading to widespread destruction, understanding how to address the environmental impact, at least in terms of carbon footprint, it is a necessary step towards pressuring for sustainable reconstruction practices.

1.3. Research Questions

To address the gap in understanding and measuring the carbon footprint of rapid and large-scale reconstruction efforts following disasters, this thesis is guided by the following central research question:

How do large-scale post-disaster reconstruction efforts, such as those in Antakya, Turkey, impact carbon emissions?

Additionally, the study aims to address the following relating research sub-questions:

1. What are the primary factors necessary to consider in the environmental assessment of the carbon, and how do uncertainties associated with these factors influence the final estimates?
2. How can the carbon footprint of post-disaster reconstruction efforts be calculated for the case study in Antakya?
3. How following different policy pathways for housing can influence the total carbon footprint of new constructed houses?
4. What are the societal and environmental implications of the carbon emissions generated by post-disaster reconstruction efforts - for the case study of Antakya-?

2
State of the Art

This literature review examines the carbon footprint of post-disaster reconstruction, focusing on the building sector's contribution to carbon emissions. Given the limited research specifically addressing emissions from post-disaster scenarios, the review begins by exploring how CO_2 emissions from the broader construction sector are calculated in existing literature. It highlights the critical role of embodied emissions -often underestimated compared to operational emissions- and investigates the unique challenges posed by post-disaster reconstruction efforts. The review also addresses the environmental and social consequences of construction-related emissions, emphasizing their severity. Finally, strategies for mitigating these emissions and promoting sustainable reconstruction practices are discussed.

2.1. Calculating Emissions from the Building Sector

Post disaster reconstruction is known to be a complex, dynamic and unpredictable (Alawag et al. 2024). While its urgency and scale present unique challenges, the carbon footprint of reconstruction closely mirrors that of conventional construction activities in the building sector. Since, research specifically addressing reconstruction-related emissions is limited, it is helpful to examine how carbon emissions are calculated in traditional building construction.

Life Cycle Assessment (LCA) is widely recognized as the most robust and comprehensive method for quantifying emissions associated with buildings (Säynäjoki et al. 2017, Anand and Amor 2017). LCA systematically evaluates "the environmental aspects and potential impacts throughout a product's life cycle, from raw material acquisition through production, use, and disposal" (European Commission, Joint Research Centre 2010). While LCA spans all phases of a buildings lifecycle, emissions from the construction phase are consistently a key focus.

In recent years, the number of LCA studies and reviews has grown significantly (Anand and Amor 2017). These studies now cover a wide range of contexts, including variations in building function, material usage, climate, and geographic conditions (Atmaca and Atmaca 2022).

2.1.1. Building Life Cycle Stages

As shown in the conceptual diagram, in Figure 2.1, Life Cycle Assessment is split in three main stages, each capturing distinct phases of a buildings lifecycle emissions.
The **construction phase (A1-A5)** encompasses emissions from the extraction, transportation, and manufacturing of raw materials, which are then processed into construction materials. These materials are transported to construction sites, adding emissions from logistics, and further emissions arise from on-site activities. This phase accounts for both the direct emissions from construction processes and the *embodied* carbon *embedded* in the materials themselves Dixit et al. 2012.
The **operational phase (B1-B7)** includes emissions associated with building use, such as heating, cooling, lighting, and appliance operation, over a typical lifespan of 50 to 100 years. Traditionally, this phase was considered the largest contributor to lifecycle emissions, accounting for up to 90% (Pomponi and Moncaster 2016, Robati et al. 2019). Even though, advancements in energy efficiency and

stricter building standards have significantly reduced operational emissions, operational emissions are still considered the largest contributor to the buildings lifecycle (Monteiro et al. 2016, Guan et al. 2016, Dixit et al. 2012). The **end-of-life phase (C1-C4)** involves emissions from building demolition, transportation of materials, and their subsequent disposal or recycling. This phase presents opportunities to mitigate emissions by reusing and recycling materials, as highlighted by studies on circular economy approaches Chung 2017.

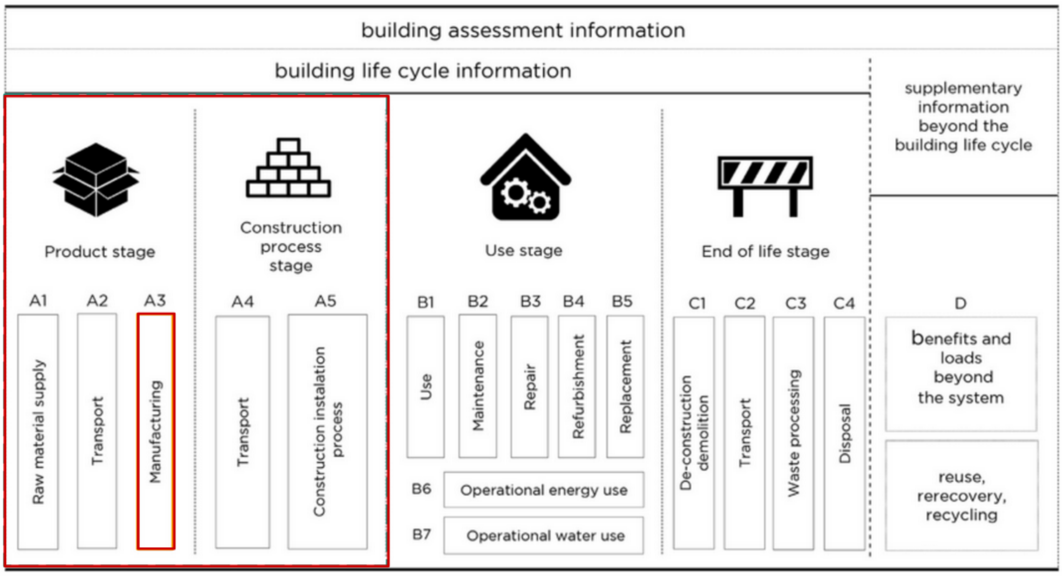

Figure 2.1: Standard life cycle stages and modules, adopted from EN 15978:2011 (NSAI). The focus of the project is specifically on the emissions produced during the **Product** and **Construction Process** stages (collectively known as the Construction Phase) of the (LCA) which can be distinguished with a red underline.

As the thesis focuses on emissions at the construction stage, it is important to examine the specific steps involved within this phase. The construction phase, can be delineated into five steps. Initially, it entails the extraction of diverse raw materials, followed by their transportation to manufacturing facilities. There, these materials undergo a multifaceted process that transforms them into construction products. This segment of the process accounts for the highest energy consumption and consequently produces the most emissions, with estimates averaging around 90% of the entire construction phase (Xiaodong et al. 2014,Zhang and Wang 2016). This is attributed to both fuel-related emissions, such as those arising from the use of fossil fuels to heat raw materials, and non-fuel-related emissions, which may stem from chemical reactions (eg. release carbon dioxide).
The process from A1 to A3 encompasses what is termed embodied emissions and aligns with the Inventory of Carbon and Energy (ICE) methodology, which measures emissions "from cradle-to-gate" and is considered the standard approach for calculating them in most of the LCA studies.
However, emissions related to the construction phase do not cease here, as the construction products must be transported from manufacturing facilities to the on-site construction location (A4). The studies show a great variety regarding the transportation emissions. Nevertheless, on average the percentages do not exceed 10% and many times there are considered negligible (Bastos et al. 2014,Atmaca and Atmaca 2015). Finally, the energy consumed on-site for operating equipment to install products and construct the building can be deemed negligible, constituting less than 1% of the total emissions in most cases (Robati et al. 2019).

Manufacturing is the primary driver of emissions during the construction phase, with cement leading the way. Cement is a cornerstone material in construction, valued for its affordability and indispensability in building projects. Estimates typically range between 30% and 60% of total GHG emissions in the total

embodied emissions (Programme 2023-09). In 2022, global cement manufacturing alone was responsible for 1.6 billion metric tonnes of CO_2 emissions, accounting for approximately 8% of the world's total CO_2 emissions Forum 2024. Following cement, steel constitutes another significant product, accounting for approximately 20% to 40% of emissions. Lastly, materials such as brick and aluminum also contribute to emissions, albeit to a lesser extent (Programme 2023-09).
The proportion of embodied emissions attributed to all the above material-products is ranging as the manufacturing processes vary from conventional process to adaptation of new eco-technology (eg. filter the emissions, re-using heat) but also from different types of materials (eg. many different types of cement).

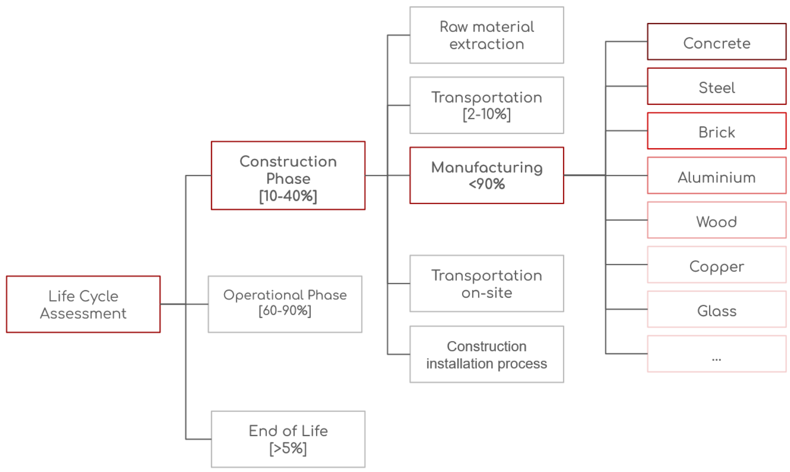

Figure 2.2: Schematic representation of the focus area within the broader framework of Life Cycle Assessment (LCA).

2.1.2. Methodologies of LCA Building Implementation

To calculate the emissions that a building emits during construction (and not only), a Life Cycle Assessment (LCA) needs to be conducted. The International Organization for Standardization (ISO) has provided some standards to guide LCA practice (ISO 2006). There are two methods within LCA that are different in nature but can be claimed to follow or fulfill the requirements of the ISO standard: process LCA and input-output (IO) LCA (Säynäjoki et al. 2017). Each method offers distinct advantages and limitations, influencing their applicability based on study objectives and data availability.

Process LCA The traditional method for conducting a Life Cycle Assessment (LCA) is process LCA Suh et al. 2004. Process LCA is a detailed, bottom-up approach that evaluates the environmental impacts of each stage in a product's lifecycle by modeling the flows of materials, energy, and emissions. The method involves gathering specific data for each process and aggregating it to assess environmental impacts. For example, to calculate emissions from cement manufacturing (stage A3), one would collect data on the electricity and fuel consumed during production and multiply it by the quantity of cement used in the construction. An example of an application is the study by Zabalza Bribián et al. 2009, which used Process LCA to evaluate the environmental performance of concrete, wood, and steel structures in residential buildings. While the goal is to include all major material and energy flows Bilec et al. 2010, process LCAs often exclude upstream processes due to data shortages and the significant workload required for detailed modeling Matthews et al. 2008.

Input - Output LCA On the other hand, Input-Output(IO) LCA examines the interconnectedness of economic activities across different sectors of the economy. Introduced by Leontief 2018 in the 1970s, IO LCA uses input-output tables that document economic transactions between industries. More specifically it shows the purchase flows between economic sectors and the value added by each sector, thus enabling allocation of the environmental output of each sector to the studied system according to monetary values. This approach provides more holistic view of the environmental consequences of economic production and consumption patterns, and achieves (at least theoretically) full system completeness Suh et al. 2004. Furthermore, performing IO LCAs is also time-effective and assessment models are often available free of charge Hendrickson et al. 2010. It tends to be less precise at the process level and may include broad estimates that lack specificity Stiebert et al. 2019. As Pöyry et al. 2015 mentions the method is usually based on national average sectors and is therefore unable to distinguish different manufacturing processes of similar products from each other. Thus, IO LCA is not a suitable method for comparing different products within one industry Suh et al. 2004.

Hybrid LCA To address the limitations of Process LCA and Input-Output (IO) LCA, the Hybrid LCA method was developed. This approach integrates the detailed, process-specific data of Process LCA with the broader economic scope of IO LCA, combining the strengths of both methodologies Hendrickson et al. 2010. The framework proposed by Treloar et al. 2000 demonstrated that Hybrid LCA enables reliable environmental assessments while requiring less time and fewer resources than standalone Process LCA Pöyry et al. 2015.
For example, Hong et al. 2015 used Hybrid LCA to assess the environmental impacts of residential and commercial buildings in South Korea, Pierobon et al. 2019 used Hybrid LCA to compare cross-laminated timber (CLT) structures with conventional concrete buildings, demonstrating the potential for significant reductions in embodied emissions. Similarly, Omar 2018 applied Hybrid LCA to industrialized building systems in Malaysia, finding improved accuracy in energy and emissions quantification compared to other LCA approaches, while Bilec et al. 2010 Bilec et al. 2010 demonstrated the utility of Hybrid LCA in evaluating the life cycle emissions of a parking garage construction project. While Hybrid LCA is often regarded as the most effective method for assessing environmental impacts in complex systems Crawford 2011, Stiebert et al. 2019 argues that its application remains limited due to the sophistication and complexity of integrating diverse datasets.

Table A.1 summarizes the advantages and disadvantages of all of the three approaches, as adapted from Stiebert et al. 2019.

2.2. Construction Emissions

Academic and policy efforts have historically focused almost exclusively on addressing operational emissions (Pöyry et al. 2015). For example, policies have emphasized lowering the energy requirements of buildings through building codes and the promotion of low-energy design strategies (Skillington et al. 2022). To illustrate better with an example, 41 countries have implemented mandatory residential building codes targeting operational energy use, and at least 85 countries have introduced energy certifications, ratings, or labels for buildings to encourage energy-efficient designs (IEA 2019). Similarly, the European Unions 2020 mandate for all new buildings to comply with nearly Zero Energy Building (nZEB) standards (EU 2010).

While reducing operational energy use is essential, it is increasingly evident that these efforts alone are insufficient to meet global climate targets (Pomponi and Moncaster 2016). Recent research highlights that construction emissions, particularly embodied emissions, represent a substantial and often overlooked share of the building sectors total carbon footprint.

This growing focus on construction emissions can be attributed to two key factors. Firstly, advancements in building's energy efficiency have shifted the balance of lifecycle emissions. As operational emissions decline due to improved efficiency measures, **the relative significance of construction-phase emissions grows** (Robati et al., 2019). Historically, it was posited that the ratio of embodied to operational impacts in building lifecycles was approximately 1:10 (Ramesh et al. 2010); however, this assumption is now outdated. For example, Röck et al. 2020 conducted a literature review of over 650 buildings and found that construction processes contribute approximately 20% of total lifecycle greenhouse gas (GHG) emissions in standard buildings (those meeting minimum energy efficiency standards). For highly energy-efficient buildings, embodied emissions constitute an even larger share, ranging from 45-50% of total lifecycle emissions. Other studies confirm this trend. Crawford 2011 found that embodied emissions could exceed 50% of a buildings lifecycle emissions, while Ibn-Mohammed et al. 2013 reported cases in the UK where these emissions reached up to 70%. Similarly, Chastas et al. 2016 identified ranges from 26% in low-energy buildings to nearly 100% in nZEBs.

Secondly, the **temporal allocation of emissions has become a critical consideration** (Säynäjoki et al. 2012). Unlike operational emissions, which are distributed over a building's 50-100-year lifespan, construction-related emissions are concentrated within a short period, typically during the first two to three years of a buildings life. This results in a **carbon spike**, where a substantial amount of GHGs is released in a brief time-frame, creating a steep initial rise in the emissions profile. Over time, the rate of emissions declines significantly during the operational phase. Figure 2.3, adapted from Röck et al. 2020, illustrates an example of this concept by comparing standard and advanced energy-efficient buildings. In standard buildings, the "break-even" point -where cumulative operational emissions equal upfront construction emissions- occurs in around 10 years (Figure 2.3a). For energy-efficient buildings, this point can be delayed to 35 or even 50 years (Figure 2.3b), depending on the analysis method. This carbon spike can account for up to one-third of total GHG emissions over a 50-year lifecycle, even for buildings designed to minimize operational emissions.

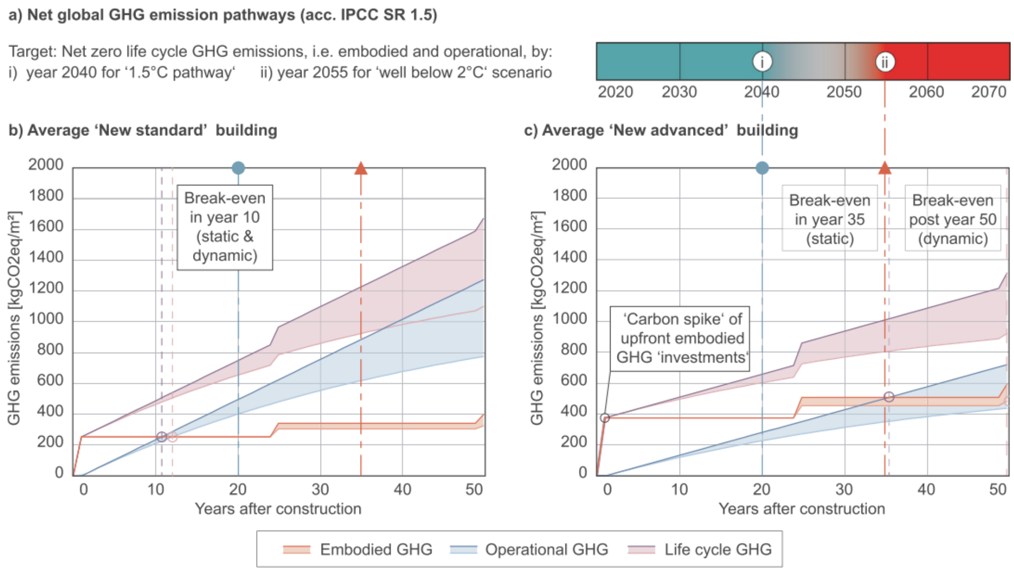

Figure 2.3: Carbon spike as illustrated in the work of Röck et al. 2020. Comparison of the carbon spike from buildings following current energy performance regulations and highly energy-efficient buildings.

2.3. Post-Disaster Re-Construction Emissions

The carbon spike of construction becomes even more pronounced in the context of post-disaster where reconstruction of critical infrastructure and buildings require vast amounts of materials, energy, and labor in a compressed time-frame. The situation is expected to worsen in the coming years as climate-induced disasters become more frequent and severe due to the escalating climate crisis (on Climate Change IPCC). According to the United Nations, the number of major disasters globally rose dramatically from 4,212 between 1980 and 1999 to 7,348 between 2000 and 2019, alongside a substantial increase in economic lossesfrom $1.63 trillion to $2.97 trillion (United Nations Office for Disaster Risk Reduction (UNDRR) 2020). These numbers indicate that the increase of natural disasters, aligns with a higher number of collapses or damaged buildings and infrastructure.

For example in Australia, the 2019-2020 "Black Summer" bushfire season destroyed more than 3000 homes and damaged an additional 1,000 structures, requiring extensive reconstruction efforts that significantly increased emissions (Wood 2020). Similarly, Hurricane Beryl in 2024 caused near-total destruction on the Caribbean island of Carriacou, where 98% of the homes were damaged or destroyed, displacing approximately 20,000 people (hur 2024).
In Norway, projections suggest that rising sea levels, combined with increased precipitation and flooding, could damage more than 110,000 buildings located less than 1 meter above normal sea level by 2100 (Almas and Hygen 2012). In the United States, Hauer et al. 2016 estimate that rising sea levels could expose 3.4 million homes to 10% of the population or a higher risk of flooding by 2100, potentially displacing more than 13 million people.

The need to build additional housing for these displaced populations has spurred a growing body of research, on post disaster reconstruction (PDR) topics. Yi and Yang 2014 review on PDR literature, found that the number of papers per year increased from 25 in 2002 to 126 in 2012. Notably, a sharp growth between 2009 and 2011 was observed, likely driven by the global focus on major disasters such as Chinas Wenchuan earthquake in mid-2008 and Japans tsunami in early 2011. More recently, a bibliometric analysis of PDR research from 2010 to August 2021 found fluctuations in the rate of published papers but with an overall increasing trend (Baarimah et al. 2021).

Research on Post-Disaster Reconstruction (PDR) primarily focuses on themes such as waste management (Szu-Hsien 2018; Habib 2019), stakeholder analysis, resource allocation, infrastructure challenges, resilience, and vulnerability (Ismail et al. 2014), reconstruction approaches, sustainable reconstruction (Ismail et al. 2014), and governance (Xiao et al. 2022).

However, while the rapid increase in emissions from reconstruction activities is acknowledged, very few studies directly calculate or analyze the associated carbon footprint in the PDR field. For instance, Yi and Yang 2014 reported that they didn't find any study focusing on the carbon footprint of PDR activities. Similarly, Ongpeng et al. 2019, after searching keywords like reconstruction and carbon footprint, identified only three papers. Among these, Zhong et al. 2024 applied a partial Life Cycle Assessment (LCA) (limited to construction phases A1-A5) to simulate carbon emissions from urban road network restoration after flooding.While Zuo et al. 2018 looked to how to reducing carbon emissions related to the transportation of minerals in UK comparing road and railways, with not direct connection though to post disaster reconstruction.

Several studies looking to the carbon footprint of PDR focus on the effect of temporary structures or shelters (Kuittinen 2016). Ali and Mourshed 2021 compared two types of temporary housing - prefabricated and container shelters-used in Syrian refugee camps. Using a comparative LCA approach, the study found that container shelters exhibited a 3.89% higher embodied carbon footprint than prefabricated structures, despite both having the same base area. Furthermore, the work of Ogo 2018 estimated the total embodied carbon of shelter materials in the 2010 Haiti Earthquake reconstruction. The LCA revealed that the amount of emissions, is nearly equivalent to the host countrys annual emissions.

Except of looking to the carbon footprint of temporary structure there are few studies looking directly to the carbon footprint of permanent housing and infrastructure. Pan et al. 2014 estimate the carbon footprint of housing reconstruction, following the Great East Japan Earthquake. Emissions were calculated by multiplying the reconstruction area by a fixed CO_2 factor per square meter. While this method provided a straightforward estimation, it failed to account for the uncertainties inherent in reconstruction activities Lastly, Ongpeng et al. 2019 proposed a Mixed Integer Linear Programming (MILP) model to minimize urban reconstruction carbon footprints by optimizing contractor allocation. Emissions were calculated by taking into account the parameters ofv(distance, emission factor, material weight). By using as a case study Philippines, they show that having local and no local construction companies in the region of the reconstruction project resulted to an increase of 36.89% carbon footprint (from 27,675 tons of CO_2 to 20,216.25 tons of CO_2).

Insights of the carbon footprint of reconstruction efforts can also be retrieved from post-conflict settings. For instance, the reconstruction of Gaza was estimated to generate around 60 million tonnes of CO_2 emissions, comparable to the annual emissions of countries like Sweden or Portugal Benjamin Neimark 2024. Similarly, Mihai 2023 examined the carbon impact of rebuilding Ukraine, underscoring the environmental consequences of such large-scale reconstruction efforts.

2.4. Potential Impact of re-construction emissions to the environment and society

Environmental Cost The added carbon footprint due to (re)-construction can perpetuate the climate change problem, creating a cycle where increased emissions contribute to more frequent and severe climate-related disasters (on Climate Change IPCC). For example, hurricanes, floods, and wildfires become more intense and common as global temperatures rise, which in turn leads to more instances of post-disaster recovery that generate additional carbon emissions Lemke et al. 2007.

The extraction of raw materials for reconstruction also has profound ecological consequences. For instance, Sovacool et al. 2018 emphasize how large-scale resource extraction during reconstruction exacerbates environmental degradation, often leaving ecological scars long after human recovery efforts have subsided.
The process of rebuilding generates also significant construction waste, including hazardous debris. Improper waste management of disaster debris, which often includes hazardous materials, exacerbates these issues by contaminating soil and water, stressing local ecosystems Srinivas and Nakagawa 2008. Additionally, Félix et al. 2013 found that temporary housing solutions, which are often hastily constructed, contribute to increased waste and long-term environmental footprints, particularly in regions lacking robust waste management systems.
Similarly, the removal of sand and gravel from riverbeds disrupts marine ecosystems, reduces water quality, and affects aquatic food chains (UK Green Building Council 2024). Moreover, construction activities can release pollutants into the soil, adversely affecting its quality and harming plant and animal life (Sandil and Kumar 2022).

In summary, reconstruction imposes significant environmental costs, with carbon emissions driving a damaging climate feedback loop, but also causing ecological harm from material extraction and waste mismanagement.

Social Cost Beyond environmental harm, the emissions added due to large-scale reconstruction also affect society - not only locally- but globally. This can be due to alterations in agricultural productivity, human health risks, property damages from increased flood risk, and changes in energy system costs, or other economic disruptions that result from the additional CO_2 contributing to climate change.

One way to assess the impact on the society is through the Social Cost of Carbon (SCC). The SCC is a famous economic concept used to quantify the monetary value of the long-term damage caused by emitting one tonne of carbon dioxide (CO_2) into the atmosphere. The SCC is expressed in terms of dollars per tonne of CO_2 and serves as a critical metric for policymakers and economists to evaluate the benefits of reducing greenhouse gas emissions versus the costs of implementing such reductions. The calculation of the SCC is complex and involves modeling factors such as; agricultural productivity loss, scenarios for population, economy and emissions, changes in vulnerability and relative prices with development; the rate of degradation of carbon dioxide from the atmosphere; the rate and level of global warming; the uncertainties about impacts and risk aversion, and the discount rate;Taconet et al. 2021,Tol 2023. The effect of any of these factors can create wide variances between different values on other models. For example, the discount rate is considered a critical factor influencing SCC estimates and determines the present value of future climate damages. Higher discount rates reduce the present value of future harms, yielding lower SCC estimates, while lower rates increase the SCC Kaufman et al. 2020.

Model estimates of the SCC vary substantially. For example, Nordhaus 2014 estimated the SCC to be approximately equal to $43 per ton, while Wang et al. 2019 reported a wide range of values, spanning from -$50 to $8752 per ton of carbon. Additionally, Tol 2023 highlighted that in the past decade, SCC estimates have risen from $9 to $40 per ton for high discount rates and from $122 to $525 per ton for low discount rates. This variability underscores the influence of underlying assumptions and methodologies on SCC estimates.

2.5. Mitigation of construction emissions

Understanding the significance of emissions from the construction sector, Pomponi and Moncaster 2016 sought to address how they could potentially be mitigate. By reviewing systematically the existing literature (having a final cut of 77 papers), they identified 17 distinct mitigation strategies as extracted from the studies and are summarized in Table 2.5. [1].

Table 2.5 highlights that the most extensively researched mitigation strategy involves using materials with inherently lower embodied energy (EE) and embodied carbon (EC) (Mitigation Strategy 1). Alternative materials such as timber, bamboo, or wood have been proposed to replace high-carbon materials

[1]While Pomponi and Moncaster 2016's focus was limited to embodied emissions, it is important to note that these emissions constitute at least 90% of total construction-related emissions Xiaodong et al. 2014

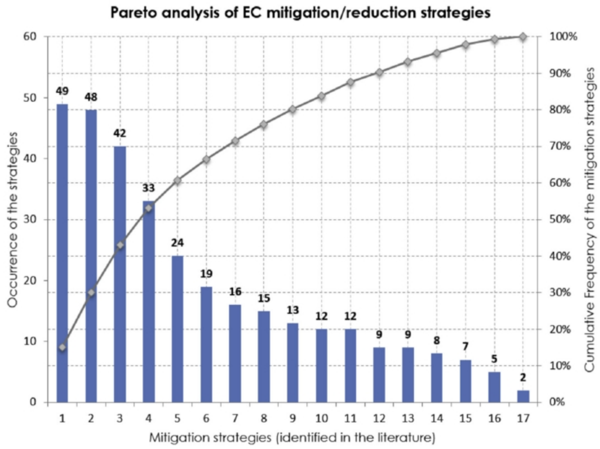

MS	Description
1	Practical guidelines for a wider use of low-EC materials
2	Better design
3	Reduction, re-use and recovery of EE/EC intensive construction materials
4	Tools, methods, and methodologies
5	Policy and regulations (Governments)
6	Refurbishment of existing buildings instead of new built
7	Decarbonization of energy supply/grid
8	Inclusion of waste, by-product, used materials into building materials
9	Increased use of local materials
10	Policy and regulations (Construction sector)
11	People-driven change (key role of all BE stakeholders)
12	More efficient construction processes/techniques
13	Carbon mitigation offsets, emissions trading, and carbon tax
14	Carbon sequestration
15	Extending the building's life
16	Increased use of prefabricated elements/off-site manufacturing
17	Demolition and rebuild

Figure 2.5: Details of the mitigation strategies (MSs) identified in the literature.

like concrete and steel, which are known for their intensive carbon footprint Yu et al. 2011. For instance, Venkatarama Reddy 2009 examined stabilized mud blocks as a substitute for load-bearing brickwork and reported a nearly 50% reduction in embodied costs. While, You et al. 2011 found that steel-concrete structures, when compared to masonry-concrete structures, could achieve a 4.2% reduction in CO_2 emissions.

Another prominent strategy is optimizing building design (Mitigation strategy 2 with 48 papers found). This includes adopting better design practices, and integrating life cycle assessments (LCA) early in the design phase. The high influence that a better design can have, was shown in the work of Acquaye and Duffy 2010, where he conducted an input-output analysis of Irelands construction sector, revealing that improved design practices could reduce indirect emissions by 20%.

The third most common strategy explored is reduction, re-use and recovery of EE/EC intensive construction materials. The difference with the first strategy can be subtle. Strategy 1 is more about substituting a material with another. While material optimization aims to reduce the use of an intensive carbon material either by reusing, recovering, or blending it with another material to use less of the intense. For instance, García-Segura et al. 2014 noted a 720% reduction from substituting Portland cement with blended alternatives.

Some other mitigation strategies include the use of more advanced tools and methodologies, such as Building Information Modeling (BIM) and LCA software, or government policies and regulations to facilitate the transition to lower embodied carbon materials. Dhakal 2010 documented that policy-driven changes in construction practices reduced emissions by 50% in Japan and China. Overall it is agreed that policies that either set standards for embodied carbon, or implement carbon taxes, or provide incentives for the use of low-carbon materials can encourage the adoption of sustainable practices across the construction sector.

In terms of building utilization, refurbishment of existing structures is highlighted as a more sustainable option compared to new construction, as retrofitting preserves the embodied energy of existing materials, significantly reducing the need for new materials and the associated emissions. In accordance with that Gaspar and Santos 2015 assessed the potential saving for a detached house in Portugal built in the late 1960 s, concluding that refurbishment would be 22% more efficient than demolition and rebuild, while Power 2010 show that the EC of an average refurbishment project to bring an existing house up to modern standards is around one third of that of a new house.

Furthermore, some other strategies to address the emissions, although less well researched is integrating waste and by-products into construction materials aligns with circular economy principles. Intini and Kühtz 2011 found that using recycled PET for thermal insulation in residential building could lower environmental impacts by 46% of the embodied emissions. Reducing transportation emissions through local material use is another effective measure; Crishna et al. 2011observed that between 2% up to an 84% reduction in emissions can be saved based on the stone type and the country of origin, and mainly than importing it.

Overall, Pomponi and Moncaster 2016) concluded that a pluralistic approach is necessary, as no single mitigation strategy is sufficient to achieve a significant reduction in embodied carbon. They found that over 80% of the studies reviewed combine at least two strategies to effectively mitigate CO_2 emissions. This underlines the need for a holistic approach to addressing embodied carbon in the construction industry.

2.6. Uncertainty Analysis

From the few reviewed studies that analyzed the carbon footprint in reconstruction, no evidence was found of uncertainty analysis being applied to any parameter. This omission aligns with the standards for conducting LCA, which do not mandate uncertainty analysis ISO 2006. However, even in cases where parameter values are directly adopted, such as the CO_2 factor for Japan Pan et al. 2014 or the ton CO_2/ton-kilometer factor used in disaster simulations in the Philippines Ongpeng et al. 2019, uncertainty analysis remains absent.

Uncertainty analysis involves quantifying the uncertainty in model inputs, parameters, or outputs to understand its impact on the model's behavior and outcomes. It aims to identify, assess, and reduce uncertainty in modeling processes, which is crucial for ensuring the reliability and robustness of model predictions Helton and Davis 2003.

2.6.1. Uncertainty Analysis in a Policy Context

Uncertainty analysis is vital for understanding the robustness of models, especially in complex systems such as climate modeling, engineering design, and policy analysis. More specifically, for the latter, it helps modelers and decision-makers assess the confidence in model predictions and the potential range of outcomes under varying conditions. For policymakers, it informs risk assessment, guides resource allocation, and supports decision-making under uncertainty by highlighting areas where more data or research is needed (Der Kiureghian and Ditlevsen 2009).

In the white paper of Haasnoot 2011, they categorize type of uncertainty about the model based on location, level, and nature.

Location: The location of where the uncertainty is detected. For instance it can be **Contextual Uncertainty**, meaning that external forces or changes outside policymakers' control, such as economic shifts or climate change, which affect the system being modeled. Otherwise, it can be **System Response Uncertainty**. In this case, the uncertainty is about how the system responds to external forces and policy interventions, often stemming from model structure uncertainty or parameter uncertainty. Moreover, **Model Parameter Variability** can exist due to limited or imprecise data, calibration issues, or inherent randomness in the system. Lastly, **Stakeholder Preference Uncertainty**, which refers to uncertainty regarding the relative importance and preferences of stakeholders involved in the policy-making process, which can change over time (Walker and Marchau 2003).

Level of Uncertainty: Ranges from complete determinism (where everything is known precisely) to total ignorance (where nothing is known) and four levels in between (A.1). The level of uncertainty and the challenge they create when modeled are famously captured by Donald Rumsfeld answer at a U.S. Department of Defense news briefing; *As we know, there are known knowns these are things we know we know. We also know there are known unknowns that is to say we know there are some things we do not know; but there are also unknown unknowns the ones we don't know we don't know. It is the latter category that tends to be the difficult one* (Upton and Cook 2014).

Nature of Uncertainty: Includes aleatory (inherent variability) and epistemic (lack of knowledge). Aleatory uncertainty is irreducible, while epistemic uncertainty can be reduced through further research and data collection (Walker and Marchau 2003).

2.6.2. Uncertainty Analysis Methods

The uncertainty of some levels, location, and nature can be successfully be explored and understood with mathematical methods and models. Several methods exist for uncertainty analysis, each suitable for different modeling contexts. One of the most common is **Monte Carlo Simulation (MCS)**. This is one of the most widely used methods for uncertainty analysis. It involves running the model many times (often thousands of times) with randomly sampled inputs based on their probability distributions (Janssen 2013). The outcomes form a distribution that represents the uncertainty in the model's predictions. A more efficient sampling method than basic random sampling used in Monte Carlo simulations is **Latin Hypercube Sampling (LHS)**. LHS divides the range of each input variable into equally probable intervals and ensures that the entire input space is explored systematically (Rajabi et al. 2015). In comparison with Monte Carlo, it provides better coverage of the input space with fewer samples compared to simple random sampling, which can reduce computational costs but still requires a large number of model evaluations for high-dimensional problems (Song and Kawai 2023). Moreover, **Bayesian Uncertainty Analysis** incorporates prior knowledge (in the form of prior distributions) along with observed data to update the probability distributions of the uncertain parameters. Bayesian methods use Bayes' theorem to combine prior information with evidence from data to produce a posterior distribution (Becker et al. 2012). It allows the incorporation of expert knowledge and prior data into the analysis, providing a systematic framework for updating uncertainty. Computationally intensive, especially when dealing with complex models or a large number of uncertain parameters (Liang and Mahadevan 2015).

While uncertainty analysis focuses on quantifying the uncertainty in model outputs given uncertain inputs, sensitivity analysis determines how changes in model inputs affect the outputs. Sensitivity analysis identifies the most influential factors on the model's behavior, guiding model refinement and uncertainty reduction efforts (Saltelli and Annoni 2010). The Three Common Sensitivity Analysis Modes:

- **Factor Prioritization:** Identifies the uncertain factors that have the most significant impact on model output variability. It helps prioritize efforts to reduce uncertainty in the most influential factors, thereby reducing output variability.
- **Factor Fixing**: Aims to identify factors that have negligible impact on the model output, allowing them to be fixed at nominal values to simplify the model and reduce computational effort without significantly affecting the results.
- **Factor Mapping**: Examines how variations in inputs affect the output.

The literature reviewed demonstrates significant progress in measuring and mitigating emissions in the construction sector, particularly through the widespread use of Life Cycle Assessment (LCA) methods. Numerous studies have developed reliable frameworks to quantify both operational & embodied emissions, and a broad set of mitigation strategies is being explored. However, studies that isolate the impact of the construction phase remain limitedand those focused specifically on post-disaster reconstruction are even rarer.

Research specifically addressing the carbon footprint of post-disaster reconstruction (PDR) remains sparse. When such studies do exist, they often rely on overly simplified methodssuch as applying a fixed CO_2 factor per square meterwithout accounting for the variability and uncertainty that define real reconstruction scenarios. The urgency, scale, and unpredictability of post-disaster contexts make emissions highly dynamic, yet the literature largely fails to capture this complexity or its resulting carbon impact.

Moreover, as climate-induced disasters grow in frequency and severity, the role of reconstruction as a contributor to emissions has been largely overlooked. One noticeable omission in the current literature is the lack of uncertainty analysis, even though parameter uncertainty is particularly relevant in post-disaster settings, where data is often incomplete or evolving.

Therefore, there is a need for models that can estimate emissions with confidence and hence support decision-making in post-disaster recovery planning.

3

Case Study: Antakya

On February 6th, Turkey and Syria experienced two devastating earthquakes within nine hours of each other. The first quake, with a magnitude of 7.8 Richter (R), struck southern Turkey near the northern border of Syria, while the second, measuring 7.5 R, hit approximately 95 kilometers southwest (See Figure 3.1). The regions vulnerability to seismic hazards was well-known due to its tectonic setting, influenced by the Dead Sea and East Anatolian faults, as well as the Cyprus arc. This susceptibility was tragically confirmed by the recent earthquakes, which reached a maximum Mercalli intensity of XII, indicating extreme devastation (Mendoza et al. 2018).

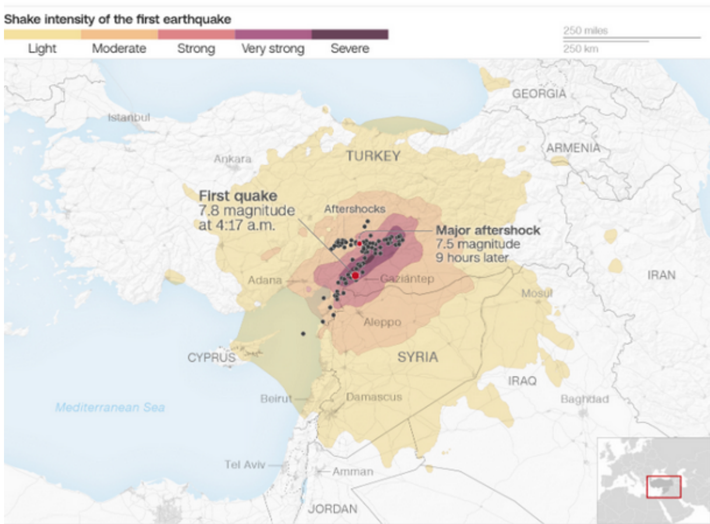

Figure 3.1: The map illustrates the area impacted by the earthquake as recorded until 2:30 pm local time on February 7th, 2023. Source CNN

The impact on Turkey was profound, affecting nearly 16 million people, with 9.1 million experiencing direct consequences and a confirmed death toll surpassing 50,000 (Ahmed et al. 2023). Beyond human casualties, extensive infrastructure damage was reported across 11 provinces in southwest Turkey, including Hatay, Kahramanmaras, Sanliurfa, Diyarbakir, Adana, Adiyaman, Malatya, Osmaniye, Kilis, and Elazig. The destruction was exacerbated by side effects that amplified ground motion, leading to resonance in mid-rise and high-rise buildings (Song et al. 2024).

The Disaster and Emergency Management Presidency (AFAD) reported that approximately 710,000 buildings sustained significant damage, with roughly 280,000 structures collapsed/severe damage. This disaster surpassed the destruction caused by the 1999 Marmara Earthquake, which had been a pivotal moment for improved disaster preparedness, urban planning, and societal awareness. This highlights the vulnerability of the regions constructed environment and underscores the inadequacy of certain seismic code standards in specific areas (Ozturk et al. 2023).

Antakya bore the brunt of the 7.8 R magnitude earthquake, with the estimated destroyed infrastructure to range between 60-80% (for instance see map of damage assessment in figure 3.2 taken from Foster+ Partners that defines as demolished/heavily damaged 65% of the buildings).

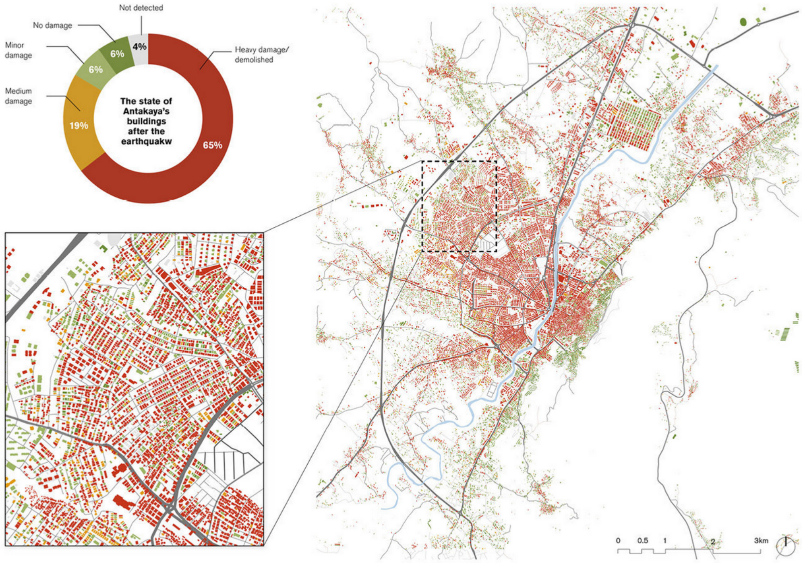

Figure 3.2: Map of damage to Antakya after the Turkey-Syria earthquakes in February 2023. @Foster + Partners

Figure 3.3: Satellite images before and after the earthquake in Hatay (taken from Google Satellite).

Antakya historically known as Antioch, has a rich cultural and historical heritage, spanning over two millennia. It was a prominent city in the ancient world, serving as a center for Hellenistic culture and playing significant roles during the Roman, Byzantine, and Ottoman periods. This history has resulted in a diverse cultural and architectural landscape, reflecting the city's role as a crossroads for various civilizations and religions. Its status as a melting pot of diverse religious communities has shaped a unique cultural tapestry, evident in its religious monuments and practices (Dalrymple 1997).

The growth as an urban center has been marked by its function as the administrative heart of Hatay province during the early years of the Republic of Turkey (Ozdemir 2024). Prior to 1939, the city saw enhancements in health, education, and infrastructure, which attracted rural populations and contributed to its expansion. By the mid-20th century, the city's population reached approximately 27,000, establishing Antakya as the largest city in the province. Initially, its growth was fueled by agriculture and related industries. However, from the 1970s onward, the services sector expanded, driven by international trade and investments in health, education, and administration (Çetin 2013). This expansion led to suburbanization and unregulated construction, often lacking adequate engineering standards. By 2009, the population exceeded 200,000, reflecting rapid urbanization that has introduced various infrastructural challenges (Yüksel 2021). As of 2022, the population had grown to approximately 400,000 (Turkish Statistical Institute 2022).

It is part of a seismically active region, at the intersection of the African, Arabian, and Anatolian tectonic plates. This geological setting makes the area prone to significant seismic activity. The East Anatolian Fault, one of the most active fault lines in Turkey, runs near the city, contributing to its history of frequent and sometimes severe earthquakes. The tectonic dynamics of this region result in a complex pattern of seismicity, including both shallow and more profound seismic events. These conditions have historically led to numerous earthquakes in and around Antakya, with some of the most notable occurring in antiquity, such as the earthquakes in 115 AD. and 526 AD., both of which caused widespread destruction and loss of life. The ongoing tectonic movement continues to pose a risk for future seismic events, something that was confirmed in the recent devastating earthquake.

Analyzing the environmental implications of reconstruction efforts, in terms of emitted CO_2 in the atmosphere, in a city such as Antakya can provide valuable insights to understand the broader environmental impact of post-disaster rebuilding efforts, while it could highlight the need to decision-makers for considering more sustainable and resilient reconstruction policies.

4

Method

In this section, the methodology for estimating the carbon footprint of post-disaster reconstruction is outlined (Figure 4.1), and the way it was applied to the case study of Antakya, Turkey is presented.

First step was the collection of data. The focus was on three key parameters: (1) Gross Floor Area (GFA), which refers to the ground floor area of a building in square meters; (2) the Number of Floors per building; and (3) the CO_2 Factor, which represents the carbon emissions released into the atmosphere after constructing 1 meter square of a building, (expressed in kg CO_2eq/m^2). For the case study, Gross Floor Area and the Number of Floor were collected from spatial data from the Hatay Municipality, and the CO_2 Factor through literature review. Interestingly enough, there was discrepancy in the literature regarding which of the construction stages were taking into consideration at each paper (from A1 to A5) when calculating the CO_2 Factor range. However, all studies consistently included the embodied emissions during the manufacturing stage (A3), that is considered to be the stage during the construction phase that is responsible for the vast majority of CO_2 emissions.

In Step 2, the collected data underwent cleaning and processing to ensure it is ready for use in the model.

In step 3, a range of values was assigned to the variables with uncertainty. In an ideal scenario-such as a controlled, small-scale construction project-each model parameter could be potentially assigned a precise, fixed value. However, in large-scale construction projects, data are often incomplete or imprecise, meaning that the models parameters do not have one precise value. The model is designed to handle such uncertainties by accepting either fixed values or a range of possible values where the true value of the parameter is likely to lie. In the next step (step 4), the variables are fed into the model to estimate the total CO_2 emissions. For each building, the model calculates the product of Gross Floor Area (GFA) (units: m^2), the Number of Floors (integer), and the CO_2 Factor (kg CO_2eq/m^2) to determine the total emissions for that building. This process is repeated for all buildings in the dataset, and the individual emissions are summed to yield the total CO_2 emissions for the entire case study area. Mathematically, this process is represented by the following equation:

$$TotalCO_2 = \sum_{i=1}^{n} GFA_i \times Floors_i \times CO_2Factor_i \tag{4.1}$$

where i represents each building and n is the total number of buildings. To account though for the uncertainty in the model's parameters, the model applies equation 4.1 through the use of Monte Carlo (MC) simulations. Initially, MC simulations are run by varying One parameter At a Time (OAT) while holding the others constant. Additionally, Sobol indices are calculated to quantify the influence of each parameter. Finally, a comprehensive MC simulation is conducted with all variables varying *simultaneously.* The findings from MC *simultaneously* form the **main results** of the study.

To assess the broader significance of these emissions, the Social Cost of Carbon (SCC) is calculated by using the **main results** from the MC simulations.

Having understood the societal and environmental impacts of these emissions, it is important from a policy analysis perspective to develop strategies that could potentially mitigate the effect of post-disaster reconstruction. In this study, we evaluate two potential policy approaches: one focuses on promoting sustainable construction practices, and the other emphasizes the construction of energy-efficient buildings.

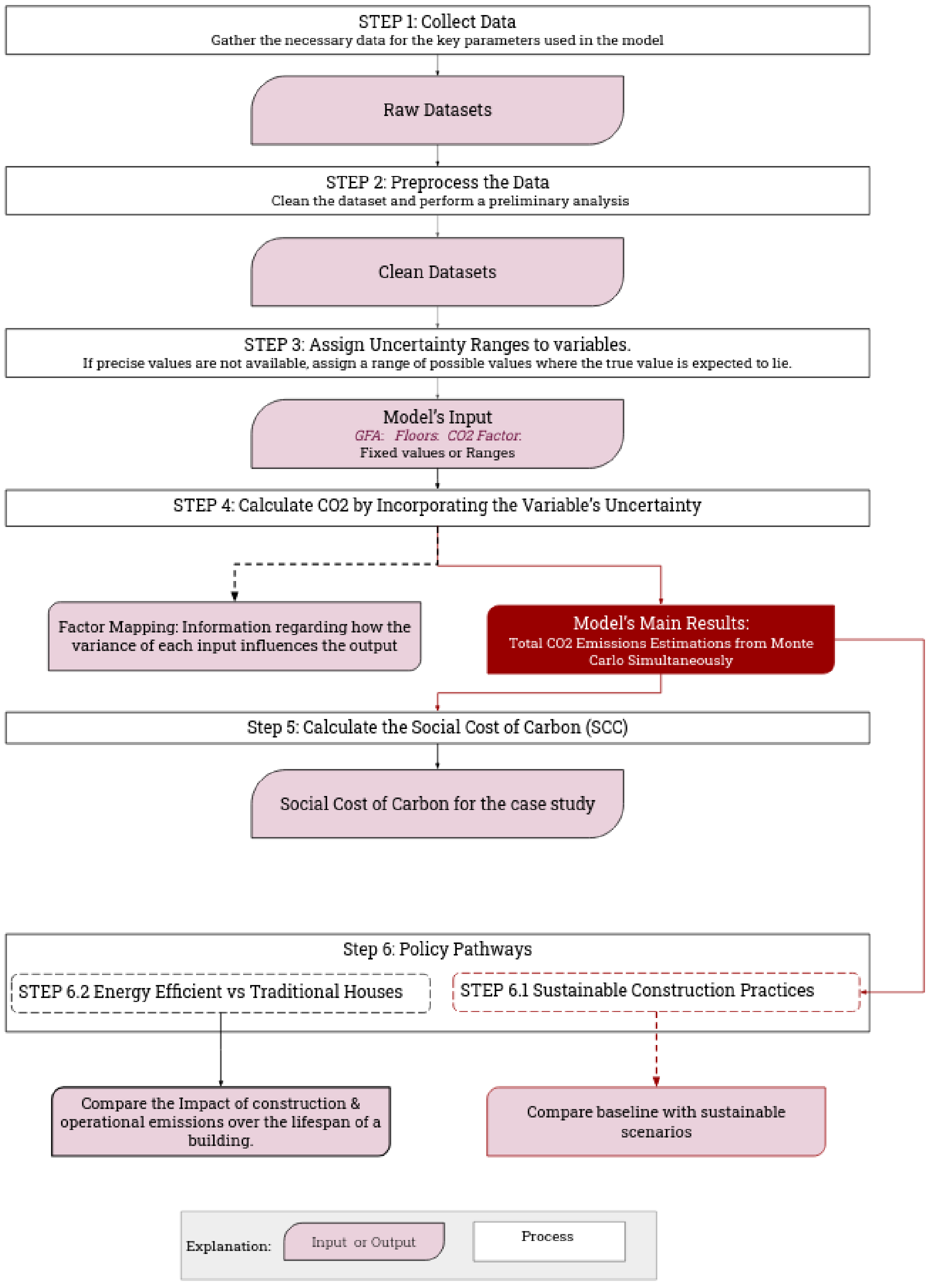

Figure 4.1: Flowchart of the Research Method, where it shows how the output of each step is the input of the next step. More details relating to each step can be found in Figures A.3

4.1. Data Collection

First step consists of gathering data for the key parameters.
The building's footprint, defined by the Gross Floor Area and Number of Floors, represents the total square meters of a building. This information is typically available in urban planning documents such

as city master plans[1], planning permits, or construction reports. Gross Floor Area is usually presented in square meters or in digital formats (e.g., shapefiles or GeoJSON), which can easily be converted to the required units for analysis.

The Number of Floors variable provides an indication of the buildings vertical scale, though it may not always specify the exact number of floors. Common metrics for expressing this dimension are outlined in Table A.2.

Unlike building footprint data (FFA and Number of floors), the CO_2 Factor is typically not included in reconstruction or master plans. This value is determined by the building's specific characteristics, varying based on factors such as construction materials, transportation logistics, and building practices. Data for the CO_2 factor is generally obtained from Life Cycle Assessment (LCA) studies or if it has been conducted an environmental product declaration (EPD) [2].

4.1.1. Gross Floor Area & Number of Floors

In the case study of Antakya, for the variables Gross Floor Area and Number of Floors were derived from spatial data collected by digitizing high-resolution images of reconstruction plans provided by the Hatay Metropolitan Municipality (figure A.4). This raw spatial data were provided in various shapefiles with with each entry/row corresponding to a building that will be constructed in Antakya.

4.1.2. CO_2 Factor

The CO_2 Factor was determined through a comprehensive literature review focusing on Life Cycle Assessments (LCAs) of residential buildings (diagram of the literature review can be seen in figure 4.2). Two main strategies were employed for the search: keyword-based queries and the snowball technique. The predefined keyword strings were used across multiple academic databases, with the primary focus on Google Scholar, ScienceDirect, and Scopus. The snowball technique helped expand the search by identifying additional relevant studies through citations, references, and expert reports.

Initially, over 200 papers were identified. These papers were filtered in two stages: first by publication year, prioritizing studies published after 2000, and then through abstract review. Studies on non-residential structures, such as dormitories (eg. Huberman and Pearlmutter 2008), temporary refugee housing (Atmaca 2017), or schools (Muñoz et al. 2017), were excluded to ensure the focus remained on residential buildings.

Next, the review narrowed to papers relevant to the climate of Hatay, Turkey. According to the Köppen climate classification system[3], Hatay has a "hot dry-summer" Mediterranean climate (Csa). Therefore, LCAs from regions with similar climates, including Morocco, Algeria, Portugal, southern Spain, France, Italy, Greece, Lebanon, and Israel, were considered (see figure A.5). This final step narrowed the selection to 34 relevant papers, which were then subjected to meta-analysis to derive the CO_2 Factor.

[1]A Master Plan is a strategic document outlining long-term goals for land use, infrastructure, housing, and sustainability, guiding future urban development.

[2]EPDs are a form of life cycle assessment and are the standard way of quantifying the impact of a product or system on the environment. Declarations may include: Manufacturer, Company Information,Product Identification Information,Life Cycle Assessment (LCA) Methodology,Product Category Rules (PCR), Data on raw material acquisition, Content of materials, Chemical substances, Efficiency and energy use, Emissions (to air, soil, and water), Waste generation, Analysis of the LCA Results

[3]The Köppen climate classification is a widely used system that divides climates into five main groups based on seasonal precipitation and temperature patterns Rubel and Kottek 2011.

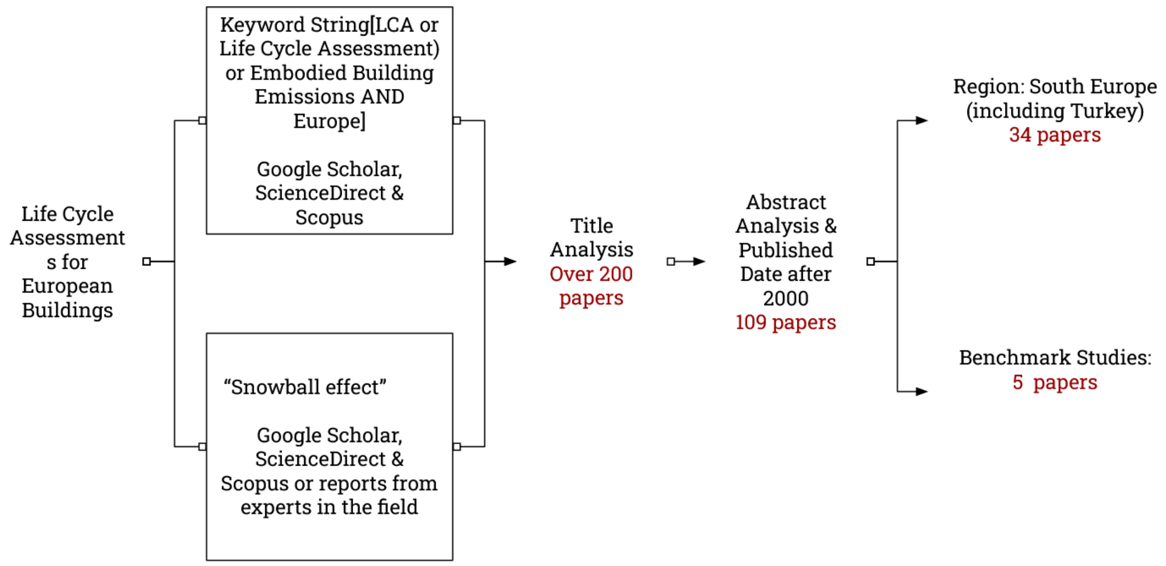

Figure 4.2: Overview of LCA literature review.

4.2. Data Pre-processing

4.2.1. Gross Floor Area & Number of Floors

The process of preparing spatial data for analysis involved three key steps: data cleaning, data transformation, and preliminary analysis, as illustrated in Figure 4.3 which consists of Data Cleaning, Data Transformation, and Preliminary Analysis.

Figure 4.3: Flowchart outlining Step 2 of the methodology for spatial data.

Data Cleaning The initial raw data, provided in multiple shapefiles representing different aspects of the reconstruction plans, and hence they needed to be merged. This process combined data relating to the geographical boundaries, land use categories, residential zones, and detailed building data into a single comprehensive dataset. Next, the handling of missing data was addressed. If possible, the missing values on columns with key information was filled by reviewing the available data, otherwise the data were excluded from the research. To ensure the dataset was relevant to the studys objectives, irrelevant columns and rows that did not contribute to the analysis, such as non-residential buildings or unnecessary information, were removed. Finally, spatial consistency was ensured by standardizing all data to the same Coordinate Reference System (CRS), specifically the 2D geographic CRS: EPSG:4326.

Data Transformation The next step was to ensure the data was in the correct units. The *Gross Floor Area* was provided as coordinate points outlining the building's footprint. This was easily converted to square meters (m^2) using straightforward geometric calculations, with no uncertainty introduced.

The Density column, which needed to be converted into Number of Floors, was more challenging. Density was classified as low, medium, or high, each corresponding to a range of building stories. Since exact floor counts were unavailable, ranges were assigned to each category in step 4. For cases requiring a fixed floor count, average values were set as: 2 floors for low, 5 for medium, and 9 for high Density.

Preliminary Analysis To inspect the data and spot potential anomalies a preliminary analysis was conducting.
The spatial data were mapped onto a geographic representation, assisting to the data inspection. First, a map displaying the urban plan of Antakya was produced, showing various zones such as industrial areas, commercial spaces, social infrastructure, mixed-use regions, and protected areas. Additionally, a map focusing exclusively on residential buildings was created, with each building color-coded based on its*Density* classification (low, medium, or high). To ensure consistency with the *housing.shp* dataset, a comparative map overlay was performed, checking whether each low, medium, or high-density building (*building.shp* file) corresponded correctly to the designated*Density* zones of the *housing.shp* file.
Then, the range and distribution of the spatial data values was examined. Specifically, a histogram was created to compare the number of buildings categorized by low, medium, and high*Density*. Additionally, the square area of each residential building was analyzed to assess whether most buildings had a similar total*Gross Floor Area* and to identify any outliers. This analysis helped verify the accuracy and consistency of the dataset.

4.2.2. CO_2 Factor

Literature Review gave 34 papers, of residential buildings in countries with a similar climate as Turkey. The meta analysis process is summarized in figure 4.4 and visualized in figure 4.5.

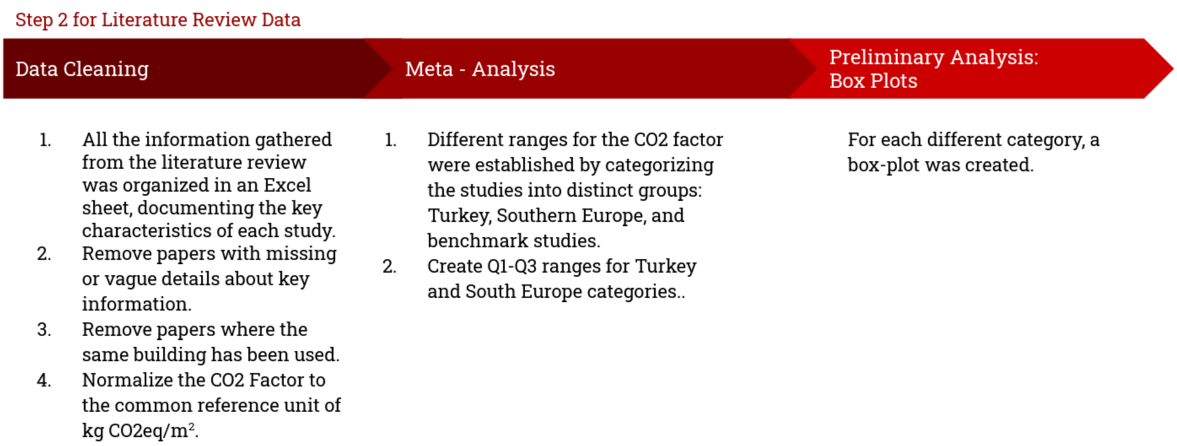

Figure 4.4: Flowchart outlining Step 2 of the methodology for literature review meta-analysis.

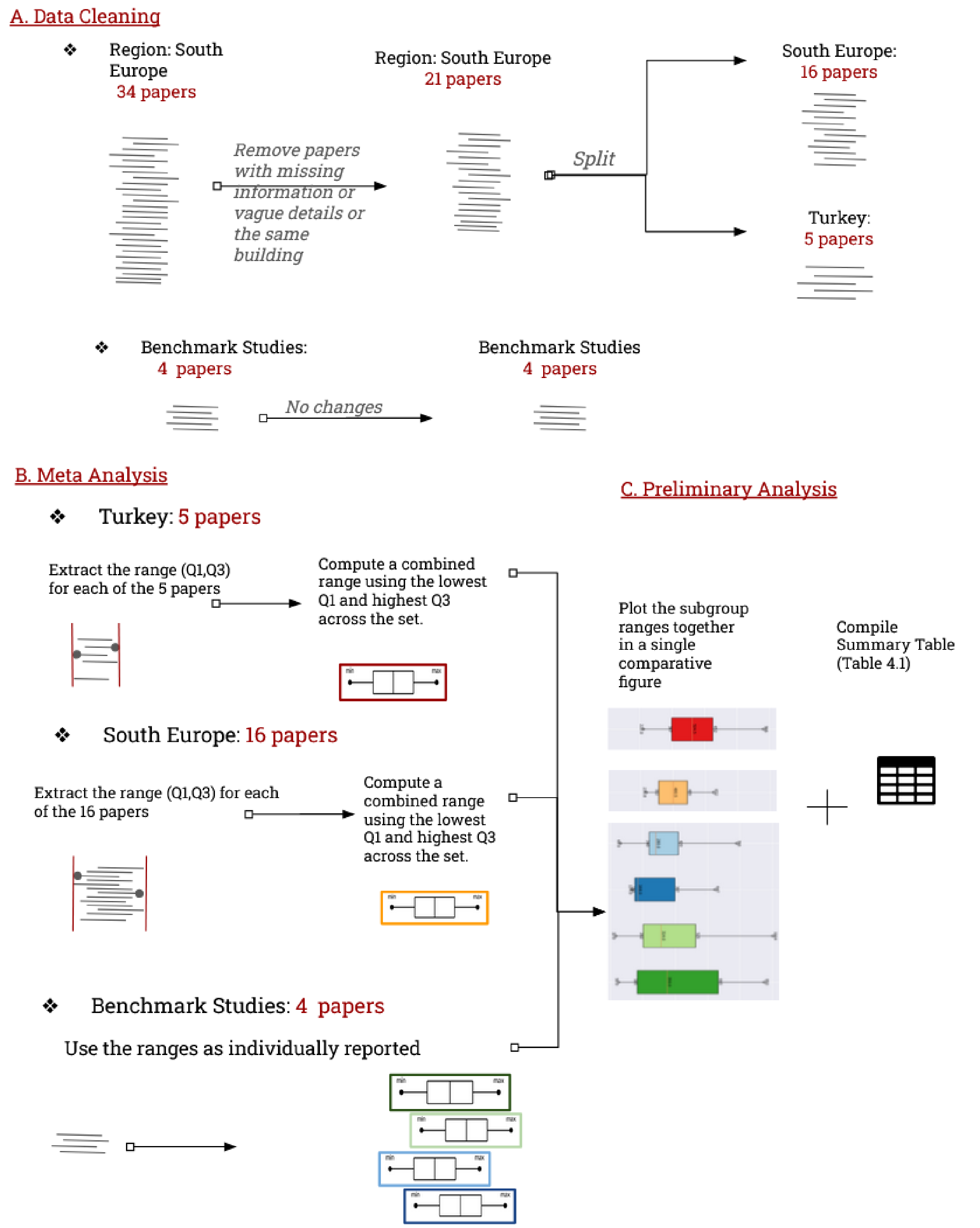

Figure 4.5: Visualization of the Data Pre-processing workflow in the Literature Review Meta-Analysis Methodology for the CO_2 Factor

Data Cleaning The 34 papers from literature review were systematically organized into an Excel database. For each study the key characteristics were recorded such as geographic location, type of building (eg. single-family homes versus multi-storey buildings), the LCA phases that were considered (from A1-A5 at each paper), Source of material intensity values (eg. ICE Version 2.0), and building size and shape (e.g., floor area, number of stories).

For each paper, it was assessed whether sufficient data were provided to calculate emissions per square meter of Gross Floor Area (GFA) or Net Floor Area (NFA). For this study, the difference between GFA and NFA was considered negligible[4]. Studies with unclear definitions of these functional equivalents were excluded, as it would not be possible to calculate the CO_2 factor (in kg CO_2eq/m^2).
Additionally, papers reporting on the same building-often by the same author-were removed to avoid duplication (e.g., Mangan and Oral 2015 and Mangan and Oral 2016). Papers set in unique environmental conditions, such as the Negev desert (Huberman and Pearlmutter 2008), were also excluded due to the peculiarities of their context.
To ensure comparability, a harmonization process was used to standardize results to a common reference unit: tonnes of CO_2 per square meter (kg CO_2eq/m^2). All values were normalized to this unit by adjusting for the reference study period and the specific square meter area used in each study.

Meta Analysis Finally, the meta-analysis categorized studies into two groups: one focusing on buildings in Turkey and another on buildings in Southern Europe. Benchmark works such as those by De Wolf et al. 2015, Röck et al. 2020, Wolf et al. 2020, Simonen et al. 2017 were also reviewed, as they compiled extensive databases on embodied emissions. The results from these studies are summarized in Table 4.1, and are illustrated as box-plots in Figure 4.6.

Name of the Paper	Year	Author	Phase	Average Value	Number of Buildings
Material quantities and embodied carbon dioxide in structures	2015	De Wolf	A1-A3	330	41
Analyze Embodied Carbon, Database of Embodied Quantity Outputs: Lowering Material Impacts Through Engineering	2020	De Wolf	A3	284.5	129
Embodied Carbon Benchmark Study: LCA for Low Carbon Construction (washington.edu)	2017	Simonen	A1-A5	363.5	222
Embodied GHG emissions of buildings The hidden challenge for effective climate change mitigation - ScienceDirect	2020	Rock	A1-A5	282.5	87
South Europe	-	-	-	524.5	127
Turkey	-	-	-	400.5	65
Overall	-	-	-	**351.79**	**684**

Table 4.1: Overview of studies used to define CO_2 emission factor ranges for Monte Carlo simulations. The first four rows are benchmark studies covering a large sample of buildings and specific LCA phases. The South Europe and Turkey rows aggregate multiple studies reviewed in this thesis; while exact LCA phases arent specified, all include at least A3 phase, which represent the bulk of the construction emissions.

Preliminary Analysis Figure 4.6 presents a comparison of seven different CO_2 factor ranges, including four from benchmark studies, two from the current research (South Europe and Turkey), and one representing the LCA of TOKI buildings. The box-plots illustrate the interquartile range (Q1 to Q3), showing where 25% to 75% of the values fall, while the black whiskers extend to indicate the full range, including outliers.

[4]GFA refers to the total floor space within a building, including areas like walls, columns, and common spaces, while NFA refers only to the usable area, excluding structural elements such as walls and corridors.

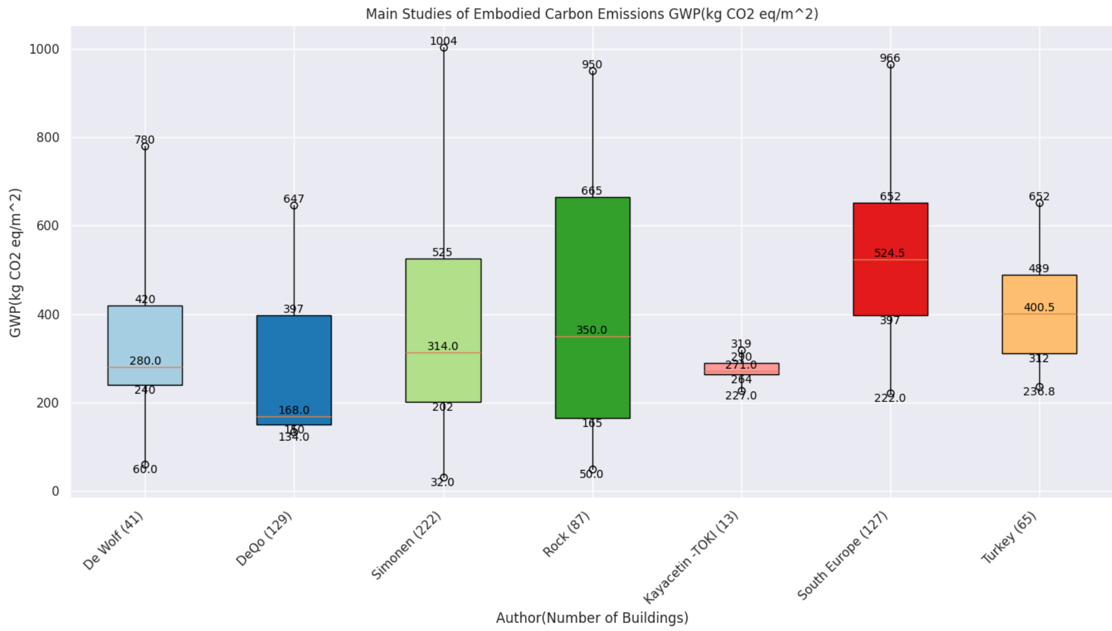

Figure 4.6: Boxplot of CO emission factors from various studies included in the analysis. The first four boxplots represent benchmark studies identified through snowball sampling during the literature review. The last two (in orange and red) reflect aggregated ranges derived from multiple studies focused on Southern Europe and Turkey, respectively.

Among the studies, Röck et al. 2020 exhibits the widest range, from 165 to 665 kg CO_2eq/m^2, indicating significant variability. This is followed by the studies of Simonen et al. 2017 and Wolf et al. 2020, which also show broad distributions, suggesting diverse practices and outcomes within their samples.

In contrast, the TOKI projects, represented by Kayaçetin and Tanyer 2020, show a much lower and more concentrated CO_2 factor, with a median value of only 271 kg CO_2eq/m^2 and minimal spread. [5]

The distributions for South Europe and Turkey, which were developed in this thesis, generally align with existing literature, exhibiting though higher medians and broader IQRs, but remain within a similar range as the other studies. Comparing the values of LCA in Turkey with the South Europe, the former has a narrower spread which maybe is the result that includes fewer studies. Overall, the CO_2 factor across all studies falls between 150 and 650 kg CO_2eq/m^2, a range that was explored in the uncertainty analysis.

4.3. Assigning Uncertainty Ranges for Model's Input

Depending on the source and accuracy of the data, the model can accept two types of inputs: either a fixed value for each building or a range of values(conceptual diagram of the process can be found in figure A.6).

4.3.1. Gross Floor Area - Fixed Values

The Gross Floor Area (GFA) for each building was provided in the raw data and can be directly transformed into square meters without introducing any uncertainty into the model. This gives a fixed

[5] TOKI houses are part of a government-led initiative to deliver affordable housing, particularly targeting low- and middle-income families. These projects often involve the construction of entire neighborhoods, complete with necessary infrastructure like schools and parks. The design of TOKI houses is typically standardized and cost-effective, enabling the rapid construction of housing units across Turkey. This approach is especially prevalent in areas affected by natural disasters or undergoing significant urban renewal, where there is an urgent need for new, affordable housing solutions. Given the extensive rebuilding efforts expected after the recent earthquake, it is anticipated that a large proportion of the new housing will be constructed by TOKI, although the share of buildings to be reconstructed is remains unknown. The CO_2 factor for TOKI projects, as observed in the study, is notably lower and shows less variability compared to other types of housing projects. However, this consistency is also certainly affected by the fact that in comparison with all the other studies, TOKI range was based in one single study.

and precise value for each building that will be constructed. [6]

4.3.2. Number of Floors or Density - Ranges

The Density provided in the raw data is a categorical variable that needs to be converted into Number of Floors for quantitative analysis. For instance, the categorical value of "low density," needs to be convert into a quantitative value, such as 2 floors. Since this precise information is not included in the dataset, uncertainty is introduced into the model when Density is being translated to Number of Floors. The process of this transformation is explained below and is visualised in figure 4.7.

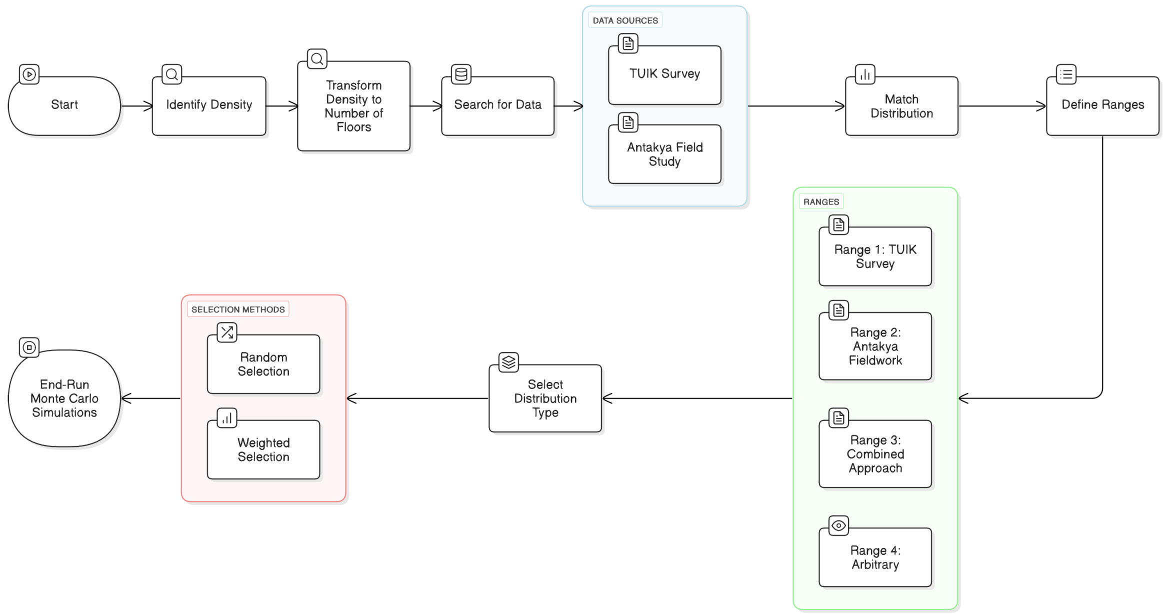

Figure 4.7: Flowchart of the process to transform the density into number of floors

To convert Density into exact floor counts, a search was made to find reliable data that can define what constitutes low, medium, and high density in Turkey. Two key datasets were found: the 2021 survey from the Turkish Statistical Institute (TUIK) (Turkish Statistical Institute 2021) and a field study conducted in Antakya (Ozdemir 2024). These datasets provided statistics on the distribution of building floors in Turkey and Antakya, respectively. The detailed statistics can be found in figure A.7. The methodology involves matching the distribution of building density in the provided spatial data to the distribution found in these datasets. For instance, if 30% of the buildings in the spatial data are classified as having low density, it is cross-reference with the TUIK data, where the 30% of the buildings with the lowest-density consist the buildings, for example having 1 or 2 floors. Similarly, this comparison is repeated using the Antakya-specific dataset to ensure a localized view (below more details of how each range was defined).

From these sources, four different ranges are developed, each establishing distinct ranges for converting Density into Number of Floors: (i) Range 1 uses data from the national TUIK survey, (ii) Range 2 is based on detailed fieldwork in Antakya, (iii) Range 3 combines insights from both the national and local datasets, and (iv)Range 4 is an arbitrary case, based on visual observations from Google Maps.

1. **Range 1: TUIK Survey National**
   The first range is grounded in the 2021 Survey on Building and Dwelling Characteristics conducted by the Turkish Statistical Institute (TUIK) [Turkish Statistical Institute, 2021]. This survey provides a comprehensive overview of the distribution of building floors across Turkey, making it a reliable source for national trends.

[6] However, it's important to note that the GFA is based on data provided by the municipality, which could change over time. To maintain consistency in this case study though, the model treats the provided data as certain, focusing on parameters with explicit uncertainty.

According to the TUIK survey, 29% of residential buildings across Turkey have 1 or 2 floors, 62% have 3 to 8 floors, and 9% have more than 9 floors. This distribution is reflective of the broader Turkish urban environment, encompassing both urban and rural areas. In our dataset, the low-density category comprises 31.6% of the buildings, which aligns closely with the TUIK figure for 1 or 2 floors. The middle-density category in our data represents 66.2%, also consistent with the TUIK range of 3 to 8 floors. High-density buildings make up 2.2% of our data, slightly lower than the TUIK figure for buildings with more than 9 floors. Based on this data, we defined the*Density* classifications as follows:

- **Low*Density*:** 1 or 2 floors
- **Middle*Density*:** 3 to 8 floors
- **High*Density*:** 9 to 12 floors

2. **Range 2: Fieldwork in Antakya**
   The second range is based on a detailed field study conducted by Ozdemir [2024], which focused specifically on Antakya. This study examined the structural characteristics of buildings in the city following the Kahramanmara Earthquakes and included an in-depth survey of 2,650 buildings across six central neighborhoods in Antakya.

   The findings from this study provide a more localized perspective, particularly relevant to Antakya's urban context. According to the study, 36% of the residential buildings in these neighborhoods have 1 to 3 floors, 62% have 4 to 8 floors, and only 2% have more than 9 floors. These figures align closely with our dataset's proportions: 31.6% of the buildings fall into the low-density category, 66.2% into the middle-density category, and 2.2% into the high-density category. It is important to note that this study focused primarily on the city center, where buildings tend to have more floors than in the suburbs. Therefore, while the data is highly relevant, it may slightly overestimate the proportion of middle-density buildings. Based on this data, we defined the*Density* classifications as follows:

   - **Low*Density*:** 1 to 3 floors
   - **Middle*Density*:** 4 to 8 floors
   - **High*Density*:** 9 to 12 floors

3. **Range 3: A Combined Approach** The third range seeks to balance the insights from both the national and local datasets. The TUIK survey, while comprehensive, might overgeneralize the distribution of floors, especially in a city like Antakya, where high-rise buildings are less common. On the other hand, the fieldwork study by Ozdemir [2024] provides valuable local insights but focuses primarily on the city center, potentially underestimating the prevalence of low-density buildings in less central areas.

   Therefore, the combined range integrates the strengths of both datasets. We assume that the overall distribution of building floors in Antakya falls somewhere between the national average and the city center's characteristics. This range uses the following classifications:

   - **Low*Density*:** 1 or 2 floors
   - **Middle*Density*:** 3 to 8 floors
   - **High*Density*:** 9 to 12 floors

4. **Range 4: Arbitrary**

   We also developed an "Arbitrary Range" based on visual observations from Google Maps, where building floors was investigated by "judging by the eye". This approach, while subjective, allows us to explore whether potential discrepancies might arise when*Density* classifications are made without empirical evidence.
   The*Density* classifications for the Arbitrary Range are:

   - **Low*Density*:** 1 to 3 floors
   - **Middle*Density*:** 4 to 7 floors
   - **High*Density*:** 8 to 11 floors

Range 1 and Range 3 may initially appear identical because they share the same range of floor values, but they differ when weights are applied. In this analysis, we consider two approaches for selecting a value from these ranges. One where the selection is random, meaning each floor count has an equal chance of being chosen, and another where weights are applied. For instance, when the model encounters the "low density" classification in both Range 1 and Range 3, it knows that this can be 1 or 2 floors. If the selection is random, there is a 50% chance of choosing either 1 or 2 floors. However, when weights are applied, the probabilities change -there might be a 40% chance of selecting 1 floor and a 60% chance of selecting 2 floors.

Overall, we apply four different ranges across two cases (see Table 4.2): one where all floor counts within each range are equally probable, and another where weighted probabilities are used, based on external data from Table A.7. This comparison helps us understand how different assumptions about building density affect the distribution of floor counts and, consequently, the model's outcome.

Range	**Density**	**Floor Range**	**1**	**2**	**3**	**4**	**5**	**6**	**7**	**8**	**9-12**
Range 1	Low	1-2	41%	59%	-	-	-	-	-	-	-
TUIK Survey	Medium	3-8	-	-	23.9%	22.4%	20.9%	19.4%	9.0%	4.5%	-
	High	9-12	-	-	-	-	-	-	-	-	25% each
Range 2	Low	1-3	30.0%	42.0%	28.0%	-	-	-	-	-	-
Antakya Field Work	Medium	4-8	-	-	-	42.0%	24.0%	15.0%	13.0%	6.0%	-
	High	9-12	-	-	-	-	-	-	-	-	25% each
Range 3	Low	1-2	45%	55%	-	-	-	-	-	-	-
Combined Approach	Medium	3-8	-	-	22.7%	24.2%	22.7%	15.2%	10.6%	4.5%	-
	High	9-12	-	-	-	-	-	-	-	-	25% each
Range 4	Low	1-3	33.3%	33.3%	33.3%	-	-	-	-	-	-
Arbitrary	Medium	4-7	-	-	-	25%	25%	25%	25%	-	-
	High	8-11	-	-	-	-	-	-	25%	25%	25% each

Table 4.2: Density Classifications, Floor Possible, and Floor Distributions for Each Range

4.3.3. CO_2 Factor - Ranges

Table 4.1 provide the ranges that will be inserted to the variable of the CO_2 Factor (except the TOKI range). In the meta-analysis shown in Figure 4.6, each boxplot represents the interquartile range (25-75%) of the CO_2 Factor values (Q1 to Q3). While boxplots are useful for visualizing data spread and variability, they provide limited information about the underlying distribution of the data.

A straightforward approach might be to assume a uniform random distribution, given that no additional distributional details are available. However, Life Cycle Assessment (LCA) studies often reveal that CO_2 Factors are not uniformly distributed ([Simonen et al., 2017]). In many cases, emissions cluster around a central value, which is more accurately represented by a normal distribution with a symmetrical spread around the mean. That said, material choices, policy standards, or regional practices can sometimes create asymmetry, leading to skewed distributionseither left- or right-skewed.

Therefore, to account for these possibilities, and in the absence of specific distributional data, we tested four potential distribution types for each boxplot: uniform, normal, and skewed distributions (both left and right). This approach ensures a broader understanding of variability.

Uniform Distribution
Initially, uniform random distributions were applied using the first quartile (Q1) and third quartile (Q3) as boundaries, with the broad distribution also considered (Figure A.8).

Normal Distribution
The normal distributions were generated under the assumption that the lowest and highest values from each study correspond to Q1 and Q3, respectively. These values are assumed to follow a normal distribution. The mean is calculated as the average of the two quartiles, and the standard deviation is estimated by dividing the range (Q3 - Q1) by four ($\frac{\text{highest} - \text{lowest}}{4}$). Results are shown in figure 4.8.

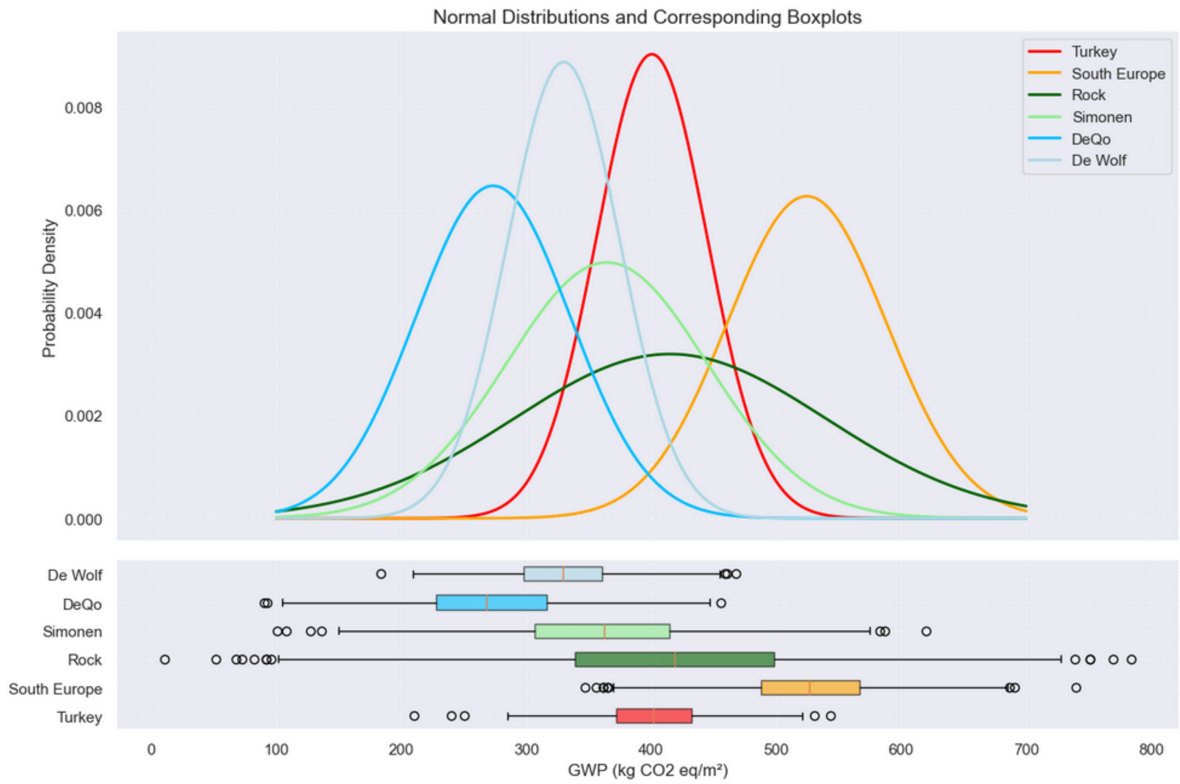

Figure 4.8: Transformation of boxplots into probability distributions. The figure displays the resulting normal distributions derived from the 6 boxplot ranges. The same approach was also applied to generate uniform and triangular distributions and can be found in Figures A.8, A.9 and A.10.

Triangular Distributions

Lastly, the triangular distribution both for left and right skew was created. The first quartile (Q1) and third quartile (Q3) served as the lower and upper bounds, while the peak of the distribution was set at one standard deviation ($\pm 1\sigma$) from the mean. For left-skewed distributions, the peak was placed at (mean $-\sigma$), and for right-skewed distributions, it was positioned at (mean $+\sigma$). This approach allowed for asymmetry in the data, reflecting real-world variability in emissions. The resulted distribution plots are presented in figures A.9 and A.10.

Additional Ranges Used in the Main Analysis

In addition to these 6 ranges, two more were added. One is the "broad" range, which spans from 134 to 665 kg CO_2eq/m^2, and represents the minimum and maximum values observed across all six boxplots. Second is the "mixture" range, that integrates all the 6 distributions. It is created by assigning equal weights to the distributions from the six boxplots, except for the Turkish distribution, which was given a higher weight due to its regional significance. The results for the -normal- "mixture" are depicted in figure 4.8 (but also see Figures A.8, A.9, A.10). These two ranges the *mixture* and the *broad* provide the most comprehensive representation of the underlying dataset. Therefore, they have been selected as the primary input ranges for the main analysis.

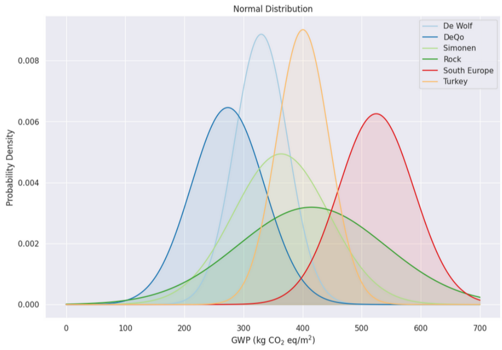

(a) Normal distribution of the different ranges explored in the literature review of LCA

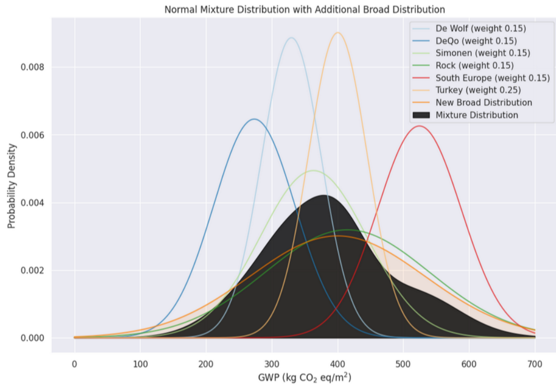

(b) Mixture Distribution

Figure 4.9: Mixture Distribution based to the CO_2 Factor for different *normal* distribution ranges

4.4. Calculate CO_2 Emissions via Uncertainty Analysis

In this step, Monte Carlo simulations were employed to estimate CO_2 emissions, as this method effectively accounts for uncertainties in key parameters. The Monte Carlo approach involves repeatedly calculating CO_2 emissions, with each simulation drawing random values from the assigned uncertainty ranges (that were established in the previous Step). By conducting thousands of simulations, the method generates a distribution of the value of all the thousand outcomes, showing the range and probability of different emission estimates.

This study applies two primary approaches: the One-at-a-Time (OAT) method, where a single variable is altered while all others are held constant, and the Simultaneous Variation approach, in which variables are varied concurrently (see schematic explanation in figure 4.10). Additionally, a Sobol sensitivity analysis is considered as an optional technique to quantify the relative contribution of each uncertain variable to the overall variability of the results.

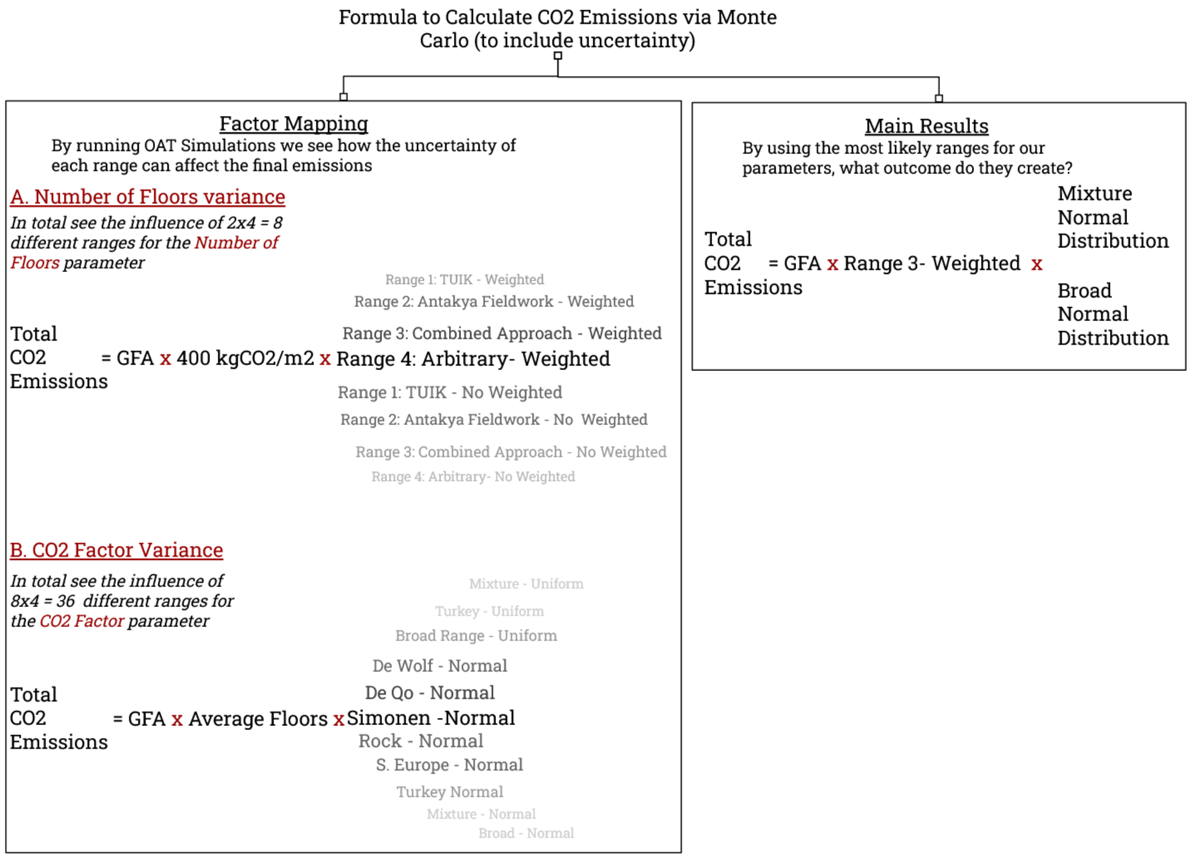

Figure 4.10: Flowchart illustrating how the parameter ranges summarized in Figure A.11 are used in the analysis. Each range was tested to assess the influence of either the *Number of Floors* or the CO_2 *Factor*, by varying one parameter at a time while holding the other constant (OAT), while only a few ranges have been used for the main results.

4.4.1. Monte Carlo One At a Time

The Monte Carlo One-at-a-Time (OAT) method shows the influence of each individual variable on the output (total CO_2 emissions) by varying one parameter at a time, while keeping all other parameters constant. These simulations were performed for all the different uncertainty ranges of each parameter (Table 4.3).

Scenario No.	OAT or Simultaneous	Number of Floors Value	CO_2 Factor Value	Distribution Type
1	OAT	Range 1: TUIK	Fixed at 400 kg CO_2eq/m^2	Random
2	OAT	Range 2: Antakya Field Work	Fixed at 400 kg CO_2eq/m^2	Random
3	OAT	Range 3: Combined Approach	Fixed at 400 kg CO_2eq/m^2	Random
4	OAT	Range 4: Arbitrary	Fixed at 400 kg CO_2eq/m^2	Random
5	OAT	Range 1: TUIK	Fixed at 400 kg CO_2eq/m^2	Weighted
6	OAT	Range 2: Antakya Field Work	Fixed at 400 kg CO_2eq/m^2	Weighted
7	OAT	Range 3: Combined Approach	Fixed at 400 kg CO_2eq/m^2	Weighted
8	OAT	Range 4: Arbitrary	Fixed at 400 kg CO_2eq/m^2	Weighted

Table 4.3: Scenarios where the CO_2 Factor is constant and the Number of Floors is varying

Next, Monte Carlo simulations using the OAT method were performed with the **Number of Floors fixed at its average value**, while the CO_2 Factor was varying. Simulations were conducted for each distribution type -uniform, normal, left-skewed triangular, and right-skewed triangular distributions -using the possible ranges for the CO_2 Factor (the six boxplots, the broad range and the mixture range). For each distribution type, the results were displayed as histogram plots, capturing the spread and likelihood of different emission outcomes for each case.

Scenario No.	OAT or Simultaneous	Number of Floors Value	CO_2 Factor Value (kg $\mathbf{CO_{2eq}/m^2}$)	Distribution Type
9-15	OAT	Low = 2, Middle = 5, High = 9	6 Boxplots & Broad Range	Random
16-23	OAT	Low = 2, Middle = 5, High = 9	6 Boxplots & Mixture & Broad Range	Normal
24-31	OAT	Low = 2, Middle = 5, High = 9	6 Boxplots & Mixture & Broad Range	Triangular - Left Skew
32-39	OAT	Low = 2, Middle = 5, High = 9	6 Boxplots & Mixture & Broad Range	Triangular - Right Skew

Table 4.4: Scenarios where the Number of Floors is constant and the CO_2 Factor is varying. All of the above scenarios can be found in detail, in table A.3

4.4.2. Monte Carlo Simultaneously

After separately analyzing the full range of uncertainties for the two parameters, the next step is to estimate CO_2 emissions while accounting for the simultaneous uncertainty in both variables. In the OAT approach, the calculations were relatively manageable, with (4 ranges x 2 distributions for *Number of Floors* as shown in Table 5.3)+(8 ranges x 3 distributions + 7 ranges x 1 distribution for CO_2 Factor as shown in Table 5.3). So in total 39 different scenarios. However, varying both parameters simultaneously significantly increases computational complexity, requiring the evaluation of (4 ranges x 2 distributions)Œ(8 ranges x 4 distributions)=256 potential scenarios. Therefore, running 256 scenarios, over a thousand of simulations for each scenario with a dataset of the magnitude of 40,000 rows can be computationally expensive.

Therefore, to balance accuracy and efficiency, we performed *MC Simultaneously* only for the most prominent uncertainty ranges. The following characteristics were used for this refined simulation:

- **Number of Floors**: The range was selected from Scenario 3, which integrates data from both a national database covering all of Turkey and a more localized database focused on the center of Antakya. Within Scenario 3, the weighted distributions were chosen to best represent the uncertainty.
- CO_2 **Factor Range**: The simulation utilized the distribution from the mixture distribution (257-530 kg CO_2eq/m^2) and a broader distribution that extends the range further (134-650 kg CO_2eq/m^2), capturing more variability in potential emissions.

An example of how the code for MC Simultaneously looks like can be found in .

Scenario No.	OAT or Simultaneous	Number of Floors Value	CO_2 Factor Value (kg $\mathbf{CO_{2eq}/m^2}$)	Distribution Type
40	Simultaneous	Range 3 - Weighted	Mixture (257-530 kg CO_{2eq}/m^2)	Weighted
41	Simultaneous	Range 3 - Weighted	Broad Range (134-665 kg CO_{2eq}/m^2)	Weighted

Table 4.5: CO_2 Emission Simulation Scenarios: Number of Floors and CO_2 Factor Ranges

4.4.3. Sobol Sensitivity Analysis

Sensitivity analysis is crucial for understanding the influence of different input parameters on a model's output. The reasons of applying Sobol when we have already investigate the parameters through Monte Carlo can be summarized in 3 reasons. First, Sobol *quantifies* the contribution of each parameter to the total variance (S1 value) beyond merely observing outcome ranges. Second, it identifies and measures interactions between parameters (ST value), revealing how they may affect each other to the final outcome. Third, Sobol serves as a comparative tool to validate and refine the findings from the Monte Carlo analysis.

In this case study, only two uncorrelated parameters were used. However, Sobol was still included for completeness and to anticipate future applications of the model. Its inclusion also allows for an interesting comparison with Monte Carlo results, showing how the two methods may differ in capturing model sensitivity.

Sobol analysis is rooted to the concept of the Shapley value from Game Theory and mathematically it decomposes the total variance $V(Y)$ of the model's output into contributions from individual inputs and their interactions. The general form for the decomposition of variance is as follows:

$$V(Y) = \sum_{i=1}^{k} V_i + \sum_{1 \leq i < j \leq k} V_{ij} + \cdots + V_{12\ldots k}$$

where:

- V_i represents the contribution of the i-th parameter alone,
- V_{ij} represents the contribution from the interaction between parameters i and j,
- $V_{12\ldots k}$ represents the contribution from the interaction among all k parameters.

Since the model contains only two parameters($k = 2$), the exact formulas can be simplify as follows:

1. **Total Variance**:

$$V(Y) = V_1 + V_2 + V_{12}$$

   where:

   - V_1 is the variance contribution of parameter X_1 (Density),
   - V_2 is the variance contribution of parameter X_2 ($CO_2 factor$),
   - V_{12} is the variance contribution due to the interaction between X_1 and X_2.

2. **First-Order Sobol Indices**: The first-order Sobol index S_i measures the proportion of the output variance attributed to a single input parameter X_i

   - For X_1:

$$S_1 = \frac{V_1}{V(Y)}$$

   - For X_2:

$$S_2 = \frac{V_2}{V(Y)}$$

   This index represents the direct effect of X_i (Density) on the output (total CO_2 emissions).

3. **Total-Order Sobol Indices**: The total-order Sobol index ST_i captures the contribution of X_i to the output variance, including both its direct effects and its interactions with other parameters:

   - For X_1:

$$S_{T_1} = 1 - \frac{V_{\sim 1}}{V(Y)}$$

   - For X_2:

$$S_{T_2} = 1 - \frac{V_{\sim 2}}{V(Y)}$$

   Here, $V_{\sim 1}$ and $V_{\sim 2}$ represent the variance of the output excluding the variance caused by X_1 and X_2, respectively.

For the case study, the Sobol analysis was conducted by using the CO_2 range derived from the mixture distribution, combined with the*Density* range from the Combined Approach (Range 3) with an equal random distribution.

4.5. Social Cost of Carbon

This section converts the estimated CO_2 emissions from the reconstruction of Antakya into monetary terms, in order to reflect their broader societal and environmental costs.

The process begins with the mean CO_2 emissions derived from the main Monte Carlo simulation results, expressed in tonnes. These emissions are then multiplied by the Social Cost of Carbon (SCC), a widely accepted economic metric that estimates the long-term societal damage caused by emitting one additional tonne of CO_2 into the atmosphere. The SCC reflects impacts such as health effects, agricultural losses, property damage from increased flood risk, and other climate-related disruptions (see Section 2 for further discussion).

The societal cost is then obtained by multiplying the mean CO_2 emissions by the standardized SCC value. For example, if the main results show that the reconstruction releases 30 tonnes of CO_2 and the SCC is $1 per tonne, the resulting cost would be $30.

Given that SCC estimates vary widely, due to differences in models and future assumptions -such as discount rates- a benchmark value of $185 per tonne [7] is adopted in this study, based on a widely recognized study of Rennert 2022. This value is 3.6 times higher than the U.S. government's previous estimate of $51 per tonne and reflects updated damage functions and socioeconomic projections.

While applying a single SCC value supports consistency and comparability in the analysis, the uncertainty surrounding this metric is acknowledged. To account for this, an alternative methodology incorporating a range of SCC values is provided in Appendix A.4.4.

4.6. Policy Pathways

This section examines potential policy pathways to reduce the carbon footprint of post-disaster reconstruction. Specifically, focuses on two key approaches.

The first approach calculates the total CO_2 emissions (with Monte Carlo) simulations, by applying a reduced CO_2 factor to a percentage of the buildings that will be reconstructed. This way, it represents a scenario where sustainable construction practices have been followed. These results are then compared to a baseline scenario where a uniform CO_2 factor is applied to all buildings (see Step 4).

The second approach assesses whether adopting a policy of constructing energy-efficient homes, could, in the long term, offset the carbon footprint that is generated during the reconstruction process. This is achieved by comparing the CO_2 factor of construction with that of building operation.

4.6.1. A. Policy Pathways: Using sustainable construction practices

There are multiple sustainable construction practices, and a systematic review by Pomponi and Moncaster 2016) outlines the practices that are most commonly explored in literature. However, selecting a policy from the ones that Pomponi and Moncaster 2016 propose, would require a detailed investigation, something that goes beyond the scope of this study. **Therefore, for this analysis, we consider as sustainable construction practices, any approach that reduces the value of the CO_2 *factor* parameter.**

Baseline scenario
The methodology begins by establishing a baseline scenario that represents standard reconstruction practices. Therefore, from the existing ranges, we selected the CO_2 emission factor that ranges from 134 to 655 kg CO_2eq/m^2 ("broad" normal distribution), as the most broad range (and also one of the two ranges that was presented as main results in step 4). [8].

Sustainable scenarios
To explore more sustainable alternatives, three sustainable reconstruction scenarios are introduced. In each scenario, a specified share of buildings is constructed using a lower emission factor range of 264290 kg $\mathrm{CO_{2eq}}/m^2$, while the rest remain within the baseline range. This lower range is based on empirical data from Kayaçetin and Tanyer 2020, which specifically assessed the embodied carbon in TOKI (Toplu Konut Idaresi) housing.

TOKI projects, developed by Turkeys Housing Development Administration, are government-led initiatives aimed at providing affordable housing. These projects often involve large-scale, rapid construction of standardized residential units using prefabricated reinforced concrete. Centralized design and procurement processes allow for reduced material waste and transportation needs, contributing to lower embodied emissions compared to typical building methods Kayaçetin and Tanyer 2020.

[7] 2020 dollars, at a 2% discount rate

[8] Meaning that in the Monte Carlo Simulations for the baseline scenario, for each building a value was taken randomly from the normal distribution of the range (134,655)

The design of TOKI houses is typically standardized and cost-effective, enabling the rapid construction of housing units across Turkey. This characteristic is especially useful in areas affected by natural disasters or undergoing significant urban renewal, where there is an urgent need for new, affordable housing solutions. Given the extensive rebuilding efforts expected after the recent earthquake, it is anticipated that a large proportion of the new housing is or will be constructed by TOKI, although the share of buildings to be reconstructed is remains unknown. This, in combination with the availability of emissions data, makes TOKI a relevant case study for exploring low-carbon construction pathways.

It is important to note, however, that this choice is based on practical considerations rather than an endorsement of TOKI as a universally ideal solution. The social and architectural implications of such standardized developments are further discussed in later sections.

In Scenario 1, 15% of the buildings are constructed using the lower CO_2 emission factor, while 85% follow standard practices. Scenario 2 assumes 30% of buildings adopt the lower emission factor, with 70% using the standard approach. In Scenario 3, 50% of the buildings are rebuilt with the lower CO_2 emission factor, and the remaining half follows the standard practices. All of the described scenarios can be seen in table 4.6.

Scenario	CO_2 Factor Range (kg CO_{2eq}/m^2)	Proportion of Buildings Using Lower CO_2 Factor	Description
Baseline	134 - 655 (broad normal distribution)	0% (all buildings use standard practices)	Represents standard reconstruction practices, where all buildings adopt the higher CO_2 emission range.
Scenario 1	15%: 264 - 290 (TOKI range) 85%: 134 - 655 (standard range)	15%	15% of buildings are built using lower CO_2 factors based on TOKI houses, while the majority follow standard practices.
Scenario 2	30%: 264 - 290 (TOKI range) 70%: 134 - 655 (standard range)	30%	30% of buildings adopt the lower CO_2 emission factor, while the rest use standard practices.
Scenario 3	50%: 264 - 290 (TOKI range) 50%: 134 - 655 (standard range)	50%	Half of the buildings use lower CO_2 factors, reflecting a significant shift toward sustainable reconstruction practices.

Table 4.6: Baseline and Sustainable Reconstruction Scenarios: CO_2 Factor Ranges and Proportions

By comparing the results of these scenarios to the baseline, helps to quantify the possible reductions in carbon emissions, if sustainable reconstruction practices were adopted. If significant, it could be an argument for following sustainable rebuilding efforts.

4.6.2. B. Policy Pathways: Energy-efficient vs traditional buildings

This section examines whether constructing energy-efficient homes can - over time- offset the carbon emissions generated during post-disaster reconstruction. While energy-efficient homes are effective at reducing operational emissions, the critical question is whether, and when, these operational savings can offset the initial "emissions spike" from construction. To address this, we introduce four energy-efficiency scenarios and compare them against a baseline scenario, over the whole lifespan of a building.

The **baseline scenario** represents a traditional building that was not affected by the earthquake, and thus doesn't emit any emissions during construction. The building model used is a five-story residential structure with a total area of 745 m^2.

The four **alternative scenarios** involve reconstructing the same building (with identical characteristics in terms of floors and area) but with different energy-efficiency upgrades. Scenario A involves the installation of photovoltaic (PV) panels, Scenario B includes vertical-axis wind turbines (VAWT), Scenario C incorporates green walls, and Scenario D combines all of these three measures. These scenarios are based on the work of Saleh et al. 2024, who provided detailed data on energy consumption and CO_2 emissions for a five-story building in Antakya (figures of the building for each scenarios can be found in Figure A.13 and a table with the calculation of the annual operation emissions in 4.7). The original data, presented in units of kWh/year/m^2, were converted to tonnes of CO_2/m^2 using a common conversion factor of 0.000233.

Therefore, for each energy-efficient scenario (A to D), we assigned a different *operational* CO_2 emission factor. In addition to operational emissions, *construction emissions* were modeled for all of the scenarios (except the baseline where construction emissions are 0). The construction emission was selected equal to 399 kg CO_2eq/m^2, a value that is the mean value of the mixture distribution (a range used in the main results and is a combination of the 6 distributions as extracted from the literature, see 4.6). Construction emissions are considered to be emitted the first two years of the building's lifespan and operational emissions for 48 years. Having in total a building with a lifespan of 50 years.

The plot that was constructed, shows on the x-axis the building's year and on the right y-axis shows the Cumulative CO_2 emissions up to that year, by summing the annual operational emissions with the initial construction emissions. By plotting the four energy efficient scenarios and the baseline scenario, we define the break-even point. The break even point is identified as the year when the cumulative CO_2 emissions from the baseline scenario equaled or exceeded those from any other scenarios.

Scenario	**Description**	**Annual Operational Emissions ($\mathbf{CO_2/m^2/year}$)**
Baseline (Business as Usual)	Assumes no buildings are destroyed or rebuilt; emissions begin from year 0 without intervention.	0.043
PV Panels	Incorporates photovoltaic panels to generate electricity on-site.	0.035
VAWT (Vertical-Axis Wind Turbine)	Uses small-scale wind turbines for supplementary power generation.	0.039
Green Wall	Adds a vegetated facade that enhances insulation and passive cooling.	0.041
All Measures Combined	Combines PV panels, wind turbines, and a green wall to maximize energy efficiency.	0.030397

Table 4.7: Summary of operational emissions across different sustainable building scenarios. Emissions are calculated per square meter per year and reflect the effectiveness of each strategy relative to the baseline.

5
Results

5.1. Raw Data Insights

The data for this study was sourced from two main avenues. First, **spatial data** provided by the Hatay Municipality contained information on two of the three key model parameters: Gross Floor Area and Number of Floors. This raw spatial data was provided in the form of shapefiles (.shp), each representing different elements of the reconstruction plans. Four primary shapefiles were used: *Border Antakya*, defining the geographical limits of the city; *Landuse,* detailing categories such as residential, commercial, and industrial zones; *Housing*, providing information on large residential areas; and most importantly, *Buildings*, which contains detailed data on all individual structures to be rebuilt. Each entry in the Buildings shapefile corresponds to a specific building, with attributes for density (low, medium, or high) and its geometry in a Coordinate Reference System (CRS), specifically the 2D geographic CRS: EPSG:4326. Figure A.14 shows how the raw data looked like.

The second source of data came from a **literature review** aimed at determining the CO_2 Factor parameter. This review yielded 34 relevant studies. These studies were all Life Cycle Assessments (LCA) of residential buildings from the below countries: Turkey, Greece, Lebanon, Italy, Spain, and Portugal. At this stage, the papers were not yet evaluated for completeness regarding the specific CO_2 Factor (in kg CO_2/m^2).

5.2. Cleaned and Processed Data

The raw data have been merged in one shapefile with 47,263 rows, each corresponding to a building. As illustrated in Figure 5.1, the spatial plan reveals that 84% of the designated buildings will be residential (colored gray), with the remaining 16% will be allocated to industrial zones, commercial spaces, social infrastructure, mixed-use areas, and protected regions. This distribution aligns closely with data from the Turkish Statistical Institute (TUIK) [Turkish Statistical Institute, 2024], which reports that 85% of land use in Turkish cities is residential. Therefore, the data accurately reflect the typical land use distribution in urban Turkey.

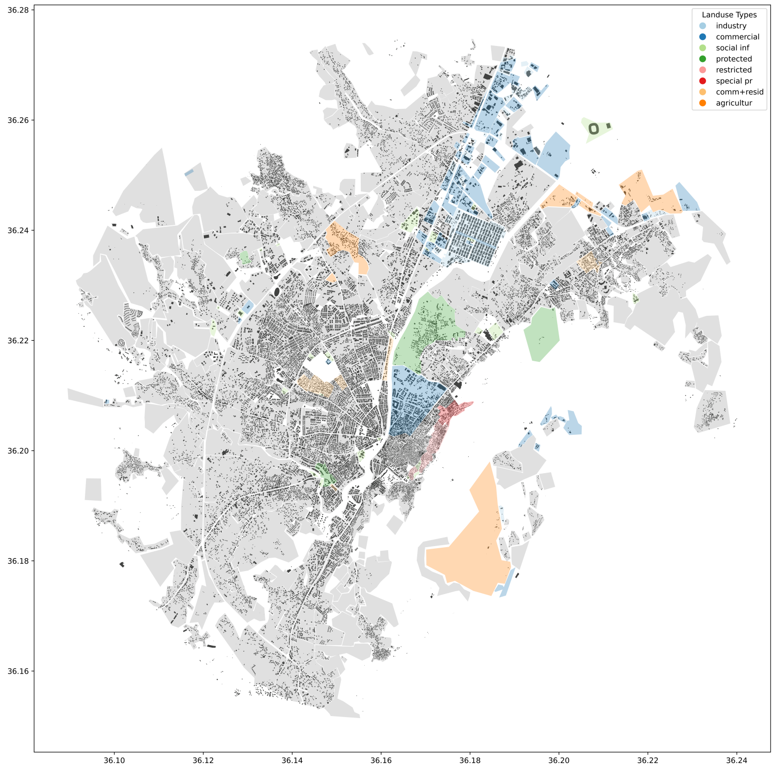

Figure 5.1: Antakya reconstruction plans based on the data from Hatay Metropolitan Municipality Hatay Metropolitan Municipality 2024 (see A.4). Color coded based on the type of landuse, with gray the residential buildings.0

After merging the datasets, an analysis was conducted to identify missing values. Approximately 15% of the dataset had missing values in the Density column. Upon further inspection, most of these missing values were linked to non-residential buildings, which were excluded from the analysis, as this study focuses solely on residential buildings. For the remaining 1% of residential buildings with missing Density values, the information was imputed using the housing.shp shapefile. The missing Density values for individual buildings were assigned based on the area's density that the building is located (Figure 5.2, which overlays building's density and area's density on the same map). The Geometry column was transformed into square meters to calculate the Gross Floor Area, and no missing values were identified in this process.

After cleaning the dataset, we conducted a preliminary analysis to explore building density patterns (Figure 5.2). A color-coded map was generated to represent density categories: low (green), medium (yellow), and high (red). These categories were based on both building density and area density, which were found to align completely across the two datasets. Non-residential buildings, shown in black, were excluded from the density classification as they are not residential buildings.

The analysis showed that most residential buildings fall into the medium-density category (yellow), with a noticeable concentration on the eastern side of the city center. Low-density buildings (green) are primarily located on the city's outskirts, as well as in the historical center, which is characterized by traditionally low-density structures (see Figure A.2). High-density buildings (red) are relatively rare and dispersed sporadically across the city.

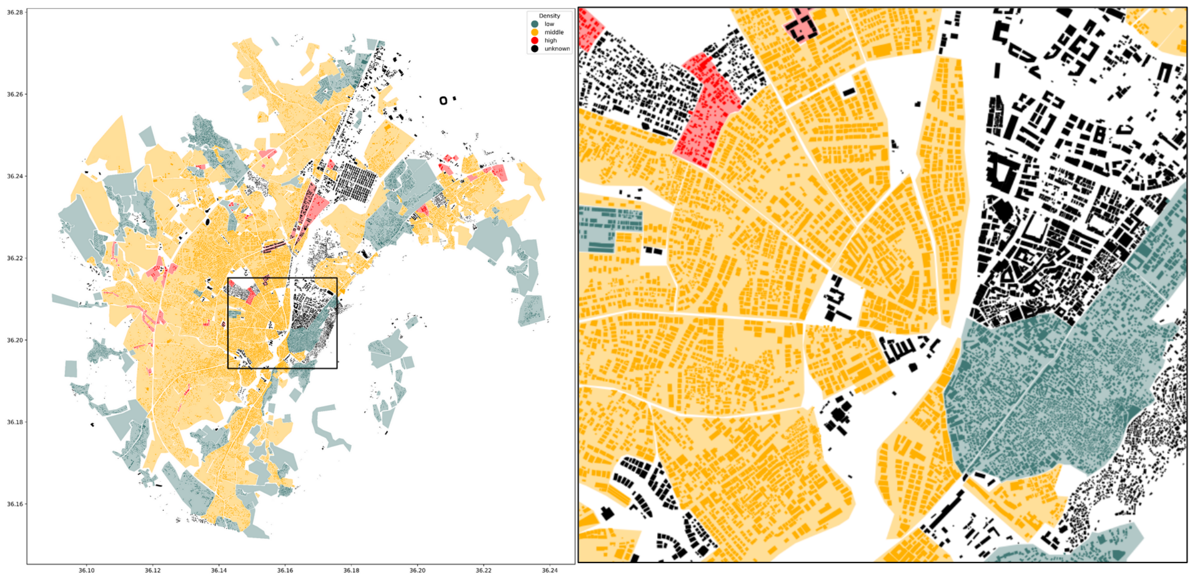

Figure 5.2: Map Visualization of the provided Spatial Data with a zoom in. The larger colored areas correspond to data from the housing.shp shapefile, while the smaller shapes represent building footprints from the Buildings.shp dataset, both color-coded by density.

Histograms of key columns were then created for analysis. First, for the Number of Floors, -expressed at this stage as density categories-, a histogram of low, medium, and high-density values was generated. The results showed that medium-density buildings account for 66.2% of the total residential buildings, low-density buildings make up 31.6%, and high-density buildings represent only 2.2%. Additionally, a histogram of the total square meters of buildings was created and is presented in Figures 5.3b and A.15, revealing that the vast majority of residential buildings have a ground floor area between 50 and 200 m^2.

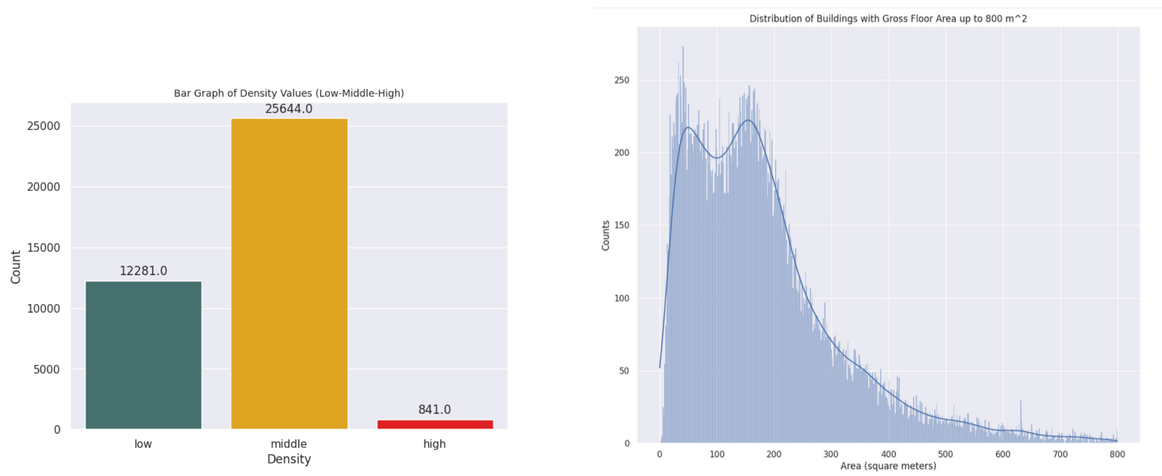

(a) Bar-graph of the Density values

(b) Histogram of the Gross Floor Area per building

Figure 5.3: Preliminary Analysis Distribution plots for the key parameters of th model

5.3. Uncertainty Ranges Assigned to Model Inputs

In Step 3 of the methodology, uncertainty ranges were defined for key model parameters. Table A.3 provides a summary of all the assigned ranges, while Figure A.11 offers a schematic overview of the possible values for the two parameters subject to uncertainty: *Number of Floors* and CO_2 *Factor*. In total, 8 distinct ranges were identified for the *Number of Floors* parameter, and 36 for the CO_2 *Factor*, all of which were used to calculate potential variations in total CO_2 emissions for Monte Carlo Simulations.

5.4. Results of CO_2 Emissions Calculation

To incorporate uncertainty into the models parameters, Monte Carlo simulations were run for all the different uncertainty ranges.

The results begin with the One-at-a-Time Monte Carlo method (Scenarios 1-39) where a single variable is altered to assess how changes in each parameter affected the outcome. Once their individual effects is understood, then for the most probable ranges for each parameter, we run Monte Carlo Simultaneously. That means that **both variables were varied simultaneously** (Scenario 40 and 41) to observe the combined influence and a final estimation for the amount of CO_2 emissions. Additionally, the Sobol sensitivity analysis results are provided to quantify the contribution of each uncertain variable to the overall variability of the outcomes, enabling a comparison with the One-at-a-Time method.

5.4.1. Results: Monte Carlo One at a Time (OAT)

Number of Floors

Scenario No.	OAT or Simultaneous	Number of Floors Value	CO_2 Factor Value	Distribution Type
1	OAT	Range 1: TUIK	Fixed at 400 kg CO_2eq/m^2	Uniform
2	OAT	Range 2: Antakya Field Work	Fixed at 400 kg CO_2eq/m^2	Uniform
3	OAT	Range 3: Combined Approach	Fixed at 400 kg CO_2eq/m^2	Uniform
4	OAT	Range 4: Arbitrary	Fixed at 400 kg CO_2eq/m^2	Uniform

Table 5.1: Scenarios where the CO_2 Factor is constant and the Number of Floors is varying

Scenario 1 to 4: Uniform probability In this simulation, for each scenario, the selection of the number of floors within a given density category (*low, middle, or high*) was based on equal probability (see Table 5.1). This implies that within each density category(eg. low), every possible floor number from has an equal chance of being selected during the Monte Carlo simulations. For instance in Scenario 1, when a building has a low density, there is an equal random probability of being 1 or 2 floors.

The results are based on 1000 simulations and are illustrated in Figure A.17. In these plots, the first three vertical axes represent the transformation of Density categories into specific floors. The final vertical axis on the right side of the plot represents the total CO_2 emissions (measured in tonnes) resulting from all the different combinations of floors. Figure A.17 specifically presents the results for Scenario 3 and Scenario 4, while detailed figures for each scenario are available in Figure 5.4.

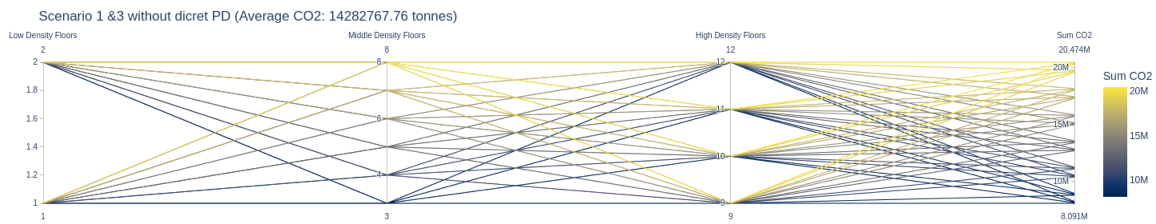

Figure 5.4: One at a time variation of Density Ranges (without discrete probability density) for the Range 3 - Combined Approach

Some key observations can be drawn from Figure 5.4 and the respective plots of the other ranges.

Firstly, the **total CO_2 emissions exhibit a wide range**, with outcomes spanning from approximately 10 million tonnes to nearly 20 million tonnes. This significant spread underscores the impact that different floor configurations can have on overall emissions. More importantly, the results underscore how evolving reconstruction plans, which may shift floor area allocations or change zoning regulations, can significantly alter total emissions outcomes. Floor count decisions directly influence built area, material use, and structural loadall of which drive embodied emissions. As urban plans develop and densities are adjusted (whether for regulatory, economic, or social reasons), these shifts can scale up to have a major environmental impact. Therefore, the flexibility or uncertainty in floor planning becomes a key factor in emissions forecasting and carbon accounting in post-disaster reconstruction.

Moreover, when comparing the different ranges, including Range 4 (which was arbitrarily defined), **there is no substantial difference in the overall ranges of the CO_2 emissions**. This suggests that the particular definitions of the ranges (Range 1-Range 4) have a relatively minor impact when probabilities are not weighted. In other words, the similarity in outcomes across the scenarios, indicates that the equal probability assumption leads to a similar distribution of results, regardless of the scenario specifics.

Scenario No.	OAT or Simultaneous	Number of Floors Value	CO_2 Factor Value	Distribution Type
5	OAT	Range 1: TUIK	Fixed at 400 kg CO_2eq/m^2	Weighted
6	OAT	Range 2: Antakya Field Work	Fixed at 400 kg CO_2eq/m^2	Weighted
7	OAT	Range 3: Combined Approach	Fixed at 400 kg CO_2eq/m^2	Weighted
8	OAT	Range 4: Arbitrary	Fixed at 400 kg CO_2eq/m^2	Weighted

Table 5.2: Scenarios where the CO_2 Factor is constant and the Number of Floors is varying

Scenario 5 to 8: Weighted Probabilities In this simulations, for each scenario, the selection of the number of floors within a given density category (*low, middle, or high*) was guided by the distributions outlined in Table 5.2. Then the same parallel plots were generated as shown in Figure 5.5.

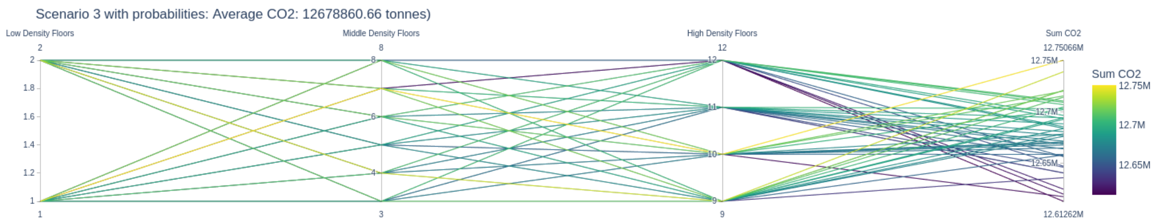

Figure 5.5: Range 3 - Combined Approach but with Weighted Probability

Key observation from the results of Figure 5.5 (and Figures A.17a, A.17b and A.17d)is that the **the incorporation of probability-weighted distributions significantly reduces the variability of the outcome (total CO_2 emissions)** compared to the previous simulations using equal probability distributions A.17). In this case, across all Scenarios, the final CO_2 output ranges between 12.6 and 13.9 million tonnes, a vast reduction from the earlier range of 10 to 20 million tonnes.

Second, the introduction of probabilities **does not result in a significant difference in the overall output across the selected scenarios (Scenarios 5 to 9)**. The most notable variation occurs between the combined approach (Range 3, Scenario 7) and the arbitrary selection (Range 4, Scenario 8), as shown in Figures A.17c and A.17d. Range 3 produces CO_2 outputs ranging between 12.6 and 12.7 million tonnes, while Scenario 4 ranges between 13.8 and 13.9 million tonnes. However, these differences remain within the expected range of uncertainty.

In summary, introducing probability-weighted distributions reduces the variability of CO_2 emissions across the scenarios.

CO_2 Factor This section presents the results of a Monte Carlo One-At-A-Time (OAT) analysis, where the Number of Floors is fixed (Low = 2, Medium = 5, High = 9) and the CO_2 Factor varies, as defined in Step 3. Due to limited information for each range, four distribution types were tested-uniform, normal, left-skewed, and right-skewed-.

Scenario No.	OAT or Simultaneous	Number of Floors Value	CO_2 Factor Value (kg CO_{2eq}/m^2)	Distribution Type
9-15	OAT	Low = 2, Middle = 5, High = 9	6 Boxplots & Broad Range	Random
16-23	OAT	Low = 2, Middle = 5, High = 9	6 Boxplots & Mixture & Broad Range	Normal
24-31	OAT	Low = 2, Middle = 5, High = 9	6 Boxplots & Mixture & Broad Range	Triangular - Left Skew
32-39	OAT	Low = 2, Middle = 5, High = 9	6 Boxplots & Mixture & Broad Range	Triangular - Right Skew

Table 5.3: Scenarios where the Number of Floors is constant and the CO_2 Factor is varying. All scenarios in detail can be found it table A.3

First, for the 8 different ranges, we used **uniform probability** to compare them. Uniform probability is the standard way when there is not additional information about the range (only the minimum and maximum values are know) as it is for this case study. The results for these scenarios (**Scenarios 9-15**), as shown in Figure A.18a.

However, a review of the literature indicates that many ranges exhibit overlap near their central values (Figure A.8), suggesting that the data may cluster around a mean. This pattern aligns with the assumptions of a **normal distribution**, where most values concentrate near the center, gradually decreasing in likelihood as they deviate from the mean. As such, for the same 8 ranges we compare then with a normal distribution(**Scenarios 16-23**), with results presented in Figure 5.6.

Given the possibility that the distribution may not be perfectly symmetrical, additional tests were conducted using **left-skewed and right-skewed triangular distributions** (**Scenarios 32-39**). These tests aimed to capture potential asymmetries in the data. The results of these tests are displayed in Figures A.18c and A.18b.

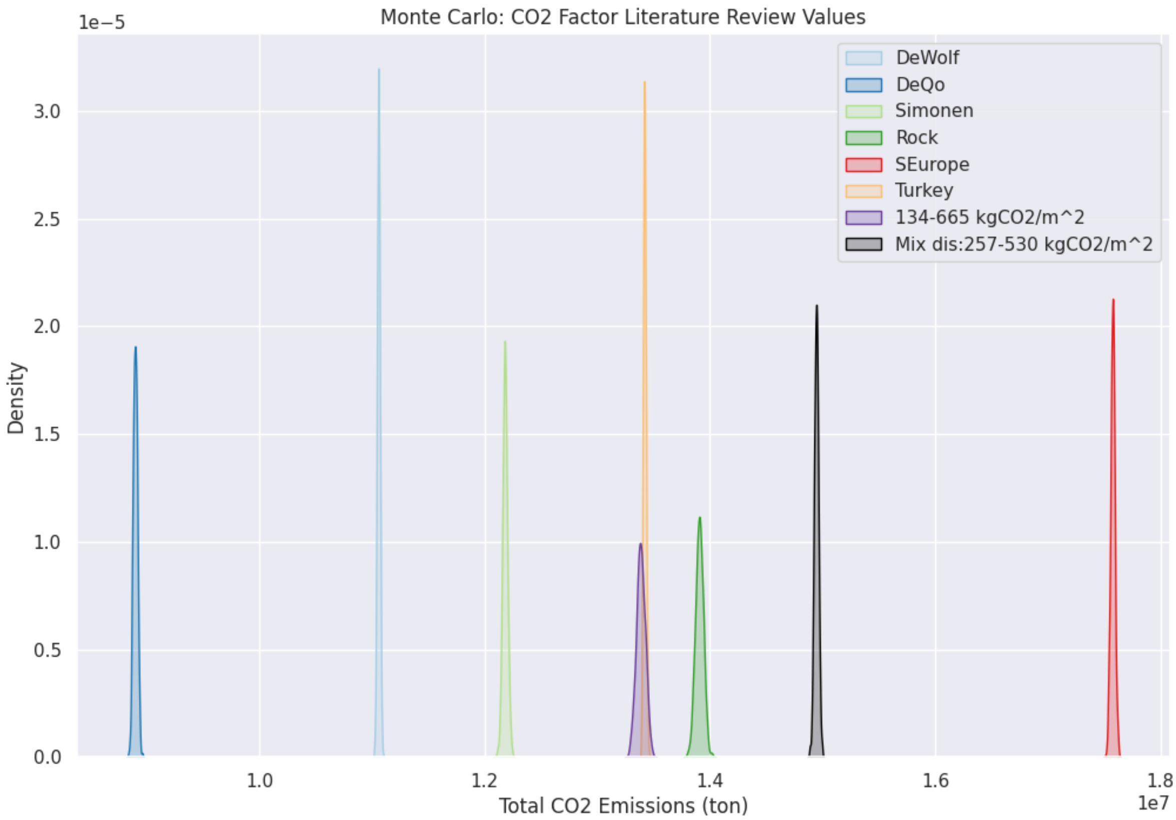

Figure 5.6: Monte Carlo Simulation with all the possible distributions

In Figure 5.6, along with Figures A.18a and A.18c, and A.18b each range of CO_2 factors consistently produces a narrow peak in the density plot of total emissions. This observation is significant, as it might seem intuitive to expect overlapping total emissions due to the overlap in CO_2 factor ranges themselves. However, the separation between emissions distributions remains clear. This effect results from the stabilizing influence of aggregating emissions over a large number of buildings and repeated simulations, which narrows the distribution of total emissions for each CO_2 factor range. This is explained in detail in section A.5.3.

5.4.2. Main Results: Monte Carlo Simultaneously

The next step focuses on the primary case where uncertainty in both key parameters, the number of floors and the CO_2 emission factor, is considered simultaneously. These scenarios differ from earlier simulations in two important ways.

Firstly, this is the only stage where both parameters vary simultaneously in the Monte Carlo simulations. Varying both together is computationally intensive, which is why this approach was not applied to all 41 ranges tested previously. Secondly, while the earlier simulations were designed to assess the individual influence of each parameter in isolation, this step tries to estimate a more realistic total emissions outcome, without caring about the individual contribution of each parameter to the final result.

As shown in Table 4.5 and Figure 4.10, the main results are drawn from two scenarios. In both, the number of floors is defined using Range 3, which applies a weighted distribution based on the *combined approach* data range. For the CO_2 factor, two distributions are considered: a broad range of 134650 kg CO_2eq/m^2 in Scenario 40, and a narrower, mixed distribution of 257530 kg CO_2eq/m^2 in Scenario 41.

The results from running again Monte Carlo for 1,000 simulations can be seen in Figures 5.7.

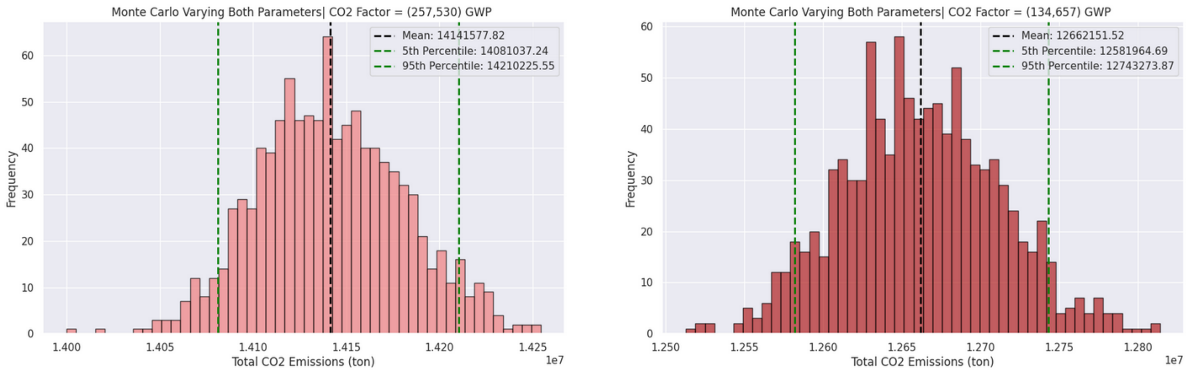

(a) Monte Carlo Results with CO_2 Factor varying based to the mixture distribution (257-530 kg CO_2/m^2)

(b) Monte Carlo Results with CO_2 Factor varying based to the broad distribution (134-650 kg CO_2/m^2)

Figure 5.7: Main Results from Monte Carlo Simulations with a variance in both of the parameters.

The results presented in Figure 5.7 provide the main estimation of the CO_2 emissions associated with the reconstruction of Antakya, incorporating the inherent uncertainties in both the CO_2 Factor and building density.

For each plot in Figure 5.7, we calculated the 90% interval that gave the ranges of (14.1, 14.2) and (12.6, 12.7) with units tons of CO_2. Combining them into one by taking the minimum and maximum value from both, we ended up with the range of (12.6,14.2) and has a mean value of 13.4 CO_2 tonnes. To put this figure into perspective, 13 million tonnes of CO_2 represent approximately 3% of Turkey's total annual emissions.

5.4.3. Sobol Sensitivity Analysis Results

To gain a deeper understanding of the uncertainty in CO_2 emissions calculations for the reconstruction of Antakya, a Sobol sensitivity analysis was conducted. Unlike the previous Monte Carlo One-At-A-Time (MC OAT) approach, which allowed us to observe the effect of each parameter on the final emissions outcome, the Sobol analysis provides insight into the relative influence of each parameter without producing a specific total emissions result. Instead, Sobol quantifies how much each parameter contributes to the overall variance in emissions.

The Sobol analysis was conducted with both parametersCO_2 factor and Number of Floorsallowed to vary. The CO_2 factor was tested across two distributions: the mixture range and a broad range. For the Number of Floors parameter, the Combined Approach (Range 3) was applied with an equal random distribution.
The results for the mixture range, shown in Figure 5.8 and detailed in Table 5.4.

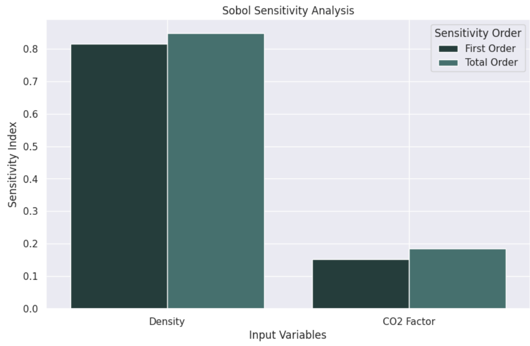

Metric	Number of Floors	CO_2 Factor	Interaction
ST	0.857	0.174	-
ST Confidence	0.067	0.017	-
S1	0.827	0.143	-
S1 Confidence	0.068	0.036	-
S2 (Interaction)	-	-	0.031
S2 Confidence	-	-	0.093

Table 5.4: Sensitivity indices (ST, S1, S2) and confidence intervals for each variable.

In the table 5.4 (or otherwise the results visualized in Figure 5.8), Number of Floors emerges as the dominant factor influencing the variance in total CO_2 emissions, with a total sensitivity index (ST) of 0.857. In other words, it means that Number of Floors parameter is responsible for 85.7% of the total variance in the output of a model. This is substantially higher than the CO_2 Factor, which has an ST of 0.174 [1].

The first-order sensitivity index (S1) closely aligns with the total sensitivity, indicating that the interaction between Number of Floors and the CO_2 Factor is minimal, as reflected by a low interaction term (0.031). Moreover, the narrow confidence intervals further confirm the robustness of these estimates, indicating that the sensitivity analysis results are reliable.

On the surface, these findings suggest that the density parameter overwhelmingly drives the output variance. However, this results seem to contradict with the results of the Monte Carlo simulations of One At a Time where also the influence of parameter's variation to the outcome's variation was examined (explained in detail in the Discussion section).

5.5. Social Cost of Carbon

This section presents the estimated Social Cost of Carbon (SCC) associated with the CO_2 emissions resulting from the reconstruction of Antakya. Based on Monte Carlo simulation results, the estimated CO_2 emissions fall within an uncertainty range of 12.6 to 14.2 million tonnes, with a mean value of 13.4 million tonnes.

As outlined in the methodology, a benchmark SCC value from Rennert 2022 is used to quantify the societal impact. **Applying this SCC value to the mean emissions estimate of 13.4 million tonnes leads to a total societal cost of approximately $2.37 billion**. In other words, the estimated long-term economic damages to society from the CO_2 emissions generated by the rebuilding process in Antakya amount to around $2.4 billion. For context, the total estimated cost of reconstruction following the Turkey-Syria earthquake (across all affected regions, not just Antakya) is roughly $100 billion.

It is important to emphasize, however, that the SCC is not a fixed value. It varies significantly depending on the underlying assumptions used in its calculation, including the choice of model, discount rate, and climate scenario. For a more detailed analysis that incorporates this uncertainty, refer to the alternative methodology presented in Appendix A.5.4. Moreover, the SCC serves as a tool for informing policy

[1] It must be noted that the ST doesnt need to add up to 1 because ST includes both the direct effects and the interaction effects of a variable. This is because some of the variance in the output might be accounted for by the interaction between multiple variables, leading to overlap in the contribution to variance, which can cause the sum of ST values to be greater than 1.

decisions, an estimation, it does not directly reflect the actual costs that individuals or businesses will bear.

5.6. Policy Pathways Evaluations

5.6.1. A. Policy Pathways: Using sustainable construction practices

As described in the Methodology section, additional Monte Carlo simulations were performed to evaluate the potential reduction in CO_2 emissions when incorporating lower-carbon construction methods.

Traditional construction is modeled using a CO_2 emission factor following a normal distribution between 134 and 655 kg CO_{2eq}/m^2.

In contrast, sustainable construction is represented using a narrower, lower range of 264290 kg CO_{2eq}/m^2, based on values derived from TOKI (Toplu Konut Idaresi) housing. TOKI housing projects, implemented by Turkeys Housing Development Administration, use prefabricated reinforced concrete and standardized designs. These methods enable faster construction, reduce material waste, and minimize emissions from transport and site workresulting in a lower embodied carbon footprint compared to conventional methods. While not a universal model for sustainability, the TOKI approach offers a documented example of low-emission construction that is planned for large-scale use in the Antakya reconstruction.

To explore its impact, three scenarios were modeled in which 15%, 30%, and 50% of buildings follow the lower TOKI-based emission factor, with the remainder following the baseline distribution.

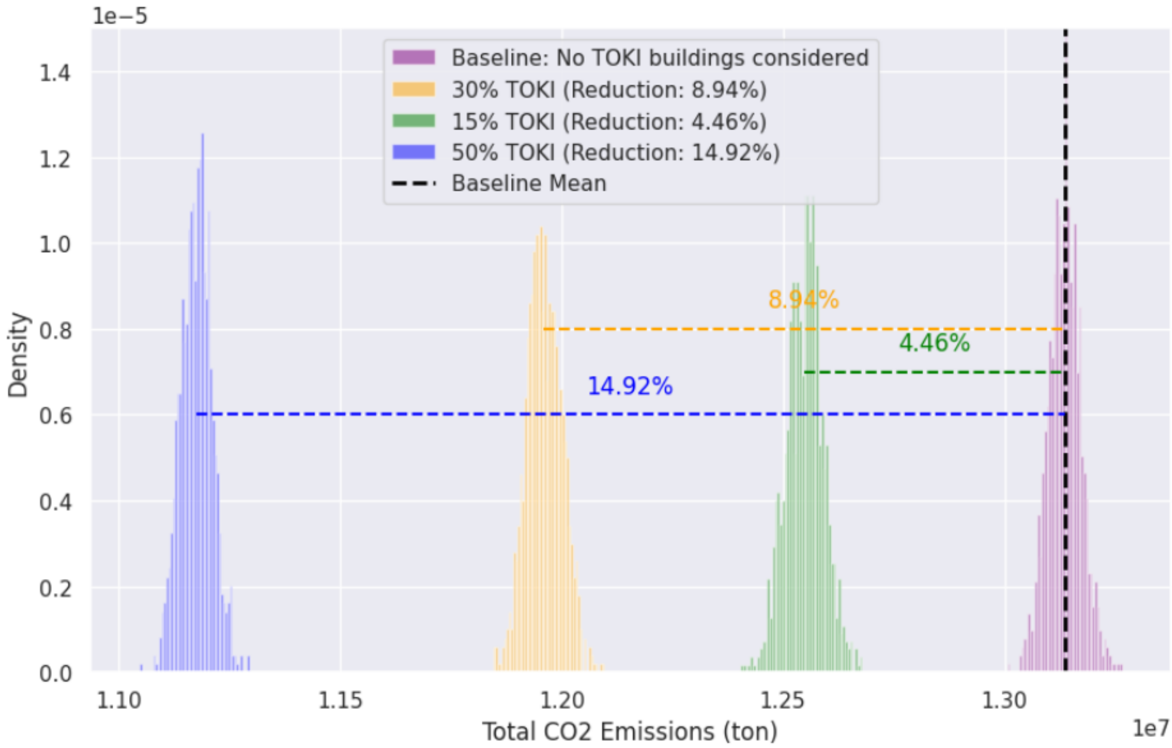

Figure 5.9: Total CO_2 emissions under different shares of sustainable/TOKI -based construction

The graph illustrates how different proportions of Sustainable/TOKI houses affect total CO_2 emissions during the construction phase. In the baseline scenario, shown in purple, where no TOKI buildings are considered, CO_2 emissions are at their highest, as expected, with the mean emissions being approximately 13.5 million ton of CO_2 (highlighted also by the dashed black line). When 15% of the buildings are TOKI houses (green), CO_2 emissions decrease by 4.46%, as indicated by the leftward shift in the density curve. Increasing the proportion to 30% (orange) results in an 8.94% reduction in emissions, with a more pronounced shift to the left. The most significant reduction, 14.92%, occurs when 50% of the buildings are TOKI houses (blue), showing the greatest leftward shift and the lowest CO_2 emissions.

These findings suggest that increasing the proportion of sustainable buildings, such as TOKI houses in the case of Antakya, could significantly reduce emissions. However, while this reduction is promising, it is essential to acknowledge the criticisms of TOKI buildings, which are usually perceived as lacking aesthetic diversity and disregarding Turkey's architectural heritage (Devrim 2016), a concern particularly relevant for Antakya, a city with significant historical and cultural value.

5.6.2. B. Policy Pathways: Energy-efficient vs traditional buildings

This section presents the results of the different policy pathways modeled to assess their impact on carbon emissions in post-disaster reconstruction. Various scenarios, including the use of sustainable technologies like PV panels, vertical-axis wind turbines, and green walls, are analyzed to determine how effectively they reduce operational emissions. These specific scenarios have been selected because the operational emissions of each scenario have been calculated for the specific area of Hatay, in the work of Saleh et al. 2024. The results focus on identifying the break-even point, where emissions savings from these measures outweigh the initial carbon cost of construction and are presented in Figure 5.10.

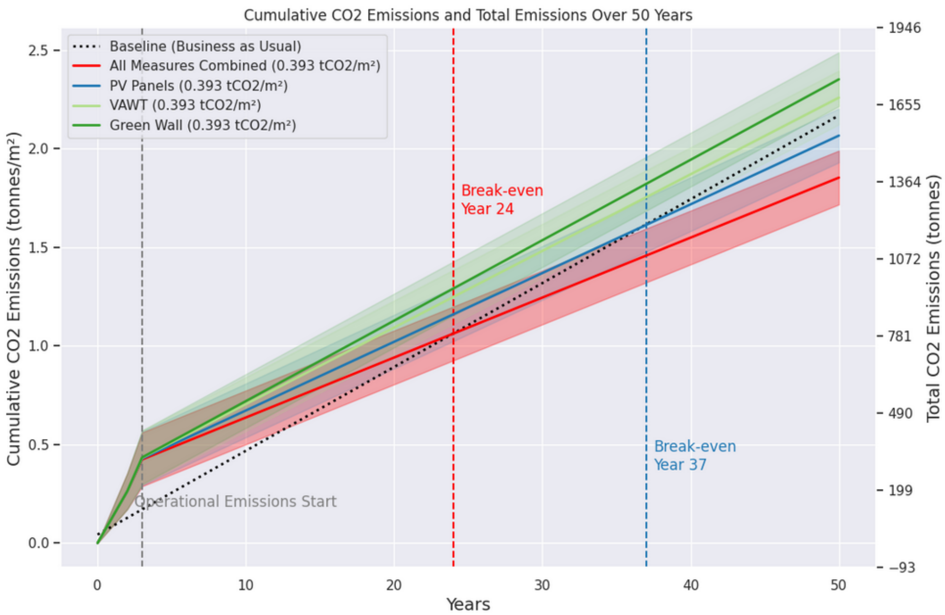

Figure 5.10: Break even point at 24 years with CO_2 Factor for construction equal to the mean value of 393 kg CO_2 eq/m^2 while showing the range for CO_2 factor from 257-530 kg CO_2 eq/m^2. The y-axis on the right shows the total tonnes of CO_2 for a building of a 5 multi-storey building of 745 m^2

In Figure 5.10, the shaded areas indicate the range of the CO_2 Factor, while the vertical lines mark the break point for the mean value of 393 kg CO_2 eq/m^2 (more details about the shade area for each scenario can be found in Figure A.24). In the figure, only two scenarios demonstrate a lower cumulative CO_2 impact compared to the baseline scenario over time.

PV Panels (Break-Even in 37 Years): In this scenario, where photovoltaic (PV) panels were integrated into the building, the break-even point was reached after 37 years. This indicates that the operational CO_2 savings generated by the PV system would offset the embodied emissions from construction after nearly four decades. The relatively long time frame reflects a gradual accumulation of savings, despite the reduction in annual emissions provided by the panels. However, this estimate is sensitive to assumptions about the lifespan and performance of PV technology. If panels are replaced earlier than expected, or if future technologies offer higher efficiency or lower embodied emissions, the actual break-even point could differ significantlyeither improving or worsening the outcome.

A better result is presented for the "**All Measures Combined (Break-Even in 24 Years)**", which combines all energy-saving measures -PV panels, Vertical-Axis Wind Turbines (VAWTs), and a green wall-and achieves a break-even point in 24 years. Although this scenario reaches break-even sooner than PV panels alone, it underscores that even with multiple energy-saving technologies, which collectively reduce emissions by nearly 30% over a 50-year period, it still takes a substantial amount of time to fully offset the initial emissions from construction. Additionally, as shown on the right y-axis in Figure 5.10, over a 50-year lifespan, a traditional building is projected to emit approximately 1,640 tonnes of CO_2 (mean value), whereas an energy-efficient building is estimated to emit about 1,365 tonnes (mean value).

However, we must note that the break even point is highly sensitive to the CO_2 factor. Further analysis in Figure 5.11 shows that under optimal conditions, with a low CO_2 construction factor, the break-even point can be achieved in as little as 13 years. In contrast, with a higher construction CO_2 factor of 530 kg CO_2 eq/m^2, the break-even is delayed to 36 years. This variation demonstrates the significant impact that the construction CO_2 factor has on overall emissions, despite being concentrated in only the initial two years of the building's life.

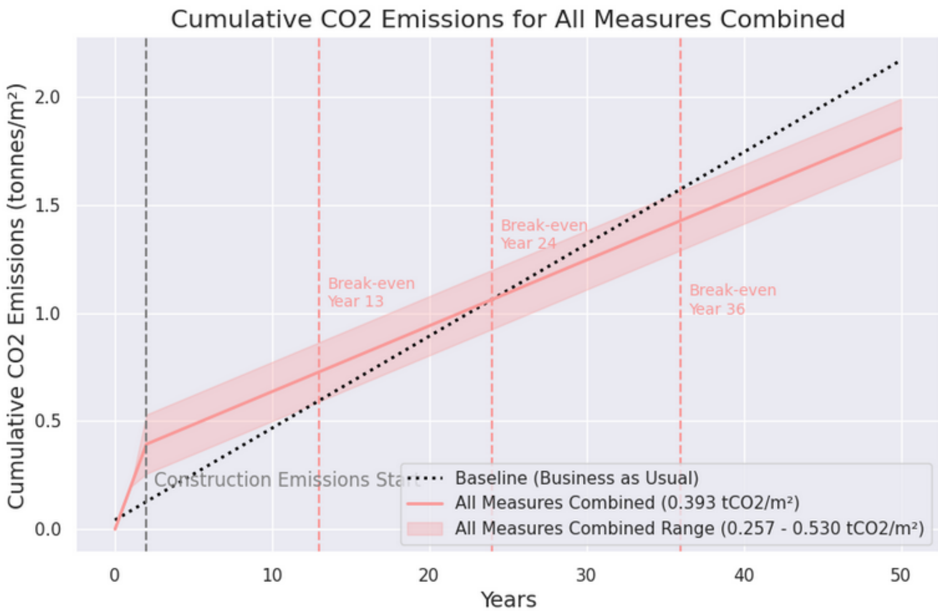

Figure 5.11: Break even point at 13, 24 and 36 years based on the minimum, mean and maximum value of the CO_2 Factor range.

6

Discussion

6.1. Key Findings

Total CO_2 Emissions The total emission for reconstructing Antakya will be **between 12.6 to 14.2 million tonnes of CO_2**. This result was calculated by using Monte Carlo Simulations, where both key parameters -Number of Floors and CO_2 Factor- were varied simultaneously (as shown in section 4.4.2).

To put this into perspective, this amount represents approximately **3% of Turkey's total annual CO_2 emissions** or it is equivalent to **emissions from about 3 million passenger vehicles driven for one year.** It is important to note that these figures pertain only to the reconstruction of Antakya (of approximately 38,000 residential buildings) and do not encompass the broader region affected by the earthquake. If we extend this analysis to estimate the carbon footprint of rebuilding efforts across Turkey, considering the need to reconstruct at least 500,000 buildings, the total CO_2 emissions respectively will range from 150 to 169 million tonnes, which would account for about 29.6% of Turkey's annual CO_2 emissions. This amount is approximately equal to the total annual carbon emissions of a country like Netherlands or Philippines (Crippa et al. 2022).

Social Cost of Carbon Quantifying CO_2 emissions from reconstruction serves not only as a numerical estimate but as a foundation for understanding the broader societal costs of these emissions. In this study, we applied the Social Cost of Carbon (SCC) framework to Antakyas reconstruction, estimating that rebuilding could impose societal costs of approximately \$ 2.4billion.

This figure underscores the practical relevance of incorporating carbon accounting into disaster recovery planning. It reveals that reconstruction, while necessary, carries a substantial environmental and economic burden that is often invisible in conventional cost assessments. These emissions represent a form of deferred societal costexternalized and spread over timewhich can no longer be ignored in light of global climate goals.

However, this analysis also brings to light a fundamental trade-off. On one hand, there is an urgent need to meet housing demand and restore infrastructure for affected communities. On the other, there is the long-term monetary and environmental cost associated with carbon emissions. Balancing these competing priorities is a key challenge for policymakers. Recognizing this tension does not mean halting reconstruction, but rather encourages strategies that can reduce emissionssuch as adopting low-carbon building materials, improving energy efficiency, or integrating sustainability into rebuilding plans.

Ultimately, integrating SCC into disaster recovery frameworks can help policymakers make more informed decisions by attaching a tangible economic value to carbon emissions. This allows for more holistic cost-benefit analyses and strengthens the case for sustainable reconstruction practices that protect both people and the climate.

Uncertainty Analysis In comparison with the few previous studies on the carbon footprint of post-disaster reconstruction, such as Pan et al. 2014, this thesis advances the methodology by incorporating uncertainty analysis. Here, parametric uncertainty analysis is central to the approach, providing not only greater confidence in the models outcomes but also a deeper understanding of the outcome's variation. Using both Monte Carlo OAT and Sobol Analysis, this study examined the impact of parameter uncertainty on the total emissions estimate.

A key insight concerns the *Number of Floors* parameter. The Hatay Municipality provided initial data on building density (low, medium, high) that was converted into number of floors by using transformation ranges. These ranges were defined in multiple ways, from using detailed, pre-earthquake distribution floors data to arbitrary estimates based on Google Maps street views. Surprisingly, despite this contrasting levels of precision, these methods yielded to similar estimates.
More importantly though, the output (total CO_2 emissions) varied widely, from 8.1 to 20.5 million tonnes. To address this sensitivity, we applied weighted probabilities, which substantially narrowed the emissions range between 12.6 and 13.9 million tonnes. Therefore, these findings suggest that uncertainty parameter is possible to be mitigated by applying weighted probabilities. However, the potential challenge is the availability of data for defining weighted probabilities , which may vary by case study. Usually though, some reliable statistics at the city, provincial, or national level, can be retrieved [1].

For the second uncertain parameter, the CO_2 Factor, eight distinct ranges were defined, analyzed, and compared using uniform, normal, and skewed probability distributions. Despite significant overlap among these CO_2 Factor ranges (Figure 4.9b), the Monte Carlo simulations produced outputs with narrowly distributed, bell-shaped histograms and low standard deviations (Figure 5.6). The underlying reason for this behavior is discussed in detail in Section A.5.3.
What is crucial to highlight here is that in scenarios where the total building area is substantial and remains relatively consistent across simulations, selecting a single CO_2 Factor may give the impression of low sensitivity to this parameter. However, when multiple CO_2 Factor ranges are plausible, precision becomes essential, as even small shifts in the parameter range can result in significant differences in emissions outcomes.

The results discussed above were obtained using Monte Carlo simulations with a One-At-A-Time (OAT) approach, supplemented by Sobol analysis for comparison. Sobol confirmed that no correlation between the parameters exists, but also revealed that Number of Floors accounted for 85.7% of the total variance in the model's output with the CO_2 Factor contributed only for the 17% of the total variance in the model's output.
This comes in contrast with the results of the MC OAT, where it was seen the sensitivity of the model to the range of the CO_2. This is because Sobol can only be applied with an equal random distribution across ranges, and the CO_2 Factor is restricted to a single range, something that as said already leads to small standard deviation. Therefore, while Sobol indicates that Number of Floors is the most influential parameter, this conclusion is true only when based on one singular range for the CO_2 Factor and a relatively loosely defined Density.

Sustainable Policy Pathways

Scenario of sustainable construction practices Through uncertainty analysis (Monte Carlo OAT of CO_2 Factor), it was possible to explore whether integrating sustainable construction methods could meaningfully reduce the total $\mathrm{CO_2}$ emissions associated with the reconstruction of Antakya. A simplified model was created to estimate how emissions change under different adoption rates of sustainable building practices.

The lower $\mathrm{CO_2}$ factor used in the sustainable scenarios (264-290 kg $\mathrm{CO_{2eq}}/m^2$) was selected based on a published empirical study by Kayaçetin and Tanyer 2020, which specifically measured the embodied emissions of TOKI (Toplu Konut Idaresi) housing. TOKI was chosen not because it represents an ideal form of sustainable development, but because it is a real, documented case with both available data and anticipated large-scale application in Antakyas post-earthquake reconstruction. This makes it a pragmatic reference point for modeling, particularly in the absence of more localized life-cycle assessments for alternative low-emission construction techniques.

[1] Please note that this approach assumes the reconstructed city will maintain a building density similar to that of the pre-disaster environment, whether at a local or broader scale.

The results demonstrate that increasing the proportion of buildings that are build following sustainable practices by 15%, 30%, and 50% can reduce CO_2 emissions by 4.46%, 8.94%, and 14.92%, respectively (5.9). This can be a significant reduction to the total CO_2 emissions that could potentially lead to a smaller environmental impact of this large scale disaster. However, this considered a very preliminary analysis, being mostly a **proof of usefulness** of the model, that shows how the environmental benefit of sustainable building practices can be crudely estimated.

Moreover, adopting TOKI houses as the sustainable model introduces a further dimension to the discussion: the intersection of sustainability with cultural and aesthetic considerations. TOKI housing is practical and cost-effective, making it a viable choice in large-scale, resource-constrained rebuilding efforts. Yet, TOKI buildings are frequently critiqued for their perceived lack of architectural diversity and for neglecting Turkeys cultural heritage (Devrim 2016).

In Antakya, a city known for its historical and cultural significance, the use of standardized TOKI-style buildings may accelerate reconstruction and lower carbon emissions, but at the potential cost of erasing it's architectural identity. This underscores the need to reconcile environmental performance with social and cultural values.

Scenario of energy-efficient vs traditional buildings Another approach to reducing the carbon impact of reconstructing focuses not on using sustainable construction practices, but on building energy-efficient houses. This analysis examines whether the initial CO_2 emissions from construction can eventually be offset by the reduced operational emissions of advanced, energy-efficient buildings. Section 5.6.2 explores this by applying a CO_2 Factor for construction ranging from 257 to 530 kg CO_2 eq/m^2 and using operational emission values from Nakamura et al. 2024.

By comparing a traditional five-story building with a new, energy-efficient building (offering a 30% reduction in operational emissions), the analysis shows that it will take an average of 24 years to offset the initial construction emissions, which are produced within just 2 years of construction.
Additionally, the payback period for offsetting these initial emissions varies significantly, ranging from 13 to 36 years, depending on the initial CO_2 (construction) Factor. If the average CO_2 (construction) Factor is around 250 kg CO_2 eq/m^2, the offset occurs in 13 years. However, if the average CO_2 (construction) Factor is around 530 kg CO_2 eq/m^2, the offset period extends to 36 years. This variability underscores the importance of addressing the initial carbon spike from construction.

Both of these findings are consistent with existing literature on the significance of the carbon spike in construction. Several studies emphasize the growing share of emissions released during the construction phase over a buildings lifespan Robati et al. 2019, such as Röck et al. 2020. For instance, Röck et al. 2020 shows that in specific cases, embodied emissions can account for up to 50% of total lifecycle emissions in energy-efficient buildings, while Pöyry et al. 2015 stresses that focusing solely on operational emissions underestimates the full climate impact of the built environment. Moreover, the aspect that construction emissions have a more direct and immediate impact on climate crisis than future emissions, is something that also needs to be taken into consideration when shaping policies.

6.2. Model Evaluation

The **primary purpose** of the model is to estimate the post disaster carbon emissions, in a real case study, using Monte Carlo simulations. It achieves this by combining three key parameters: Gross Floor Area, Number of Floors, and the CO_2 Factor. To account for uncertainty, the model allows inputs to be provided as either fixed values or ranges. These ranges, defined by the modeler, can be continuous or discrete, weighted or unweighted, and follow specific probability distributions or remain uniformly random. This flexibility makes the model **adaptable to various case studies**, enabling it to handle missing or uncertain data effectively.

While this adaptability is a strength, its value depends on whether the models results can be considered reliable. Reliability is closely tied to accuracy, but validating accuracy is inherently challenging. In practice, the true carbon emissions from reconstruction are unlikely to ever be calculated, making direct comparisons between the models output and actual values impossible. Nevertheless, the model compensates for this limitation by incorporating uncertainty analysis. With only three input parameters, it is feasible to assess the influence of each variable on the final output, providing **transparency and confidence in the results.**

However, while the model can handle uncertainty effectively, the quality of the results is closely tied to the quality of the input data (*garbage in - garbage out*). Limited or poorly defined data can significantly affect the precision of the outputs. This was evident with the *Number of Floors* parameter in Section 5.4.1. Initial data for this variable were poorly defined, resulting in emissions estimates ranging widely from 8 to 18 million tonnes of CO_2. Such a broad range is not particularly useful. It was only after incorporating complementary data to reduce the uncertainty in this parameter that the results became more precise and meaningful. This demonstrates that while the model can handle uncertainty, its effectiveness depends on the availability and quality of data to constrain that uncertainty. Therefore, to improve model accuracy, the use of better data-not necessarily more, but higher quality. For example, access to detailed floor plans or exact pre-disaster building heights would reduce the need for probabilistic assumptions. Similarly, localized, project-specific $\mathrm{CO_2}$ factors from regional LCA studies would improve precision over generalized literature values. These enhancements would reduce uncertainty and make the model outputs more actionable.

The computational cost also emerged as a practical challenge. While Monte Carlo simulations are effective for representing uncertainty, they are **time-intensive**. Running simulations where multiple parameters vary simultaneously required several hours per scenario. For example, running the full simulation set for the main resultswhere both parameters varytook between 7 and 8 hours on a standard machine. This can potentially be improved by using more focused method such as LHS that usually can produce similar results to Monte Carlo with fewer iterations, and hence greatly reducing computation time while maintaining variability.

The **ease of obtaining reliable data** varies across the three parameters. The CO_2 Factor is not typically provided directly but can often be derived from Life Cycle Assessment (LCA) studies. There is a plethora of LCA studies in the literature, offering emission factors for a wide range of materials and construction scenarios. While LCA methods face some criticism regarding that the methodology is not be standarise across literature (Source), they remain the main way for estimating building carbon footprints. For highly specific case studies, however, finding precise CO_2 Factor values may become challenging due to the peculiarities of the case study in the type of materials, climate, or construction practices used.
For *Gross Floor Area* and *Number of Floors*, the availability of data often depends on local sources such as governments, municipalities, or engineering firms. In the Antakya case study, data from the Hatay Municipality, though incomplete, were supplemented with broader sources like national statistics. Together, these sources produced reliable estimates. For large-scale disasters, which often affect extensive areas and populations, data collection is typically more robust. Technological advancements, such as high-resolution satellite imagery and AI-driven damage assessments, are also improving the precision and accessibility of data. By employing these tools, it becomes feasible to approximate the pre-disaster built environment and estimate reconstruction emissions effectively.

The model serves as a **practical tool for preliminary decision-making** in post-disaster reconstruction, offering transparent and straightforward estimates that are easily comprehensible to policymakers and stakeholders. Its simplicity ensures accessibility, enabling users to quickly understand how the results are derived. However, while the model provides a methodology for estimating the total CO_2 emissions caused by reconstruction, this alone is insufficient for shaping comprehensive policies. Effective policy development requires comparing various scenarios to evaluate the impact of different approaches on total emissions.

Although this thesis explores sustainable construction scenarios, the models limitations restrict its use to preliminary analyses. Key constraints, detailed in the section below, include oversimplification of construction processes, exclusion of parameter interdependencies, and the omission of critical factors such as cost and time constraints. While these estimates are basic and insufficient as standalone arguments, they provide a valuable starting point for identifying and evaluating promising policy pathways.

This narrow approach restricts its capacity to explore the nuanced impacts of different policy pathways on overall carbon emissions. However, the model's primary aim is to highlight the significance of CO_2 emissions in post-disaster reconstruction rather than delve into specific policy details. It serves as a preliminary step, providing a broad estimate of the potential scale of impact that sustainable practices could have (Röck et al. 2020). This approach underscores the urgency of considering carbon emissions but stops short of offering detailed guidance on how specific policies should be crafted or implemented to achieve emissions reductions.

The model is best suited for estimating CO_2 emissions and calculating the Social Cost of Carbon (SCC) with a level of confidence, which was the primary objective of the thesis. However, its application in policy comparison would require further development and refinement. The true value of the model lies in demonstrating how CO_2 emissions and uncertainty can be effectively combined to analyze real-world reconstruction scenarios. Its application to a case study shows how even with data gaps, meaningful insights can be generated, offering a practical framework to guide decision-making in similar large-scale projects.

6.3. Limitations

There are several limitations regarding the model. Firstly, there is an**oversight of Recycling and Waste Management** side of the situation. The model's CO_2 factor does not account for the potential reduction in emissions from recycling the vast amount of construction waste generated after a disaster. For example, in the case study of Antakya, the debris is estimated to be over 100 million cubic meters (or about 200 million tons). This volume, presents a significant opportunity for material reuse and recycling, which can considerably lower the embodied carbon in new construction materials. Recently, the United Nations Development Programme (UNDP) and the Ministry of Environment, Urbanization, and Climate Change (MoEUCC) have completed two model facilities for the safe processing and recycling of this debris (18 months after the disaster UNPD, Relief Web). Incorporating recycling practices could potentially lower the embodied carbon in new construction materials, but thorough research is necessary to understand up to what level.

In addition, by **consolidating various emission sources into a single CO_2 facto**r, the model simplifies complex interactions within the construction process. While this approach offers a practical estimate, it may overlook critical aspects such as the use of low-carbon materials, energy-efficient construction methods, and regional variations in material sourcing, all of which can significantly impact the overall carbon footprint. The model could potentially evolve in a way that include multiple ranges implemented in once to the model, based on specific assumptions about the embodied emissions or transportation of the materials.

The uncertainty inherent in the Social Cost of Carbon index also poses challenges. Another important limitation, emphasized in the results, is the complexity of defining the Social Cost of Carbon (SCC) and the variability in the monetary cost estimates it produces. While the model incorporates SCC to illustrate the long-term societal costs of carbon emissions, these estimates are highly sensitive to assumptions about future economic growth, technological advancements, and climate impacts. Even small changes in variables like the discount rate can lead to significant fluctuations in the results, making it challenging to assign a precise monetary value to reconstruction-related emissions.

The limitations of the model extend to **the way that energy-efficient buildings emissions were calculated**. While the model explores the use of energy-efficient buildings, it does not consider that constructing such buildings might initially involve a higher CO_2 factor due to the use of sophisticated materials and technologies (Röck et al. 2020). Moreover, the analysis focuses primarily on technologies like PV panels, VAWTs, and green walls, that the values of reduction of the operational emissions were derived only from one study (which was specifically looking though to a building in Antakya). In addition, the sustainability scenarios are evaluated as static snapshots without considering future advancements. Changes in building standards, material technologies, and the energy grid over time can significantly alter the operational emissions of buildings. For example, as the energy grid becomes greener, the operational emissions from buildings with renewable energy technologies may decrease more rapidly than anticipated. This dynamic aspect is not reflected in the current model. Lastly, covering other practices such as advanced insulation or smart energy management systems is necessary to be looked to have a holistic approach.

Finally, the models integration of s**ustainable reconstruction policies** is limited, as it **simplifies complex dynamics** by merely adjusting the CO_2 factor within predefined scenarios. It does not fully capture the complexities of policy implementation or the diverse benefits of emerging sustainable construction practices and materials science innovations. Moreover, the model overlooks the potential for increased CO_2 emissions resulting from the use of materials with higher embodied energy in sustainable buildings (Giordano et al. 2015).

7

Conclusions

7.1. Research questions

7.1.1. Sub-questions

What are the primary factors necessary to consider in the environmental assessment of the carbon, and how the uncertainties associated with these factors, influence the final estimates?

In the environmental assessment, total emissions were calculated using three primary parameters: Gross Floor Area (GFA), Number of Floors, and the CO_2 Factor, each contributing to the final outcome with varying degrees of uncertainty.

Gross Floor Area (GFA) represents the total floor space to be reconstructed. As in this thesis, detailed data were provided, no uncertainty analysis was performed to see how it will influence the outcome. However, in other case-studies, incomplete data or discrepancies between planned and actual reconstruction could introduce uncertainty to that parameter.

Secondly the **Number of Floors** parameter shows how many floors each building will be, and when multiplied with the GFA gives the total reconstructed area. For Antakya's case, specific values for floors were unavailable, and density categories (low, medium, high) were provided instead. Hence having limited information about this parameter, and transforming it to quantitative ranges, the study revealed significant sensitivity to this variable. More specifically, loosely defined ranges (*meaning for example low density can be 1 or 2 floors*) caused wide variability in emissions estimates (8.1 to 20.5 million tonnes). However, this can be mitigated when applying weighted probabilities (*low density will be 60% more likely 1 floor than 2 floors*). Applying weighted probabilities reduced the outcome's range to be only between 12.6 to 13.9 million tonnes.

Lastly, the third parameter was the CO_2 **Factor**, defined as how much carbon is emitted per square meter of building constructed. The influence of the CO_2 Factor on the outcome is complex. When defined as a single range, it has minimal influence to the outcome. However, the situation changes when multiple ranges are introduced. Monte Carlo simulations (OAT) revealed that slightly different factor distributions could result in distinct CO_2 total emissions results, even when ranges overlap largely. This sensitivity becomes critical in large datasets, where the CO_2 Factor's influence to the result can rival that of the Number of Floors.

How can the carbon footprint of post-disaster reconstruction efforts be calculated for the case study in Antakya?

The carbon footprint of post-disaster reconstruction in Antakya was calculated using the three mentioned parameters: Gross Floor Area (GFA), Number of Floors, and the CO_2 Factor. Gross Floor Area was treated as fixed parameter, derived from the spatial data provided by the Hatay Metropolitan Municipality. For Density, the spatial data provided information regarding the percentage of building with the categorical value of low, medium, and high and hence there was uncertainty to convert these values to number of floors. For each category, a discrete range of values was assigned. The CO_2 Factor, representing the carbon emissions per square meter, was extracted from a comprehensive review of Life Cycle Assessment studies, considering mainly two ranges: a broad range (134-655 kg CO_2 eq/m^2) and a narrower range (257-530 kg CO_2 eq/m^2), while also the CO_2 Factor for the studies of Antakya is considered.

The combination of these parameters was used to estimate total emissions through Monte Carlo simulations, capturing uncertainties in Number of Floors and CO_2 Factor. The calculated emissions ranged between 12.6 and 14.2 million tonnes of CO_2, with a mean value of 13.4 million tonnes. The implementation of this framework in Antakya demonstrates its applicability and utility of the model. Moreover, uncertainty analysis for the case study showed that it can handle limited data, and produce results that are reliable and practical. Therefore, this indicate that the developed framework's could be useful for similar reconstruction projects.

What are the societal and environmental implications of the carbon emissions generated by post-disaster reconstruction efforts - for the case study of Antakya-?

Environmentally, the additional CO_2 emissions into the atmosphere exacerbate the greenhouse effect, contributing to global warming. This, in turn, leads to more frequent and severe climate-related disasters, such as floods, hurricanes, and wildfires. The emissions generated during reconstruction, whether from material production, transportation, or construction processes, create a reinforcing loop: as climate change drives more disasters, the need for reconstruction grows, thereby increasing emissions further. In the case of Antakya,the reconstruction efforts are estimated to add between 12.6-14.2 million tonnes of CO_2 to the atmosphere.

These emissions carry also **societal implications**[1]. By taking a standard value for the SCC -even though that can range widely- these emissions could result in societal costs of approximately $2.4 billion. These costs represent long-term economic damages, including environmental degradation, health impacts, and climate-related disruptions. While essential for recovery, such emissions highlight the hidden burden borne by society. Integrating these costs into disaster management discussion, could potentially emphasize the need for sustainable and climate-resilient rebuilding strategies to support both environmental and societal well-being.

How following different policy pathways for housing can reduce the total carbon footprint of new constructed houses?

This thesis explored two key pathways: incorporating sustainable construction practices and promoting energy-efficient building technologies.

The first approach examined the potential impact of adopting sustainable construction practices.[2] Scenarios were analyzed where 15%, 30%, and 50% of houses were built sustainably. For Antakya, the results showed that total CO_2 emissions could be reduced by 4.46%, 8.94%, and 14.92%, respectively. Therefore, this policy could offer considerable reductions in emissions during the construction phase, directly addressing the carbon footprint at its source.

The second approach evaluated the long-term benefits of constructing energy-efficient homes compared to the previous existing "traditional designs". By incorporating technologies that reduce operational emissions by up to 30%, the analysis found that these energy-efficient buildings could offset their initial construction emissions over an average of 24 years. Notably, the "offset" period varies widely from 13 to 36 years (see Figure 5.10), based on initial construction emissions -produced within just two years. Overall it showed that it is indeed possible to offset the construction emissions but is massively depend on the construction factor.

[1] With societal impacts, we consider the effects on human health, economic stability, and social welfare from the released of additional carbon into the atmosphere.

[2] Examples of sustainable practices considered are summarized in Table X. Options X-X2 and X will be translated to the model as a lower CO_2 factor.

These scenarios provide a preliminary understanding of sustainable reconstruction policies, serving as indicators of promising options rather than standalone decision-making tools. While they highlight the most viable approaches, further research is needed to fully assess and optimize their impact.

7.1.2. Main Research Question

How do large scale post disaster reconstruction efforts, such as those in Antakya, Turkey, impact carbon emissions?

Large-scale post-disaster reconstruction can significantly impact carbon emissions, creating a sharp and concentrated carbon spike over a short timeframe. Reconstruction activities primarily rely on materials like concrete and steel, which are energy-intensive to produce and transport. This results in embodied emissions that are released predominantly during the initial two-three years of rebuilding, making this period a critical contributor to the overall environmental burden of the disaster.

In the case of Antakya, where approximately 38,000 buildings are being reconstructed, the emissions are estimated to range between 12.6 and 14.2 million tonnes of CO_2, equivalent to the annual emissions of countries like Slovenia, Lithuania and Puerto Rico. The emissions generated also highlight a climate feedback loop, where reconstruction efforts contribute to global warming, intensifying climate-related disasters that, in turn, necessitate further reconstruction and emissions. Although the Antakya earthquake was not climate-induced, its emissions mirror the pattern seen in climate-related disasters, emphasizing the inter-connectedness of reconstruction and climate change.

Overall, large-scale post-disaster reconstruction efforts significantly contribute to carbon emissions due to the rapid consumption of energy-intensive materials and resources needed for rebuilding. The Antakya case clearly illustrates the magnitude of this impact. When we quantify the emissions, we find that those generated by a single cityjust one part of the affected regioncan rival the annual emissions of entire small countries, thereby exacerbating climate change and its consequences.

7.2. Contribution

This thesis was motivated by the observation that little research has examined the environmental impacts of large-scale reconstruction projects completed in a short time frame. To address this gap, a method was developed to estimate the carbon emissions associated with such efforts, incorporating the inherent uncertainties due to limitations in the available data. This method was applied in a real-world context through a case study in Antakya, Turkey.

The study quantifies the emissions from rebuilding approximately 38,000 buildings, estimating them to be comparable to the emissions of 3 million cars. Additionally, the social cost of these emissions is calculated at around $1 billion, -based on a moderate estimation-, highlighting the significant societal burden of reconstruction activities. By providing a measurable assessment of the environmental impact of reconstruction, this study shifts the discussion of *what is the environmental impact of reconstruction*, from vague assumptions to a tangible, specific value. These values serve as a foundation for targeted policy interventions, aligning with the principle that *"you cannot reduce what you do not measure."*

7.3. Policy Implications

The findings highlight the significant environmental impact of reconstruction and its role in the climate feedback loop, where disasters lead to rebuilding, generating emissions that exacerbate climate change. By quantifying emissions from Antakya's reconstruction, this study underscores the importance of integrating measurable environmental considerations into recovery planning. Policymakers can utilize the proposed framework to advocate for sustainable practices, including low-carbon materials, debris recycling, and energy-efficient construction methods. The results also emphasize the necessity of resilient urban planning and disaster prevention strategies to reduce the need for future large-scale rebuilding. By providing a concrete estimate of reconstruction emissions, the study draws attention to the often-overlooked environmental consequences of disaster recovery, which are becoming increasingly critical as climate -and conflict- related reconstruction increase.

7.4. Further Research

Incorporating Waste Disposal and Recycling The Turkey-Syria earthquake generated over 100 million cubic meters of debris from collapsed buildings, representing a substantial source of recyclable materials. Recently, facilities have been established by the UNDP and the Ministry of Environment, Urbanization, and Climate Change to recycle this material UNPD, Relief Web). However, the model developed in this thesis does not account for the potential reductions in CO_2 emissions from reusing debris materials.
Future research should focus on developing a systematic approach to incorporate recycling scenarios into the model. This would allow for a comparative assessment of emissions with and without recycling practices, quantifying the potential environmental benefits of integrating these methods into reconstruction workflows. By addressing this gap, future work could enhance the models capacity to provide a more accurate and comprehensive evaluation of the environmental impacts of post-disaster reconstruction.

Break-down of the CO_2 Factor In addition, further research could explore the relationship between building height and the CO_2 factor, as high-rise buildings may exhibit different emissions profiles compared to low-rise structures due to economies of scale in material usage and construction practices. This analysis would offer a more nuanced understanding of how design choices, such as the number of floors, influence emissions. Moreover, the CO_2 factor could be refined by breaking it down into distinct values for each phase of construction, aligned with the A1-A5 stages in Life Cycle Assessment (LCA). This would involve separately accounting for emissions from material production (A1-A3), transportation (A4), and construction processes (A5). To achieve this, region-specific LCA data would need to be collected, capturing local variations in material sourcing, transportation distances, and construction methods. While such an approach would enhance the precision and granularity of the model, it would also introduce additional complexity and uncertainty due to the high data requirements.

Integrating SCC into Cost-Benefit Analysis The model could be expanded to include the Social Cost of Carbon (SCC) within a cost-benefit analysis. This would involve comparing the emissions and costs of different construction scenarios, such as a baseline reconstruction approach versus a sustainable alternative. By assigning a monetary value to emissions in each scenario, alongside the construction costs, policymakers could better understand the trade-offs involved. This comparison would help highlight the economic and societal advantages of sustainable reconstruction, providing a clearer picture of both immediate and future costs and benefits. Such an addition would make the model more practical for decision-making and policy development.

Bibliography

Eastern caribbean: Hurricane beryl - situation report no. 01, 2024. URL https://reliefweb.int/report/grenada/eastern-caribbean-hurricane-beryl-situation-report-no-01-7-july-2024. Accessed: 2024-12-03.

Adolf A Acquaye and Aidan P Duffy. Input–output analysis of irish construction sector greenhouse gas emissions. *Building and Environment*, 45(3):784–791, 2010.

Sirwan Khalid Ahmed, Deepak Chandran, Safin Hussein, Praveen SV, Sandip Chakraborty, Md. Rabiul Islam, and Kuldeep Dhama. Environmental health risks after the 2023 turkey-syria earthquake and salient mitigating strategies: A critical appraisal. *Environmental Health Insights*, 17, January 2023. ISSN 1178-6302. doi: 10.1177/11786302231200865. URL http://dx.doi.org/10.1177/11786302231200865.

Aawag Mohsen Alawag, Wesam Salah Alaloul, Baker Nasser Saleh Al-dhawi, Abdullah O Baarimah, Mahmood A Bazel, and Ahmed W Mushtaha. A review and bibliometric analysis of blockchain adoption within the context of smart construction projects. In *2024 ASU International Conference in Emerging Technologies for Sustainability and Intelligent Systems (ICETSIS)*, pages 805–811. IEEE, 2024.

Abdullatif Ali and Monjur Mourshed. A comprehensive analysis of container vs prefabricated emergency shelters for post-disaster reconstruction in damascus. *Napier Repository*, 2021. URL https://napier-repository.worktribe.com/output/3469493/a-comprehensive-analysis-of-container-vs-prefabricated-emergency-shelters-for-post-disaster-recon
Accessed: 2024-12-06.

Anders-Johan Almas and Hans Hygen. Impacts of sea level rise towards 2100 on buildings in norway. *Building Research and Information - BUILDING RES INFORM*, 40:245–259, 06 2012. doi: 10.1080/09613218.2012.690953.

Chirjiv Kaur Anand and Ben Amor. Recent developments, future challenges and new research directions in lca of buildings: A critical review. *Renewable and Sustainable Energy Reviews*, 67:408–416, 2017. ISSN 1364-0321. doi: https://doi.org/10.1016/j.rser.2016.09.058. URL https://www.sciencedirect.com/science/article/pii/S1364032116305524.

Adem Atmaca and Nihat Atmaca. Life cycle energy (lcea) and carbon dioxide emissions (lcco2a) assessment of two residential buildings in gaziantep, turkey. *Energy and Buildings*, 102:417431, September 2015. ISSN 0378-7788. doi: 10.1016/j.enbuild.2015.06.008. URL http://dx.doi.org/10.1016/j.enbuild.2015.06.008.

Adem Atmaca and Nihat Atmaca. Carbon footprint assessment of residential buildings, a review and a case study in turkey. *Journal of Cleaner Production*, 340:130691, March 2022. ISSN 0959-6526. doi: 10.1016/j.jclepro.2022.130691. URL http://dx.doi.org/10.1016/j.jclepro.2022.130691.

Nihat Atmaca. Life-cycle assessment of post-disaster temporary housing. *Building Research & Information*, 45(5):524–538, 2017. doi: 10.1080/09613218.2015.1127116. URL https://doi.org/10.1080/09613218.2015.1127116.

Abdullah O. Baarimah, Wesam Salah Alaloul, M. S. Liew, Aawag Mohsen Alawag, Muhammad Ali Musarat, and Khalid Mhmoud Alzubi. Current state of post-disaster reconstruction projects: A bibliometric analysis. In *2021 International Conference on Decision Aid Sciences and Application (DASA)*, pages 108–113, 2021. doi: 10.1109/DASA53625.2021.9682326.

Joana Bastos, Stuart A. Batterman, and Fausto Freire. Life-cycle energy and greenhouse gas analysis of three building types in a residential area in lisbon. *Energy and Buildings*, 69:344353, February

2014. ISSN 0378-7788. doi: 10.1016/j.enbuild.2013.11.010. URL http://dx.doi.org/10.1016/j.enbuild.2013.11.010.

W. Becker, J.E. Oakley, C. Surace, and P. Gili. Bayesian sensitivity analysis of a nonlinear finite element model. *Mechanical Systems and Signal Processing*, 30:1–15, 2012. URL https://www.sciencedirect.com/science/article/pii/S0888327012000866.

Patrick Bigger Linsey Cottrell Benjamin Neimark, Frederick Otu-Larbi. A multitemporal snapshot of greenhouse gas emissions from the israel-gaza conflict [updated pre-print]. 2024. URL http://dx.doi.org/10.2139/ssrn.4855947.

Melissa M Bilec, Robert J Ries, and H Scott Matthews. Life-cycle assessment modeling of construction processes for buildings. *Journal of infrastructure systems*, 16(3):199–205, 2010.

Hao Cai, Xinyi Wang, Ji-Hyun Kim, Arathi Gowda, Michael Wang, John Mlade, Scott Farbman, and Luke Leung. Whole-building life-cycle analysis with a new greető tool: Embodied greenhouse gas emissions and payback period of a leed-certified library. *Building and Environment*, 209:108664, February 2022. ISSN 0360-1323. doi: 10.1016/j.buildenv.2021.108664. URL http://dx.doi.org/10.1016/j.buildenv.2021.108664.

Panagiotis Chastas, Theodoros Theodosiou, and Dimitrios Bikas. Embodied energy in residential buildings-towards the nearly zero energy building: A literature review. *Building and environment*, 105:267–282, 2016.

Ara Cho. Post-tsunami recovery and reconstruction: governance issues and implications of the great east japan earthquake. *Disasters*, 38(s2):s157–s178, 2014.

Lo S. L. Chung, W. H. A comparative analysis of the impacts of different waste management strategies on carbon footprint and costs in construction industry. *Waste Management*, 69:66–75, 2017. doi: 10.1016/j.wasman.2017.08.015. URL https://www.sciencedirect.com/science/article/pii/S0956053X17306220?casa_token=aIjlxwJ-VtQAAAAA:Ayqm8E1OwOPemKv4Vi5ZT9_O2fuDDg8K09HL_zzJETlofOCFUmMV72b8VGRKJH01ZdBcfd7Bz2I.

Robert Crawford. *Life cycle assessment in the built environment*. Routledge, 2011.

M. Crippa, D. Guizzardi, M. Banja, E. Solazzo, M. Muntean, E. Schaaf, F. Pagani, F. Monforti-Ferrario, J. Olivier, R. Quadrelli, A. Risquez Martin, P. Taghavi-Moharamli, G. Grassi, S. Rossi, D. Jacome Felix Oom, A. Branco, J. San-Miguel-Ayanz, and E. Vignati. *CO2 emissions of all world countries - JRC/IEA/PBL 2022 Report*. EUR 31182 EN. Publications Office of the European Union, Luxembourg, 2022. doi: 10.2760/730164.

N Crishna, PFG Banfill, and S Goodsir. Embodied energy and co2 in uk dimension stone. *Resources, Conservation and Recycling*, 55(12):1265–1273, 2011.

William Dalrymple. *From the Holy Mountain: A Journey in the Shadow of Byzantium*. HarperCollins, 1997. URL https://www.abebooks.com/Church-St-Peter-Antioch-Dalrymple-William/22750228035/bd.

Catherine De Wolf, Frances Yang, Duncan Cox, Andrea Charlson, Amy Seif Hattan, and John Ochsendorf. Material quantities and embodied carbon dioxide in structures. *Proceedings of the Institution of Civil Engineers - Engineering Sustainability*, September 2015. ISSN 1751-7680. doi: 10.1680/jensu.15.00033. URL http://dx.doi.org/10.1680/jensu.15.00033.

Armen Der Kiureghian and Ove Ditlevsen. Aleatory or epistemic? does it matter? *Structural Safety*, 31(2):105–112, 2009. URL https://ascelibrary.org/doi/10.1061/%28ASCE%29EM.1943-7889.0000025.

Ilgim Asli Devrim. Housing policies in turkey: evolution of toki (governmental mass housing administration) as an urban design tool. *Journal of Civil Engineering and Architecture*, 10(3):284–294, 2016. doi: 10.17265/1934-7359/2016.03.006. URL http://dx.doi.org/10.17265/1934-7359/2016.03.006.

Shobhakar Dhakal. Ghg emissions from urbanization and opportunities for urban carbon mitigation. *Current Opinion in Environmental Sustainability*, 2(4):277–283, 2010.

Manish K Dixit, Jose L Fernández-Solís, Sarel Lavy, and Charles H Culp. Need for an embodied energy measurement protocol for buildings: A review paper. *Renewable and sustainable energy reviews*, 16 (6):3730–3743, 2012.

EU. Directive 2010/31. *Off. J. Eur. Union*, 53:13–35, 2010.

European Commission, Joint Research Centre. *ILCD Handbook: General Guide for Life Cycle Assessment - Detailed Guidance*. Luxembourg, 2010. URL https://eplca.jrc.ec.europa.eu/uploads/ILCD-Handbook-General-guide-for-LCA-DETAILED-GUIDANCE-12March2010-ISBN-fin-v1.0-EN.pdf. ISBN: 978-92-79-19092-6.

World Economic Forum. How cement production is being made more sustainable to cut co2 emissions, 2024. URL https://www.weforum.org/stories/2024/09/cement-production-sustainable-concrete-co2-emissions/. Accessed: 2024-11-02.

Daniel Félix, Jorge M. Branco, and Artur Feio. Temporary housing after disasters: A state of the art survey. *Habitat International*, 40:136–141, 2013. ISSN 0197-3975. doi: https://doi.org/10.1016/j.habitatint.2013.03.006. URL https://www.sciencedirect.com/science/article/pii/S0197397513000386.

Tatiana García-Segura, Víctor Yepes, and Julián Alcalá. Life cycle greenhouse gas emissions of blended cement concrete including carbonation and durability. *The International Journal of Life Cycle Assessment*, 19:3–12, 2014.

Pedro Lima Gaspar and António Lobato Santos. Embodied energy on refurbishment vs. demolition: A southern europe case study. *Energy and Buildings*, 87:386–394, 2015.

Roberto Giordano, Valentina Serra, Elisa Tortalla, Veronica Valentini, and Chiara Aghemo. Embodied energy and operational energy assessment in the framework of nearly zero energy building and building energy rating. *Energy Procedia*, 78:3204–3209, 2015. ISSN 1876-6102. doi: https://doi.org/10.1016/j.egypro.2015.11.781. URL https://www.sciencedirect.com/science/article/pii/S1876610215025138. 6th International Building Physics Conference, IBPC 2015.

Jun Guan, Zhihui Zhang, and Chenglong Chu. Quantification of building embodied energy in china using an input–output-based hybrid lca model. *Energy and Buildings*, 110:443–452, 2016.

Marjolijn Haasnoot. White paper uncertainty analysis and decision-making under uncertainty with the deltamodel white paper uncertainty analysis and decision- making under uncertainty with the deltamodel. 2011. URL https://api.semanticscholar.org/CorpusID:195815242.

Sarkar B. Tayyab M. W. Saleem M. W. Habib, M. S. Large-scale disaster waste management under uncertain environment. *Journal of Cleaner Production*, 2019. URL https://www.sciencedirect.com/science/article/pii/S0959652618335571?casa_token=oXwJzEEee98AAAAA:xVRgQZ9M86v8MowMGT7QwRGjWAPy1ZtuhxCpM1s-LZ957awah1wq3ZTFuwB66CVkpbyTPJeJ4o.

Hatay Metropolitan Municipality. Reports - hatay metropolitan municipality, 2024. URL https://hatay.bel.tr/en/page/reports. Accessed: 2025-03-24.

Mathew E Hauer, Jason M Evans, and Deepak R Mishra. Millions projected to be at risk from sea-level rise in the continental united states. *Nature Climate Change*, 6(7):691–695, 2016.

Jon C Helton and F J Davis. Latin hypercube sampling and the propagation of uncertainty in analyses of complex systems. *Reliability Engineering & System Safety*, 81(1):23–69, 2003. URL https://www.sciencedirect.com/science/article/pii/S0951832003000020.

Chris T Hendrickson, Lester B Lave, and H Scott Matthews. *Environmental life cycle assessment of goods and services: an input-output approach*. Routledge, 2010.

T. Hong, M. Jang, and C. Ji. Hybrid lca model for assessing the embodied environmental impacts of buildings in south korea. *Environmental Impact Assessment Review*, 2015.

N. Huberman and D. Pearlmutter. A life-cycle energy analysis of building materials in the negev desert. *Energy and Buildings*, 40(5):837–848, 2008. ISSN 0378-7788. doi: https://doi.org/10.1016/j.enbuild.2007.06.002. URL https://www.sciencedirect.com/science/article/pii/S0378778807001776.

Taofeeq Ibn-Mohammed, Rick Greenough, S Taylor, Leticia Ozawa-Meida, and Adolf Acquaye. Operational vs. embodied emissions in buildingsa review of current trends. *Energy and Buildings*, 66: 232–245, 2013.

UNEP IEA. Global status report for buildings and construction 2019. *UN Enviroment programme*, 224, 2019.

Francesca Intini and Silvana Kühtz. Recycling in buildings: an lca case study of a thermal insulation panel made of polyester fiber, recycled from post-consumer pet bottles. *The international journal of life cycle assessment*, 16:306–315, 2011.

Dzulkarnaen Ismail, Taksiah A Majid, Ruhizal Roosli, and Noorazam Ab Samah. Project management success for post-disaster reconstruction projects: International ngos perspectives. *Procedia Economics and Finance*, 18:120–127, 2014.

ISO14040 ISO. 14040. *Environmental managementlife cycle assessmentprinciples and framework*, 578: 235–248, 2006.

H. Janssen. Monte-carlo based uncertainty analysis: Sampling efficiency and sampling convergence. *Reliability Engineering & System Safety*, 109:123–132, 2013. URL https://www.sciencedirect.com/science/article/pii/S0951832012001536.

Laurie A. Johnson and Robert B. Olshansky. *After Great Disasters: How Six Countries Managed Community Recovery*. Lincoln Institute of Land Policy, 2016. URL https://www.lincolninst.edu/app/uploads/legacy-files/pubfiles/after-great-disasters-full_0.pdf. Accessed: 2024-12-21.

Noah Kaufman, Alexander R Barron, Wojciech Krawczyk, Peter Marsters, and Haewon McJeon. A near-term to net zero alternative to the social cost of carbon for setting carbon prices. *Nature Climate Change*, 10(11):1010–1014, 2020.

N.C. Kayaçetin and A.M. Tanyer. Embodied carbon assessment of residential housing at urban scale. *Renewable and Sustainable Energy Reviews*, 117:109470, January 2020. ISSN 1364-0321. doi: 10.1016/j.rser.2019.109470. URL http://dx.doi.org/10.1016/j.rser.2019.109470.

M. Kuittinen. *Carbon Footprint in Humanitarian Construction*. Aalto University, 2016. ISBN 978-952-60-6713-1.

P Lemke, J.F. Ren, R Alley, Ian Allison, Jorge Carrasco, Gregory Flato, Y Fujii, Georg Kaser, Philip Mote, R Thomas, and Tingjun Zhang. Ipcc, 2007. climate change 2007. synthesis report. contribution of working groups i, ii, iii to the fourth assessment report of the intergovernmental panel on climate change. geneva. *IPCC.*, 01 2007. doi: 10.1017/CBO9780511546013.

Wassily Leontief. Environmental repercussions and the economic structure: an input-output approach. In *Green Accounting*, pages 385–394. Routledge, 2018.

C. Liang and S. Mahadevan. Bayesian sensitivity analysis and uncertainty integration for robust optimization. *Journal of Aerospace Information Systems*, 12(7):590–603, 2015. URL https://arc.aiaa.org/doi/abs/10.2514/1.I010268.

Suzi Dilara Mangan and Gül Koçlar Oral. A study on life cycle assessment of energy retrofit strategies for residential buildings in turkey. *Energy Procedia*, 78:842847, November 2015. ISSN 1876-6102. doi: 10.1016/j.egypro.2015.11.005. URL http://dx.doi.org/10.1016/j.egypro.2015.11.005.

Suzi Dilara Mangan and Gül Koçlar Oral. Assessment of residential building performances for the different climate zones of turkey in terms of life cycle energy and cost efficiency. *Energy and Buildings*, 110:362376, January 2016. ISSN 0378-7788. doi: 10.1016/j.enbuild.2015.11.002. URL http://dx.doi.org/10.1016/j.enbuild.2015.11.002.

H Scott Matthews, Chris T Hendrickson, and Christopher L Weber. The importance of carbon footprint estimation boundaries, 2008.

Marcelo Mendoza, Bárbara Poblete, and Ignacio Valderrama. Early tracking of people's reaction in twitter for fast reporting of damages in the mercalli scale. pages 247–257, 2018.

F.-C. Mihai. Towards sustainable rebuilding of ukraine: The carbon footprint challenge. *Central European Economic Studies*, 2023. URL https://www.ceeol.com/search/article-detail?id=1229845.

Helena Monteiro, John E Fernández, and Fausto Freire. Comparative life-cycle energy analysis of a new and an existing house: The significance of occupants habits, building systems and embodied energy. *Sustainable Cities and Society*, 26:507–518, 2016.

Pedro Muñoz, Pilar Morales, Viviana Letelier, Luis Muñoz, and Daniel Mora. Implications of life cycle energy assessment of a new school building, regarding the nearly zero energy buildings targets in eu: A case of study. *Sustainable Cities and Society*, 32:142–152, 2017. ISSN 2210-6707. doi: https://doi.org/10.1016/j.scs.2017.03.016. URL https://www.sciencedirect.com/science/article/pii/S2210670716306539.

Tetsuya Nakamura, Steven Lloyd, and Satoru Masuda. Resident evaluation of reconstruction challenges and lessons learned from the great east japan earthquake: Recommendations for reconstruction and industrial policies 12 years after the disaster. *Economies*, 12(7), 2024. ISSN 2227-7099. doi: 10.3390/economies12070186. URL https://www.mdpi.com/2227-7099/12/7/186.

William D. Nordhaus. Estimates of the social cost of carbon: Concepts and results from the DICE-2013r model and alternative approaches. *Journal of the Association of Environmental and Resource Economists*, 1(1/2):273–312, 2014. doi: 10.1086/676035. URL https://www.journals.uchicago.edu/doi/10.1086/676035.

Moriyama H. Ogo, J. Impact assessment of temporary housing on the environment during the great east japan earthquake using lca method. *Environmental Research Quarterly*, 179:42–51, 2018. URL https://www.humanitarianlibrary.org/sites/default/files/2015/07/Carbon%20Footprint%20of%20Humanitarian%20Shelter.compressed.pdf.

WMSW. Omar. A hybrid life cycle assessment of embodied energy and carbon emissions from conventional and industrialised building systems in malaysia. *Energy and Buildings*, 2018.

Intergovernmental Panel on Climate Change (IPCC). *Poverty, Livelihoods and Sustainable Development*, page 11711284. Cambridge University Press, 2023.

Jason Maximino C. Ongpeng, Jonathan R. Dungca, Katlheen B. Aviso, and Raymond R. Tan. Minimizing the carbon footprint of urban reconstruction projects. *Journal of Cleaner Production*, 240:118222, 2019. ISSN 0959-6526. doi: https://doi.org/10.1016/j.jclepro.2019.118222. URL https://www.sciencedirect.com/science/article/pii/S0959652619330926.

Anil Ozdemir. Examining the effect of structural characteristics of antakya building stock on the damage level after the kahramanmara earthquakes. *Journal of Earthquake Engineering*, 0(0):1–30, 2024. doi: 10.1080/13632469.2024.2390088. URL https://doi.org/10.1080/13632469.2024.2390088.

Murat Ozturk, Musa Hakan Arslan, and Hasan Hüsnü Korkmaz. Effect on rc buildings of 6 february 2023 turkey earthquake doublets and new doctrines for seismic design. *Engineering Failure Analysis*, 153:107521, November 2023. ISSN 1350-6307. doi: 10.1016/j.engfailanal.2023.107521. URL http://dx.doi.org/10.1016/j.engfailanal.2023.107521.

Cui Pan, Haibo Wang, Shaopeng Huang, and Haihua ZHANG. *The Great East Japan Earthquake and Tsunami Aftermath: Preliminary Assessment of Carbon Footprint of Housing Reconstruction*, volume 35, pages 435–450. 01 2014. ISBN 978-94-007-7268-7. doi: 10.1007/978-94-007-7269-4_25.

F. Pierobon, M. Huang, and K. Simonen. Environmental benefits of using hybrid clt structure in midrise non-residential construction: An lca based comparative case study in the us pacific northwest. *Journal of Building Engineering*, 2019.

Francesco Pomponi and Alice Moncaster. Embodied carbon mitigation and reduction in the built environment what does the evidence say? *Journal of Environmental Management*, 181:687–700, 2016. ISSN 0301-4797. doi: https://doi.org/10.1016/j.jenvman.2016.08.036. URL https://www.sciencedirect.com/science/article/pii/S0301479716305746.

Anne Power. Housing and sustainability: demolition or refurbishment? *Proceedings of the Institution of Civil Engineers-Urban Design and Planning*, 163(4):205–216, 2010.

United Nations Environment Programme. Building materials and the climate: Constructing a new future, 2023-09. URL https://wedocs.unep.org/20.500.11822/43293.

Amalia Pöyry, Antti Säynäjoki, Jukka Heinonen, Juha-Matti Junnonen, and Seppo Junnila. Embodied and construction phase greenhouse gas emissions of a low-energy residential building. *Procedia Economics and Finance*, 21:355365, 2015. ISSN 2212-5671. doi: 10.1016/s2212-5671(15)00187-2. URL http://dx.doi.org/10.1016/S2212-5671(15)00187-2.

M. M. Rajabi, B. Ataie-Ashtiani, and H. Janssen. Efficiency enhancement of optimized latin hypercube sampling strategies: application to monte carlo uncertainty analysis and meta-modeling. *Advances in Water Resources*, 79:44–59, 2015. URL https://www.sciencedirect.com/science/article/pii/S0309170814002474.

Thillaigovindan Ramesh, Ravi Prakash, and Karunesh Kumar Shukla. Life cycle energy analysis of buildings: An overview. *Energy and buildings*, 42(10):1592–1600, 2010.

Errickson F. Prest B.C. Rennert, K. Comprehensive evidence implies a higher social cost of co2. *Nature*, 2022. URL https://doi.org/10.1038/s41586-022-05224-9.

Carolina Reyes, Anthony D Bertagnolli, Paul M Berube, Nathaniel Baetge, Edward F DeLong, David M Karl, Abigail Hendershot, Benjamin A S Van Mooy, Stephen J Giovannoni, John W Kirchner, Rex R Malmstrom, and Adam C Martiny. Global ocean-microbiome dataset reveals biogeography and environmental drivers of bacterial taxonomic composition. *Scientific Data*, 6(1):1–10, 2019. doi: 10.1038/sdata.2018.214.

Mehdi Robati, Daniel Daly, and Georgios Kokogiannakis. A method of uncertainty analysis for whole-life embodied carbon emissions (co2-e) of building materials of a net-zero energy building in australia. *Journal of Cleaner Production*, 225:541–553, 2019. ISSN 0959-6526. doi: https://doi.org/10.1016/j.jclepro.2019.03.339. URL https://www.sciencedirect.com/science/article/pii/S0959652619310558.

Franz Rubel and Markus Kottek. *Meteorologische Zeitschrift*, 20(3):361–365, 06 2011. doi: 10.1127/0941?2948/2011/0285. URL http://dx.doi.org/10.1127/0941?2948/2011/0285.

Martin Röck, Marcella Ruschi Mendes Saade, Maria Balouktsi, Freja Nygaard Rasmussen, Harpa Birgisdottir, Rolf Frischknecht, Guillaume Habert, Thomas Lützkendorf, and Alexander Passer. Embodied ghg emissions of buildings the hidden challenge for effective climate change mitigation. *Applied Energy*, 258:114107, January 2020. ISSN 0306-2619. doi: 10.1016/j.apenergy.2019.114107. URL http://dx.doi.org/10.1016/j.apenergy.2019.114107.

Yousif Abed Saleh Saleh, Gulden Gokcen Akkurt, and Cihan Turhan. Reconstructing energy-efficient buildings after a major earthquake in hatay, türkiye. *Buildings*, 14(7), 2024. ISSN 2075-5309. doi: 10.3390/buildings14072043. URL https://www.mdpi.com/2075-5309/14/7/2043.

Andrea Saltelli and Paola Annoni. Variance-based sensitivity analysis of model output. *Reliability Engineering & System Safety*, 91(10-11):1203–1218, 2010. URL https://www.sciencedirect.com/science/article/pii/S095183200800137X.

Sirat Sandil and Rabindra Kumar. *Soil Contamination from Construction Projects*, pages 205–244. Springer International Publishing, Cham, 2022. ISBN 978-3-030-76073-1. doi: 10.1007/978-3-030-76073-1_12. URL https://doi.org/10.1007/978-3-030-76073-1_12.

Antti Säynäjoki, Jukka Heinonen, Juha-Matti Junnonen, and Seppo Junnila. Input–output and process lcas in the building sector: are the results compatible with each other? *Carbon Management*, 8(2):155–166, 2017.

Kate Simonen, Barbara Rodriguez Droguett, Larry Strain, and Erin McDade. Embodied carbon benchmark study: Lca for low carbon construction. Technical report, University of Washington, 2017.

Katie Skillington, Robert H Crawford, Georgia Warren-Myers, and Kathryn Davidson. A review of existing policy for reducing embodied energy and greenhouse gas emissions of buildings. *Energy Policy*, 168:112920, 2022.

Chenxiao Song and Reiichiro Kawai. Monte carlo and variance reduction methods for structural reliability analysis: A comprehensive review. *Probabilistic Engineering Mechanics*, 73:103479, 2023. ISSN 0266-8920. doi: https://doi.org/10.1016/j.probengmech.2023.103479. URL https://www.sciencedirect.com/science/article/pii/S0266892023000681.

Quan Song, Yefei Ren, Baofeng Zhou, Yongqiang Yang, Aiwen Liu, Ruizhi Wen, Yajun Zhang, and Yingxin Hui. Site effects exacerbate the building damages from mw7.8 turkey earthquake, 2023. February 2024. doi: 10.21203/rs.3.rs-3947139/v1. URL http://dx.doi.org/10.21203/rs.3.rs-3947139/v1.

Benjamin K. Sovacool, May Tan-Mullins, and Wokje Abrahamse. Bloated bodies and broken bricks: Power, ecology, and inequality in the political economy of natural disaster recovery. *World Development*, 110:243–255, 2018. ISSN 0305-750X. doi: https://doi.org/10.1016/j.worlddev.2018.05.028. URL https://www.sciencedirect.com/science/article/pii/S0305750X18301761.

Hari Srinivas and Yuko Nakagawa. Environmental implications for disaster preparedness: lessons learnt from the indian ocean tsunami. *Journal of environmental management*, 89(1):4–13, 2008.

Seton Stiebert, Daniella Echeverría, Philip Gass, and Lucy Kitson. Emission omissions: Carbon accounting gaps in the built environment. Technical report, International Institute for Sustainable Development (IISD), 2019. URL http://www.jstor.org/stable/resrep21925.6.

Sangwon Suh, Manfred Lenzen, Graham J Treloar, Hiroki Hondo, Arpad Horvath, Gjalt Huppes, Olivier Jolliet, Uwe Klann, Wolfram Krewitt, Yuichi Moriguchi, et al. System boundary selection in life-cycle inventories using hybrid approaches. *Environmental science & technology*, 38(3):657–664, 2004.

Georgios Syngros, Constantinos A. Balaras, and Dimitrios G. Koubogiannis. Embodied co2 emissions in building construction materials of hellenic dwellings. *Procedia Environmental Sciences*, 38:500–508, 2017. ISSN 1878-0296. doi: https://doi.org/10.1016/j.proenv.2017.03.113. URL https://www.sciencedirect.com/science/article/pii/S1878029617301172. Sustainable synergies from Buildings to the Urban Scale.

P. Szu-Hsien. The estimation of a carbon footprint for a debris flow disastera case study in daniau community in taitung, taiwan. *International Journal of Environmental Science and Development*, 2018. URL https://www.academia.edu/download/113175713/1084-T0041.pdf.

Antti Säynäjoki, Jukka Heinonen, and Seppo Junnila. A scenario analysis of the life cycle greenhouse gas emissions of a new residential area. *Environmental Research Letters*, 7:034037, 09 2012. doi: 10.1088/1748-9326/7/3/034037.

Nicolas Taconet, Céline Guivarch, and Antonin Pottier. Social cost of carbon under stochastic tipping points: when does risk play a role? *Environmental and Resource Economics*, 78:709–737, 2021.

Richard S J Tol. Social cost of carbon estimates have increased over time. *Nat. Clim. Chang.*, 13(6): 532–536, June 2023.

GJ Treloar, PED Love, OO Faniran, and U Iyer-Raniga. A hybrid life cycle assessment method for construction. *Construction Management & Economics*, 18(1):5–9, 2000.

Turkish Statistical Institute. Survey on building and dwelling characteristics, 2021. https://data.tuik.gov.tr/Bulten/Index?p=Survey-on-Building-and-Dwelling-Characteristics-2021-45870&dil=2, 2021. Accessed: 2024-08-25.

Turkish Statistical Institute. Address-based population registration system (adnks) results dated 31 december 2022, favorite reports". https://biruni.tuik.gov.tr/medas/?kn=95&locale=en, 2022.

Turkish Statistical Institute. TÜk - turkish statistical institute, 2024. URL https://www.tuik.gov.tr/. Accessed: 2024-08-25.

UK Green Building Council. Introduction to embodied ecological impacts, 2024. URL https://ukgbc.org/news/introduction-to-embodied-ecological-impacts/?utm_source=chatgpt.com. Accessed: 2024-12-01.

United Nations Office for Disaster Risk Reduction (UNDRR). The human cost of disasters: An overview of the last 20 years (2000-2019), 2020. URL https://www.undrr.org/publication/human-cost-disasters-overview-last-20-years-2000-2019. Accessed: 2024-12-06.

Graham Upton and Ian Cook. *Oxford Dictionary of Statistics*. Oxford University Press, 2014. URL https://www.oxfordreference.com/display/10.1093/acref/9780191843730.001.0001/q-oro-ed5-00008992.

BV Venkatarama Reddy. Sustainable materials for low carbon buildings. *International Journal of Low-Carbon Technologies*, 4(3):175–181, 2009.

W.E. Walker and V.A.W.J. Marchau. Dealing with uncertainty in policy analysis and policymaking. *Integrated Assessment*, 4(1):1–4, 2003. doi: 10.1076/iaij.4.1.1.16462. URL https://doi.org/10.1076/iaij.4.1.1.16462.

Pei Wang, Xiangzheng Deng, Huimin Zhou, and Shangkun Yu. Estimates of the social cost of carbon: A review based on meta-analysis. *Journal of Cleaner Production*, 209:1494–1507, 2019. ISSN 0959-6526. doi: https://doi.org/10.1016/j.jclepro.2018.11.058. URL https://www.sciencedirect.com/science/article/pii/S0959652618334589.

Catherine De Wolf, Endrit Hoxha, Alexander Hollberg, Corentin Fivet, and John Ochsendorf. Database of embodied quantity outputs: Lowering material impacts through engineering. *Journal of Architectural Engineering*, 26(3):04020016, 2020. doi: 10.1061/(ASCE)AE.1943-5568.0000408. URL https://ascelibrary.org/doi/abs/10.1061/%28ASCE%29AE.1943-5568.0000408.

Richard Wood. Australian bushfires one year on: How black summer of death and destruction erupted. 2020. URL https://www.9news.com.au/national/australian-bushfires-black-summer-one-year-anniversary/4b61f48a-9b80-44b8-8f35-a57249f924ab. Accessed: 2024-12-03.

Yi Xiao, Ke Tian, Mingkang Yuan, Yi Ouyang, and Huan Huang. Examining the complex relationships between socioeconomic development and the improvement of ecological environment in post-disaster reconstruction: The case of wenchuan earthquake disaster area in western china. *Journal of Cleaner Production*, 337:130581, 2022. ISSN 0959-6526. doi: https://doi.org/10.1016/j.jclepro.2022.130581. URL https://www.sciencedirect.com/science/article/pii/S0959652622002220.

L. Xiaodong, Y. Fan, G. Yuanxue, and J. McCarthy. Case study of carbon footprint of residential building construction. *Materials Research Innovations*, 18(sup4):S4–72–S4–76, July 2014. ISSN 1433-075X. doi: 10.1179/1432891714z.000000000647. URL http://dx.doi.org/10.1179/1432891714z.000000000647.

Honglei Yi and Jay Yang. Research trends of post disaster reconstruction: The past and the future. *Habitat International*, 42:21–29, 2014. ISSN 0197-3975. doi: https://doi.org/10.1016/j.habitatint.2013.10.005. URL https://www.sciencedirect.com/science/article/pii/S0197397513001021.

Fang You, Dan Hu, Haitao Zhang, Zhen Guo, Yanhua Zhao, Bennan Wang, and Ye Yuan. Carbon emissions in the life cycle of urban building system in chinaa case study of residential buildings. *Ecological Complexity*, 8(2):201–212, 2011.

Dongwei Yu, Hongwei Tan, and Yingjun Ruan. A future bamboo-structure residential building prototype in china: Life cycle assessment of energy use and carbon emission. *Energy and Buildings*, 43(10):2638–2646, 2011.

Emre Yüksel. Urbanization and spatial problems in antakya. *Journal of Urban and Regional Planning*, 30(1):102–117, 2021.

Ignacio Zabalza Bribián, Alfonso Aranda Usón, and Sabina Scarpellini. Life cycle assessment in buildings: State-of-the-art and simplified lca methodology as a complement for building certification. *Building and Environment*, 44(12):2510–2520, 2009. ISSN 0360-1323. doi: https://doi.org/

10.1016/j.buildenv.2009.05.001. URL https://www.sciencedirect.com/science/article/pii/S0360132309001188.

Xiaocun Zhang and Fenglai Wang. Assessment of embodied carbon emissions for building construction in china: Comparative case studies using alternative methods. *Energy and Buildings*, 130:330340, October 2016. ISSN 0378-7788. doi: 10.1016/j.enbuild.2016.08.080. URL http://dx.doi.org/10.1016/j.enbuild.2016.08.080.

Weichen Zhong, Guy Howard, and Jeffrey Neal. Estimating the carbon footprint of post-flood urban road network restoration: A case study in carlisle. Technical report, Copernicus Meetings, 2024.

Chengchoa Zuo, Mark Birkin, Graham Clarke, Fiona McEvoy, and Andrew Bloodworth. Reducing carbon emissions related to the transportation of aggregates: Is road or rail the solution? *Transportation Research Part A: Policy and Practice*, 117:26–38, 2018.

smail Çetin. Urban development in antakya from 1940 to 2010. *Journal of Urban Studies*, 25(2):45–59, 2013.

A

Appendix

A.1. Chapter: Introduction

A.2. Chapter: State of the Art

Table 2.1 The progressive transition of levels of uncertainty from determinism to total ignorance (Walker et al. 2010).

Location	Level 1	Level 2	Level 3	Level 4
Context	A clear enough future 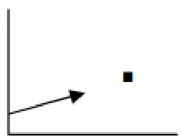	Alternate futures (with probabilities) 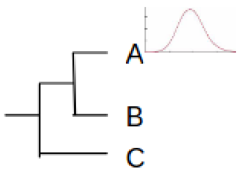	A multiplicity of plausible futures 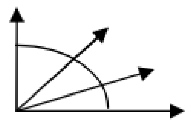	Unknown future (know we don't know) 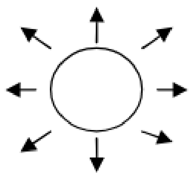
System model	A single system model	A single system model with a probabilistic parameterization	Several system models, with different structures	Unknown system model; know we don't know
System outcomes	A point estimate and confidence interval for each outcome	Several sets of point estimates and confidence intervals for the outcomes, with a probability attached to each set	A known range of outcomes	Unknown outcomes; know we don't know
Weights on outcomes	A single estimate of the weights	Several sets of weights, with a probability attached to each set	A known range of weights	Unknown weights; know we don't know

Figure A.1: The progressive transition of levels of uncertainty from determinism to total ignorance as depicted in the work of Haasnoot 2011

LCA Type	Description	Advantages	Disadvantages
Process LCA	Most common LCA type, based on bottom-up data on the energy and material flows for specific processes.	Easy to determine each process that is contributing to emissions.	Impossible to include all processes that emit GHGs, and choices must be made about what to include and how to define the system boundary. While some databases, such as ecoinvent, model infrastructure associated with the transforming activities (e.g., equipment manufacturers that supply cement, steel, and wood manufacturing facilities), it is difficult to know precisely what is included in the system boundary, and omissions may create an apples-to-oranges comparison.
InputOutput LCA	Based on a top-down approach using national statistical information on monetary transactions between sectors. Economic inputs to a sector, such as the building industry, are transformed into energy and emission flows using a partitioning and accounting of energy and emissions for the full economy.	Does not suffer from truncation error (i.e., excluding potential sources of emissions such as services like banking, advertisements, and legal services), as all emission flows are portioned and included.	Unsuitable for comparing the relative performance of different types of building materials. Associated with monetary transactions that presume an average input emission factor based on all the comprised sectors, which may or may not represent the structural building element in question. Does not include carbon sequestration, a critical element in building LCA.
Hybrid LCA	Combination of both process and inputoutput LCA.	Balances advantages of both process and inputoutput LCA.	Limited use because of sophistication and complexity.

Table A.1: Description of the main types of LCA analysis

A.3. Chapter: Case Study

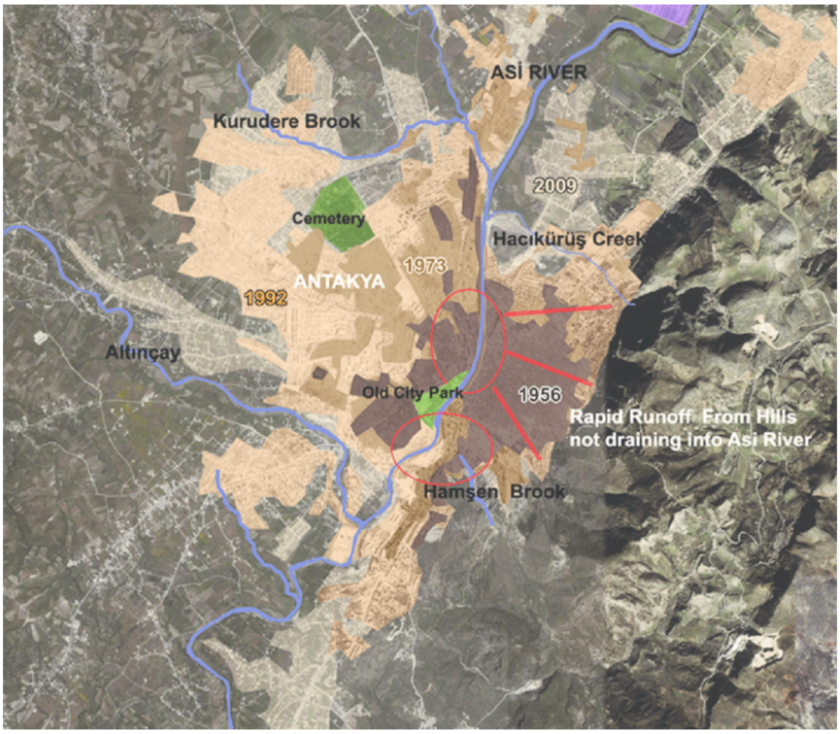

Figure A.2: Antakya's growth based on the work of X

A.4. Chapter: Method

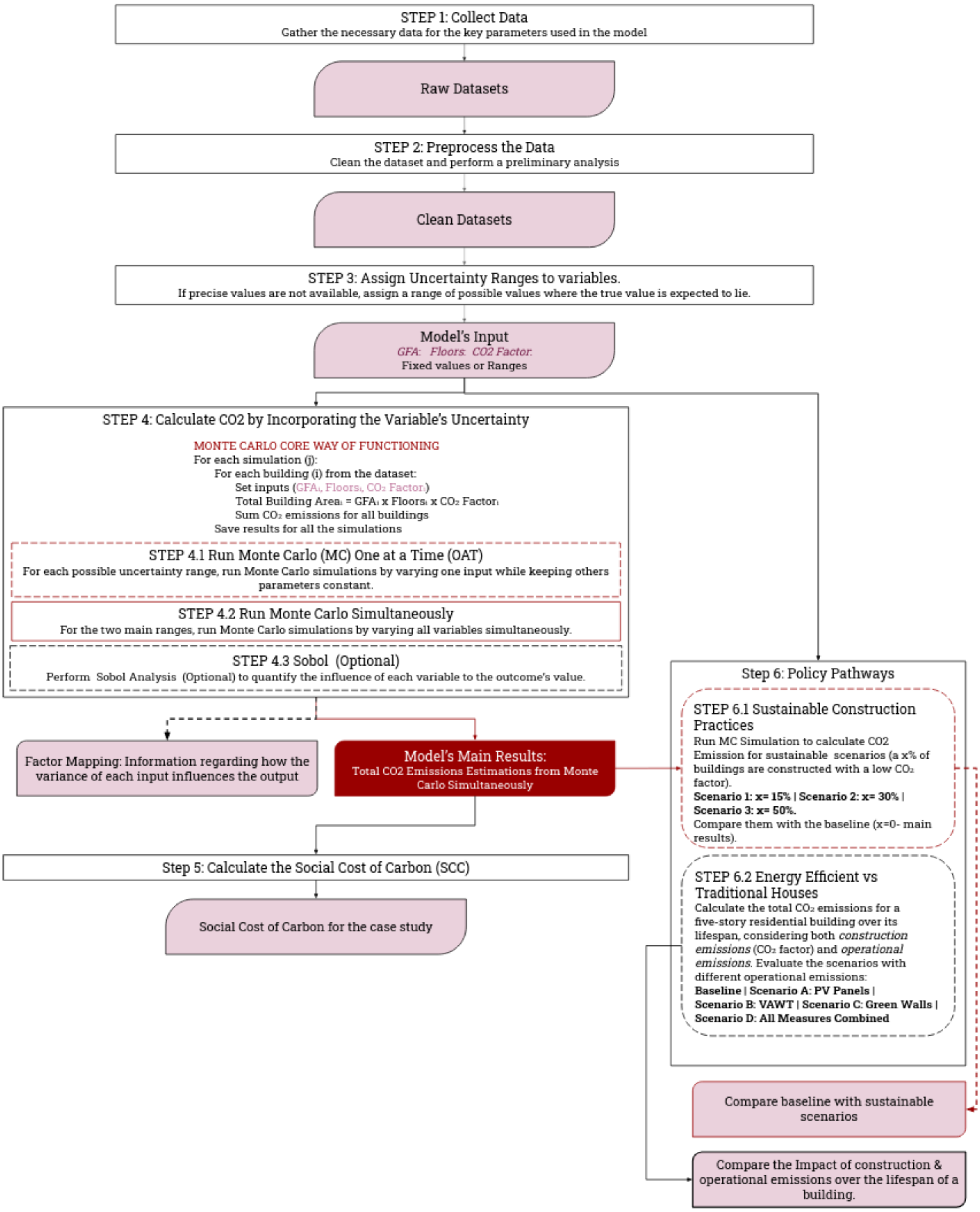

Figure A.3: Research Method with more detailed information

Name	Explanation	Formula	Units
FAR (Floor Area Ratio)	the ratio of a building's total floor area to the size of the plot on which it is built. For example, a FAR of 2.0 means the buildings total floor area is twice the ground floor area.	$\text{FAR} = \frac{\text{Gross Floor Area}}{\text{Plot Area}}$	-
Dwelling Units Per Acre (DU/acre)	Primarily used in residential projects to describe the number of housing units per unit of land area, indicating population density within a specified region.	$\text{Dwelling Units Density} = \frac{\text{Number of Housing Units}}{\text{Land Area}}$	DU/acre or DU/hectares
Number of Stories or Building Height	Represents building height, often regulated by zoning laws. It can be expressed either in terms of number of stories or absolute height in meters or feet.	-	Number of Floors, meters or feet
Qualitative Density Categories	Categorizes buildings into qualitative density terms such as low, medium, and high, often without a precise quantitative definition but generally corresponding to development intensity.	-	-

Table A.2: Key Metrics for Building Density and Area

A.4.1. Data Collection

Gross Floor Area & Number of Floors

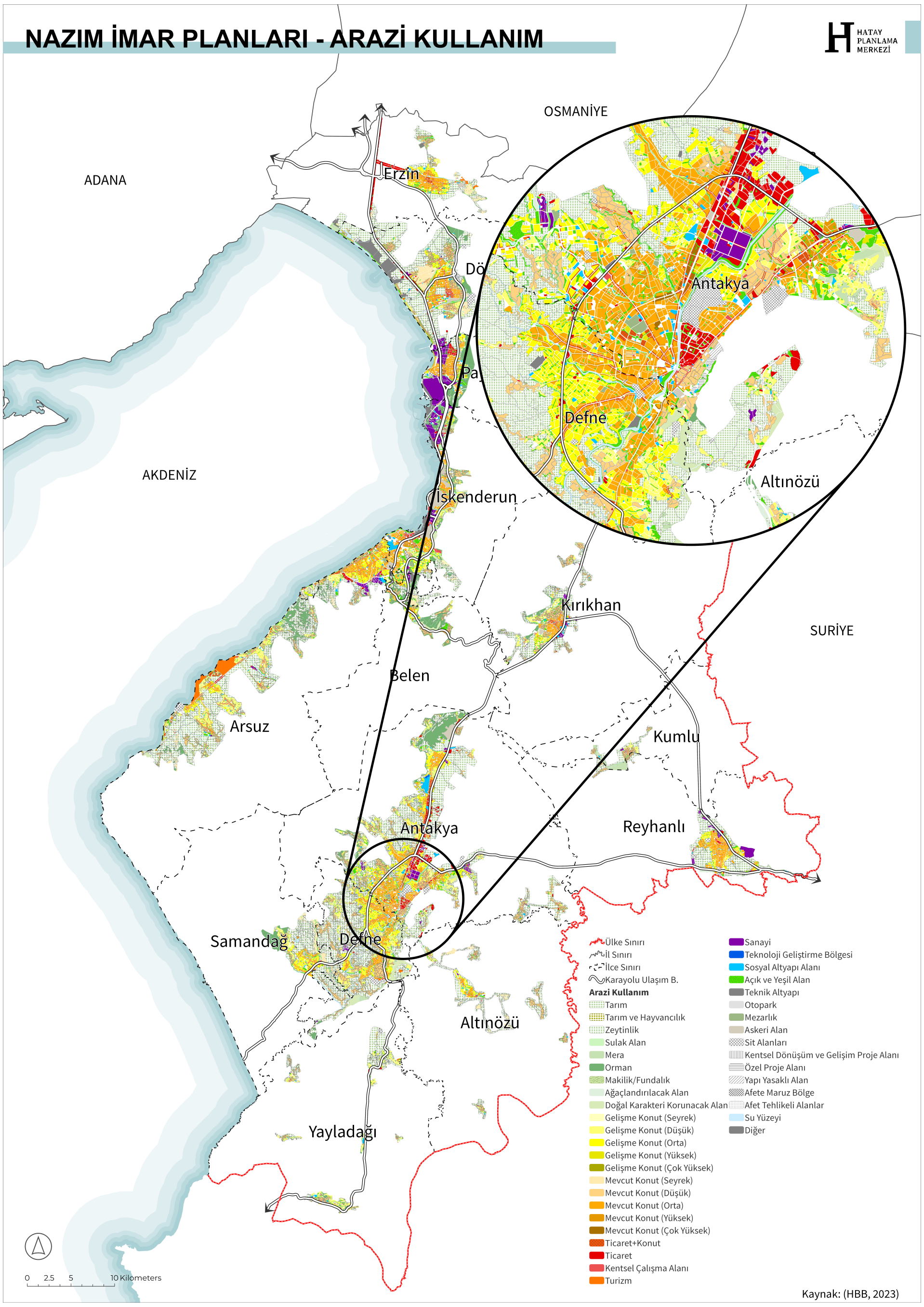

Figure A.4: Reconstruction Plans as provided from the Hatay Municipality

CO_2 Factor

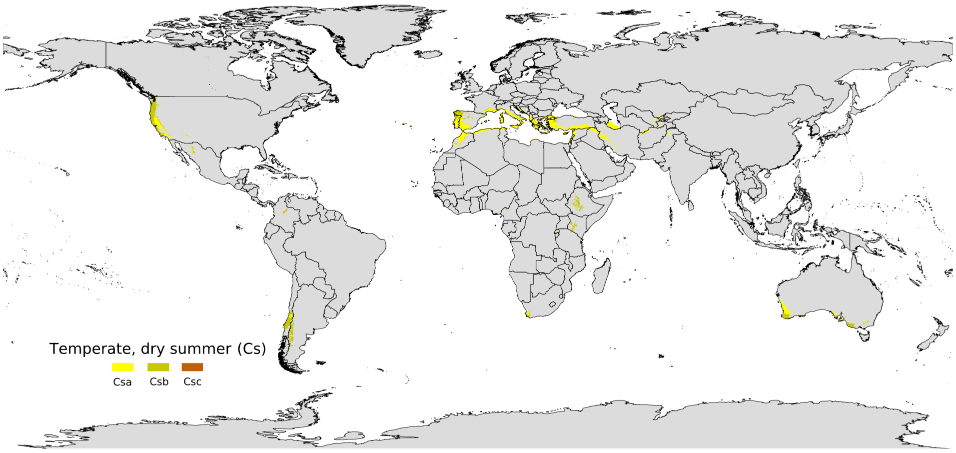

Figure A.5: Regions with climate Csa Reyes et al. [2019]

A.4.2. Assigning Uncertainty Ranges for Model's Input

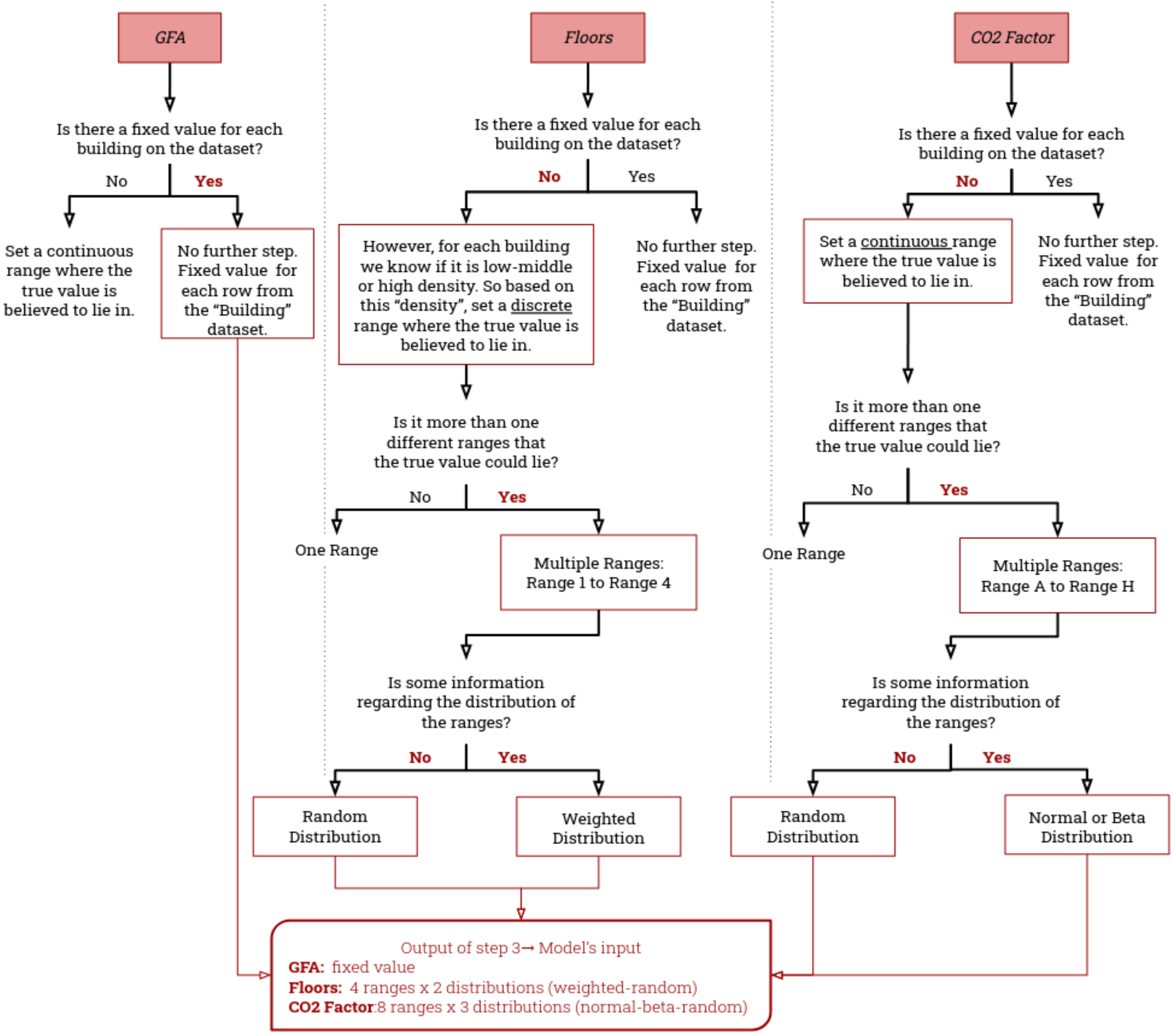

Figure A.6: Flowchart of the step 3 from the research method. *Assigning Uncertainty ranges for model's parameters.*

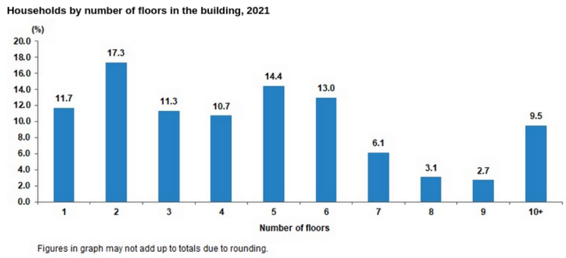

(a) Distribution of floors based on the Turkish Statistical Institute [2021]

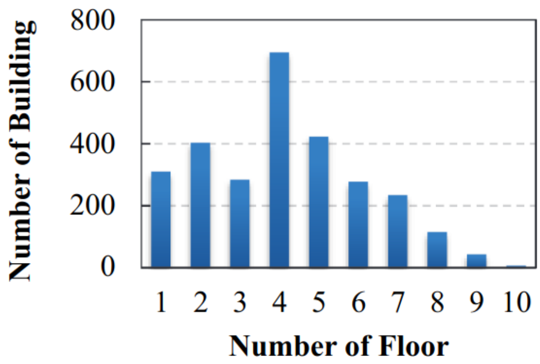

(b) Distribution of floors based on the Ozdemir [2024]

Figure A.7: Distribution of floors of the 2 datasets that have been used.

Number of Floors or Density

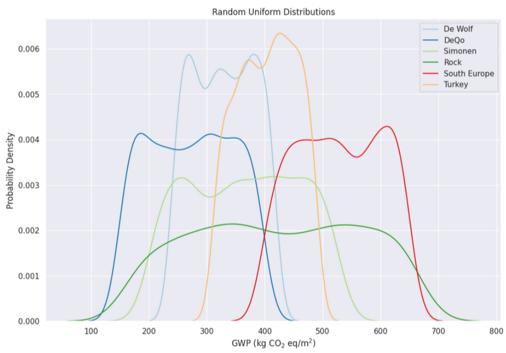

(a)

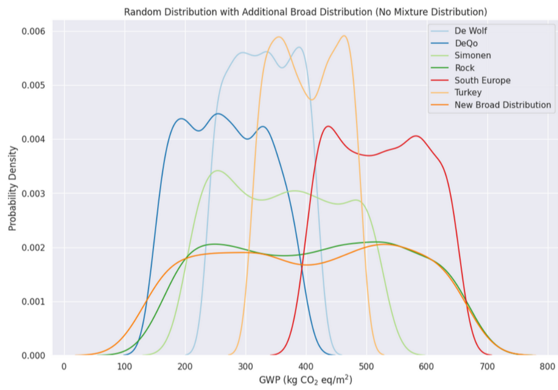

(b)

Figure A.8

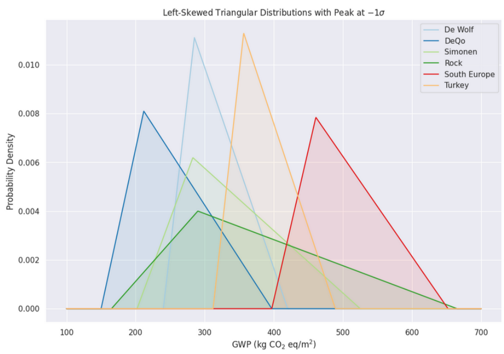

(a)

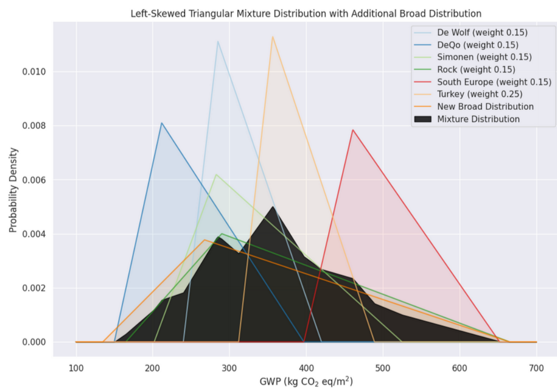

(b)

Figure A.9: Triangular Left

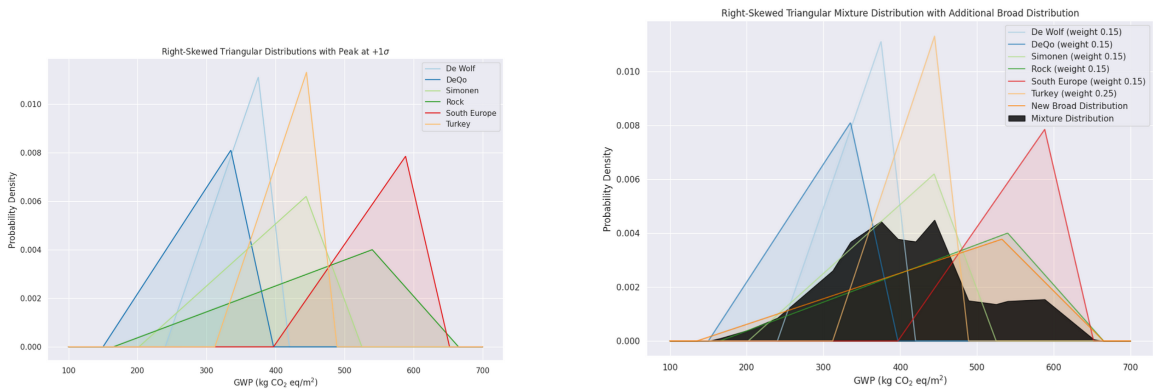

(a) (b)

Figure A.10: Triangular Right

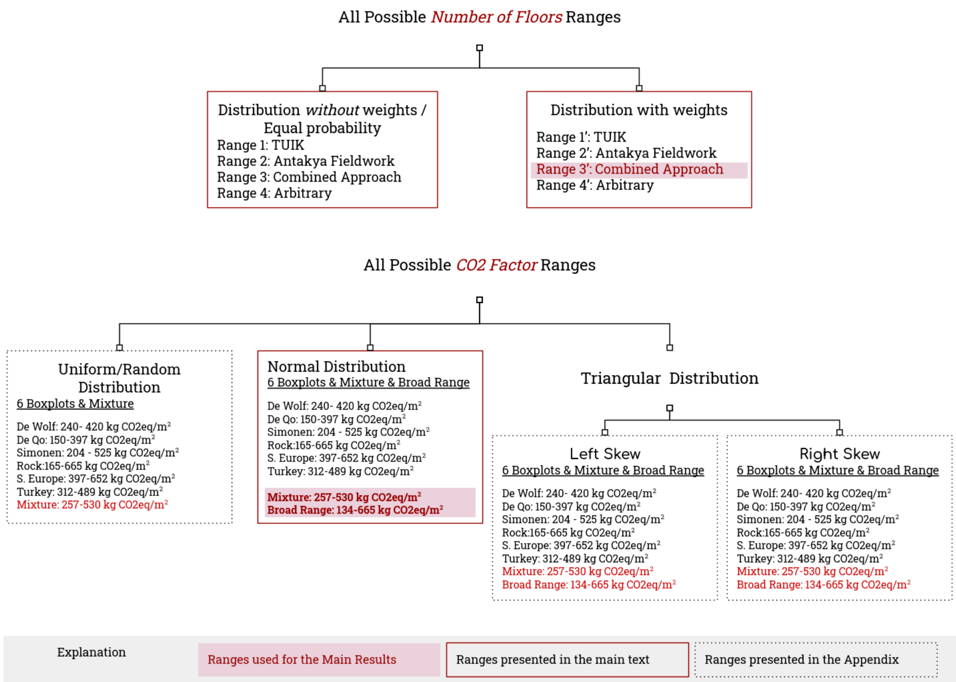

Figure A.11: All possible ranges

CO_2 **Factor**

A.4.3. Calculate CO2 Emissions

Scenario No.	OAT or Simultaneous	Number of Floors	CO_2 Factor	Distribution
1	OAT	Low (1-2), Medium (3-8), High (9-12)	Fixed at 400 kg CO_2/m^2	Random
2	OAT	Low (1-3), Medium (4-8), High (9-12)	Fixed at 400 kg CO_2/m^2	Random
3	OAT	Low (1-2), Medium (3-8), High (9-12)	Fixed at 400 kg CO_2/m^2	Random

4	OAT	Low (1-3), Medium (4-7), High (8-11)	Fixed at 400 kg CO_2/m^2	Random
5	OAT	Low (1-2) [41%, 59%], Medium (3-8) [23.9%, 22.4%, 20.9%, 19.4%, 9.0%, 4.5%], High (9-12) [25% each]	Fixed at 400 kg CO_2/m^2	Weighted
6	OAT	Low (1-3) [30%, 42%, 28%], Medium (4-8) [42%, 24%, 15%, 13%, 6%], High (9-12) [25% each]	Fixed at 400 kg CO_2/m^2	Weighted
7	OAT	Low (1-2) [45%, 55%], Medium (3-8) [22.7%, 24.2%, 22.7%, 15.2%, 10.6%, 4.5%], High (9-12) [25% each]	Fixed at 400 kg CO_2/m^2	Weighted
8	OAT	Low (1-3) [33.3%, 33.3%, 33.3%], Medium (4-7) [25%, 25%, 25%, 25%], High (8-11) [25% each]	Fixed at 400 kg CO_2/m^2	Weighted
9	OAT	Low = 2, Medium = 5, High = 9	De Wolf (240-420 kg CO_2/m^2)	Random
10	OAT	Low = 2, Medium = 5, High = 9	De Qo (150-397 kg CO_2/m^2)	Random
11	OAT	Low = 2, Medium = 5, High = 9	Simonen (204-525 kg CO_2/m^2)	Random
12	OAT	Low = 2, Medium = 5, High = 9	Rock (165-665 kg CO_2/m^2)	Random
13	OAT	Low = 2, Medium = 5, High = 9	Southern Europe (397-652 kg CO_2/m^2)	Random
14	OAT	Low = 2, Medium = 5, High = 9	Turkey (312-489 kg CO_2/m^2)	Random
15	OAT	Low = 2, Medium = 5, High = 9	Broad Range (134-665 kg CO_2/m^2)	Random
16	OAT	Low = 2, Medium = 5, High = 9	De Wolf (240-420 kg CO_2/m^2)	Normal
17	OAT	Low = 2, Medium = 5, High = 9	De Qo (150-397 kg CO_2/m^2)	Normal
18	OAT	Low = 2, Medium = 5, High = 9	Simonen (204-525 kg CO_2/m^2)	Normal
19	OAT	Low = 2, Medium = 5, High = 9	Rock (165-665 kg CO_2/m^2)	Normal
20	OAT	Low = 2, Medium = 5, High = 9	Southern Europe (397-652 kg CO_2/m^2)	Normal
21	OAT	Low = 2, Medium = 5, High = 9	Turkey (312-489 kg CO_2/m^2)	Normal
22	OAT	Low = 2, Medium = 5, High = 9	Mixture (257-530 kg CO_2/m^2)	Normal
23	OAT	Low = 2, Medium = 5, High = 9	Broad Range (134-665 kg CO_2/m^2)	Normal
24	OAT	Low = 2, Medium = 5, High = 9	De Wolf (240-420 kg CO_2/m^2)	Triangular Left-Skewed
25	OAT	Low = 2, Medium = 5, High = 9	De Qo (150-397 kg CO_2/m^2)	Triangular Left-Skewed
26	OAT	Low = 2, Medium = 5, High = 9	Simonen (204-525 kg CO_2/m^2)	Triangular Left-Skewed
27	OAT	Low = 2, Medium = 5, High = 9	Rock (165-665 kg CO_2/m^2)	Triangular Left-Skewed

28	OAT	Low = 2, Medium = 5, High = 9	Southern Europe (397-652 kg CO_2/m^2)	Triangular Left-Skewed
29	OAT	Low = 2, Medium = 5, High = 9	Turkey (312-489 kg CO_2/m^2)	Triangular Left-Skewed
30	OAT	Low = 2, Medium = 5, High = 9	Mixture (257-530 kg CO_2/m^2)	Triangular Left-Skewed
31	OAT	Low = 2, Medium = 5, High = 9	Broad Range (134-665 kg CO_2/m^2)	Triangular Left-Skewed
32	OAT	Low = 2, Medium = 5, High = 9	De Wolf (240-420 kg CO_2/m^2)	Triangular Right-Skewed
33	OAT	Low = 2, Medium = 5, High = 9	De Qo (150-397 kg CO_2/m^2)	Triangular Right-Skewed
34	OAT	Low = 2, Medium = 5, High = 9	Simonen (204-525 kg CO_2/m^2)	Triangular Right-Skewed
35	OAT	Low = 2, Medium = 5, High = 9	Rock (165-665 kg CO_2/m^2)	Triangular Right-Skewed
36	OAT	Low = 2, Medium = 5, High = 9	Southern Europe (397-652 kg CO_2/m^2)	Triangular Right-Skewed
37	OAT	Low = 2, Medium = 5, High = 9	Turkey (312-489 kg CO_2/m^2)	Triangular Right-Skewed
38	OAT	Low = 2, Medium = 5, High = 9	Mixture (257-530 kg CO_2/m^2)	Triangular Right-Skewed
39	OAT	Low = 2, Medium = 5, High = 9	Broad Range (134-665 kg CO_2/m^2)	Triangular Right-Skewed
40	Simultaneous	Low (1-2) [45%, 55%], Medium (3-8) [22.7%, 24.2%, 22.7%, 15.2%, 10.6%, 4.5%], High (9-12) [25% each]	Mixture (257-530 kg CO_2/m^2)	Normal
41	Simultaneo	Low (1-2) [45%, 55%], Medium (3-8) [22.7%, 24.2%, 22.7%, 15.2%, 10.6%, 4.5%], High (9-12) [25% each]	Broad Range (134-665 kg CO_2/m^2)	Normal

Table A.3: Scenarios for CO_2 Emission Simulations: Number of Floors and CO_2 Factor Distributions

```
# Define ranges for floors based on density with probabilities
density_to_floors_My = {
    'low': ([1, 2], [0.45, 0.55]),  # Low density floors with probabilities
    'middle': ([3, 4, 5, 6, 7, 8], [0.23, 0.24, 0.23, 0.15, 0.11, 0.04]),  # Middle
        density floors with probabilities
    'high': ([9, 10, 11, 12], [0.25, 0.25, 0.25, 0.25])  # High density floors with
        probabilities
}

# Define the number of simulations
n_simulations = 1000

# Run Monte Carlo simulation
results_free = []
for i in range(n_simulations):
    total_$CO_2$ = 0
    for idx, row in gdf.iterrows():
        # Select the number of floors based on the density and its corresponding
            probabilities
        if row['new_dens'] == 'low':
            floors = np.random.choice(density_to_floors_My['low'][0], p=
                density_to_floors_My['low'][1])
        elif row['new_dens'] == 'middle':
            floors = np.random.choice(density_to_floors_My['middle'][0], p=
                density_to_floors_My['middle'][1])
        elif row['new_dens'] == 'high':
```

```
            floors = np.random.choice(density_to_floors_My['high'][0], p=
                density_to_floors_My['high'][1])

        $CO_2$_factor = np.random.normal(0.3995, (0.665 - 0.134) / 4)
        $CO_2$_factor = np.clip($CO_2$_factor, 0.134, 0.665)  # Ensure $CO_2$ factor
            stays within the specified range
        total_sqm = floors * row['area_sqm']
        $CO_2$_emissions = total_sqm * $CO_2$_factor
        total_$CO_2$ += $CO_2$_emissions
    results_free.append(total_$CO_2$)

# Convert results to DataFrame for analysis
results_free_df = pd.DataFrame(results_free, columns=['total_$CO_2$'])

# Plot the distributions of the results as a histogram
plt.figure(figsize=(10, 6))
plt.hist(results_free_df['total_$CO_2$'], bins=50, color='#3F7774', edgecolor='black')
plt.title('Monte␣Carlo␣Varying␣Both␣Parameters|␣$CO_2$␣Factor␣=␣(134,657)GWP␣')
plt.xlabel('Total␣$CO_2$␣Emissions␣(ton)')
plt.ylabel('Frequency')
plt.grid(True)
plt.show()
```

A.4.4. Social Cost of Carbon - Alternative method

As explained in the main text, estimating a definitive SCC value is inherently complex, as it varies widely across models depending on their underlying assumptions. To address this uncertainty, the distribution of SCC values compiled in a meta-analysis by Tol [2023] is utilized. Tol synthesized 5,905 SCC estimates from 207 academic studies published before 2022. The resulting distribution is shown in Figure A.12.

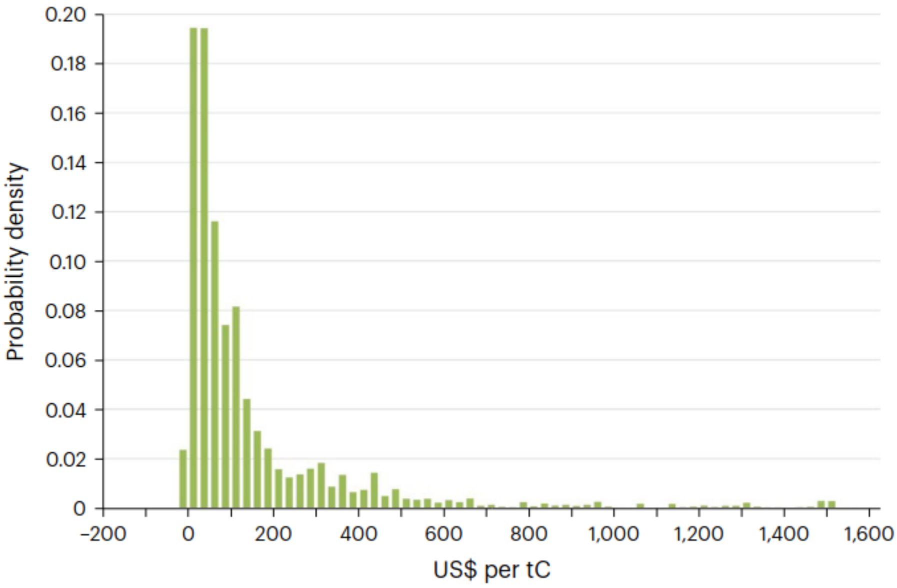

Figure A.12: Histogram of the social cost of carbon based on the work of Tol 2023

The histogram illustrates the distribution of total costs (x-axis, in USD) associated with the reconstruction-related emissions, with the y-axis representing the probability density. The distribution is highly positively skewed, covering a wide rangefrom near \$0 to around \$200 per tonne of COthough it extends beyond \$1,400.

To integrate this SCC distribution with the CO emissions estimate, each SCC value is multiplied by the mean CO emissions derived from the main results.

While a simple 90% interval using the 5th and 95th percentiles might appear suitable to summarize the central range, this method can be misleading in the case of a highly skewed distribution. It discards the tails without considering where values are most densely concentrated, potentially excluding a substantial portion of the core of the distributionparticularly when the lower tail contains high-density values.

To provide a more informative summary, a **highest density interval (HDI)** is used. A kernel density estimate (KDE) is applied to identify the mode of the distribution, and an interval is defined that includes all values with a density above 50% of the peak. This HDI approach is more appropriate for skewed distributions, as it highlights the region where values are most concentrated, offering a clearer picture of the central tendency.

A.4.5. Policy Pathways: Building Sustainable houses

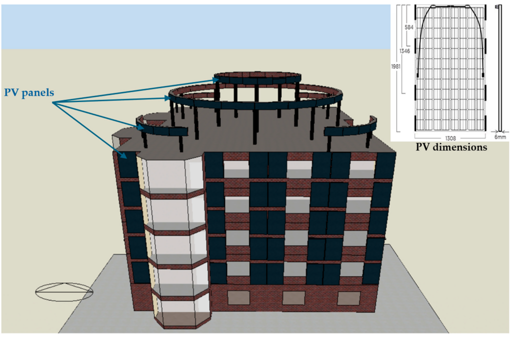

(a) Scenario A: Thin-film G Œ B 500 Bifacial PV module mounted on the case building.

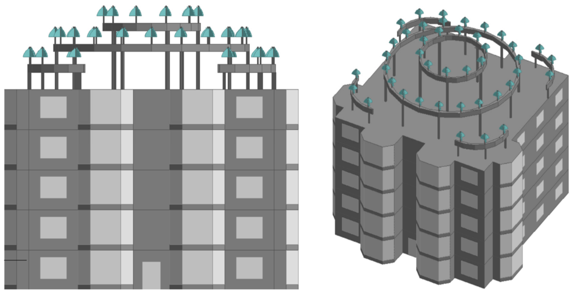

(b) Scenario B: IceWind turbines mounted on the building (developed by the Saleh et al. [2024]).

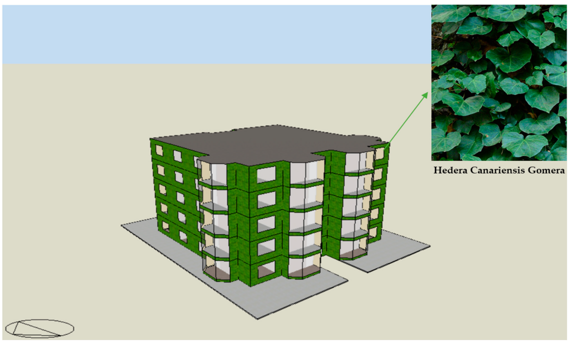

(c) Green wall for three sides of building except in the south direction.

Figure A.13: Scenarios of the energy efficient measures as taken from the work of Saleh et al. [2024]

A.5. Chapter: Results

A.5.1. Raw Data Insights

	fid	osm_id	addr_house	addr_full	damage_eve	source	damage_typ	damage_dat	building	destroyed_	addr_stree	name	addr_city	pop_num	pop_str	density	landuse	geometry
0	1.0	1.144109e+09	None	None	#TürkiyeEQ060223	cscrs	earthquake	2023-02-06	None	yes	None	None	None	7500	5001-10000	NaN	housing	POLYGON ((36.15649 36.19195, 36.15659 36.19209...
1	2.0	1.144347e+09	None	None	#TürkiyeEQ060223	cscrs	earthquake	2023-02-06	None	yes	None	None	None	1000	0-2000	NaN	housing	POLYGON ((36.16297 36.19321, 36.16302 36.19323...
2	3.0	1.139744e+09	None	None	#TürkiyeEQ060223	cscrs	earthquake	2023-02-06	None	yes	None	None	None	32500	20001-45000	NaN	housing	POLYGON ((36.16316 36.24660, 36.16322 36.24667...
3	4.0	1.139835e+09	None	None	#TürkiyeEQ060223	None	earthquake	2023-02-06	None	yes	None	None	None	15000	10001-20000	NaN	housing	POLYGON ((36.15727 36.21784, 36.15746 36.21790...
4	5.0	1.139835e+09	None	None	#TürkiyeEQ060223	None	earthquake	2023-02-06	None	yes	None	None	None	15000	10001-20000	NaN	housing	POLYGON ((36.15742 36.21831, 36.15767 36.21838...
5	6.0	1.140769e+09	None	None	#TürkiyeEQ060223	None	earthquake	2023-02-06	None	yes	None	None	None	15000	10001-20000	NaN	housing	POLYGON ((36.15718 36.21584, 36.15733 36.21589...
6	7.0	1.140777e+09	None	None	#TürkiyeEQ060223	None	earthquake	2023-02-06	None	yes	None	None	None	15000	10001-20000	NaN	housing	POLYGON ((36.15759 36.21435, 36.15786 36.21443...
7	8.0	1.141055e+09	None	None	#TürkiyeEQ060223	None	earthquake	2023-02-06	None	yes	None	None	None	15000	10001-20000	NaN	housing	POLYGON ((36.15730 36.21534, 36.15752 36.21542...
8	9.0	1.144393e+09	None	None	#TürkiyeEQ060223	None	earthquake	2023-02-06	None	yes	None	None	None	15000	10001-20000	NaN	housing	POLYGON ((36.15747 36.21594, 36.15762 36.21598...
9	10.0	1.139709e+09	None	None	#TürkiyeEQ060223	cscrs	earthquake	2023-02-06	None	yes	None	None	None	15000	10001-20000	NaN	None	POLYGON ((36.15409 36.21474, 36.15427 36.21482...

Figure A.14: The raw spatial data obtained from the Hatay Municipality, representing the digitized version of the reconstruction plans shown in Figure **??**. Key columns for analysis include Density and Geometry.

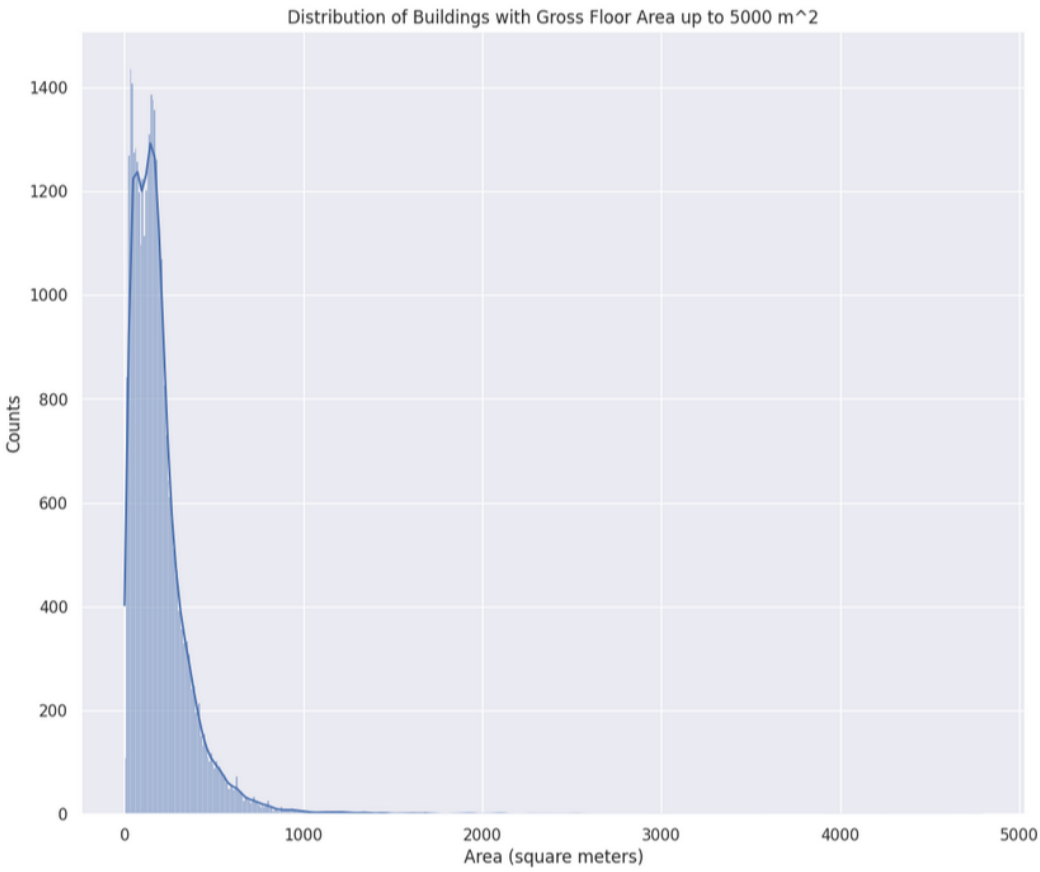
Distribution of Buildings with Gross Floor Area up to 5000 m^2
Counts
1400
1200
1000
800
600
400
200
0
0
1000
2000
3000
4000
5000
Area (square meters)

Figure A.15

A.5.2. Results of CO2 Emissions MC Simulations

OAT - Number of floors

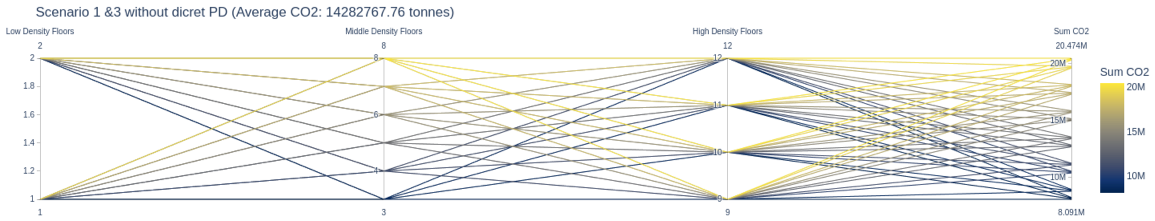

(a) Scenario 1 TUIK Survey

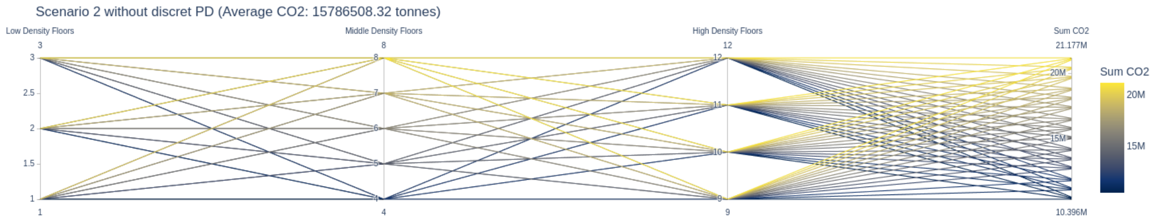

(b) Scenario 2: Antakya Field Work

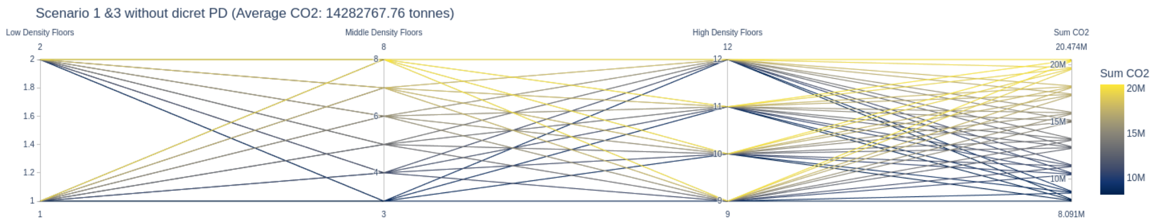

(c) Scenario 3 Combined Approach

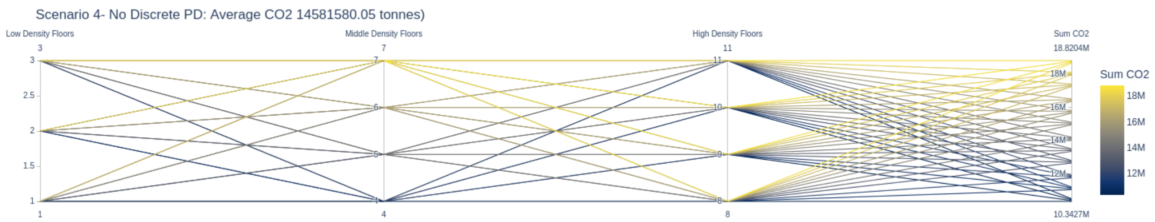

(d) Scenario 4: Arbitrary

Figure A.16: One at a time variation of Density Range (without discrete probability density)

From the above plots, it can be seen that the categorical value **middle density from the spatial data, is the most important input category**. Specifically, as illustrated in Figure **??**, when the maximum floor count in the middle-density category is capped at 8 floors, -the highest value within the 3 to 8 floors range-, the resulting CO_2 emissions are among the highest observed. However, even when the highest floor value is selected within the high-density category (12 floors), the total CO_2 emissions can still vary significantly, ranging between 8 to 20 million tonnes (**??**). This variability indicates that the middle-density category has a stronger influence on overall emissions, which aligns with expectations, as the majority of buildings fall into this category, while the high-density buildings (accounting for just 2%) have a minimal impact (Figure 5.3a).

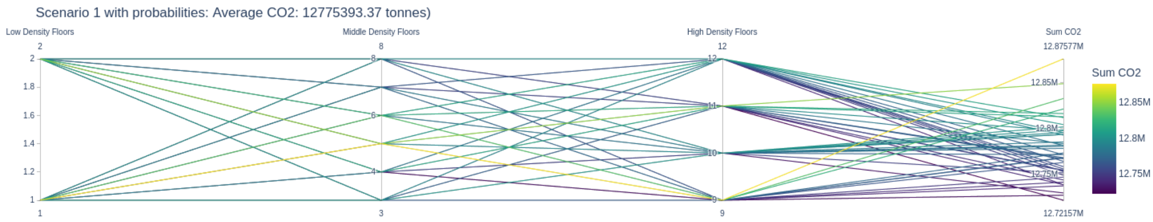

(a) Scenario 5: Range 1 - TUIK Survey

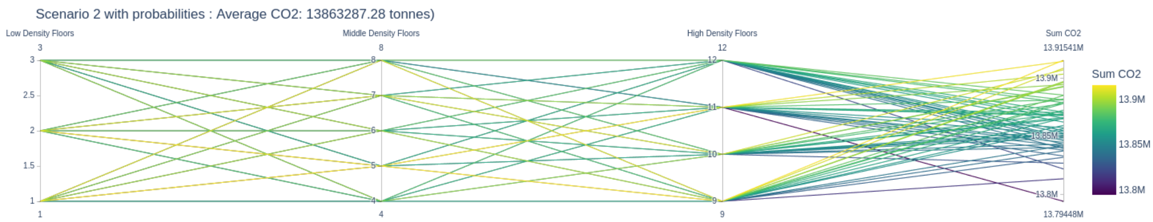

(b) Scenario 6: Range 2 - Antakya Field Work

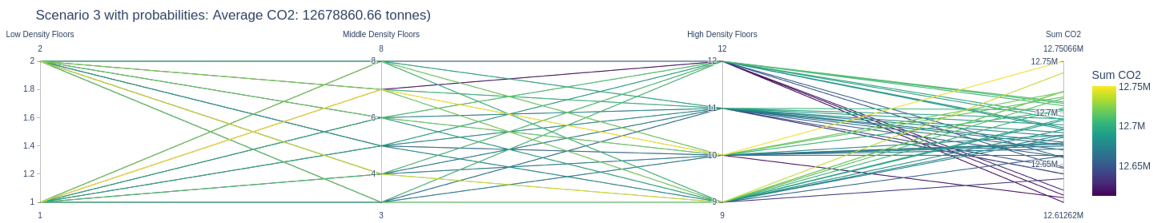

(c) Scenario 7 - Range 3 Combined Approach

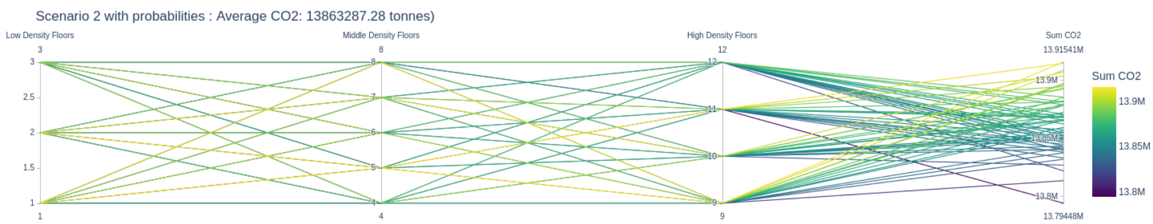

(d) Scenario 8: Range 4- Arbitrary

Figure A.17: One at a time variation of Density Range (without discrete probability density)

OAT - CO_2 Factor

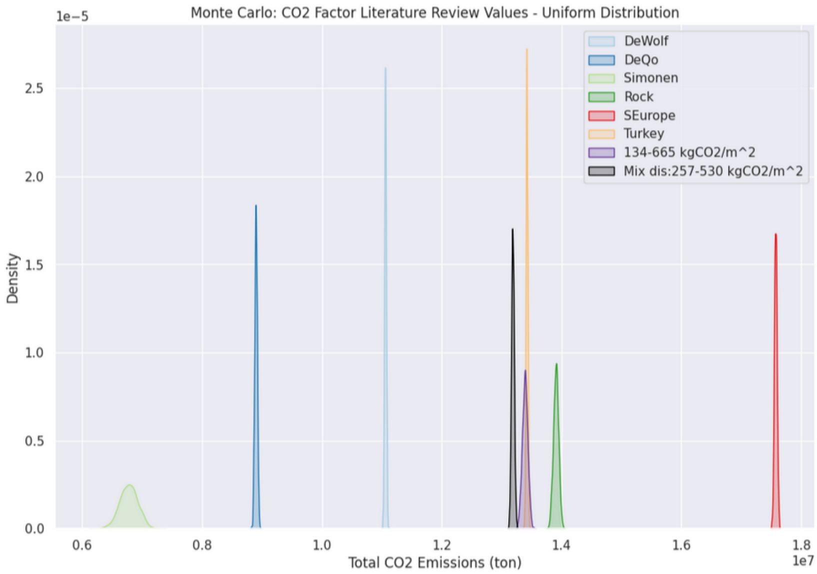

(a) Monte Carlo - Uniform distribution

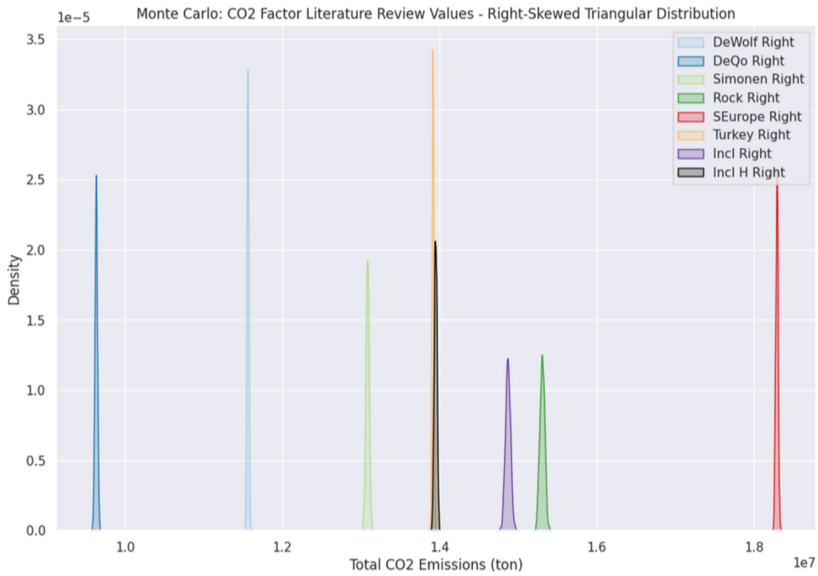

(b) Monte Carlo Triangular right skewed

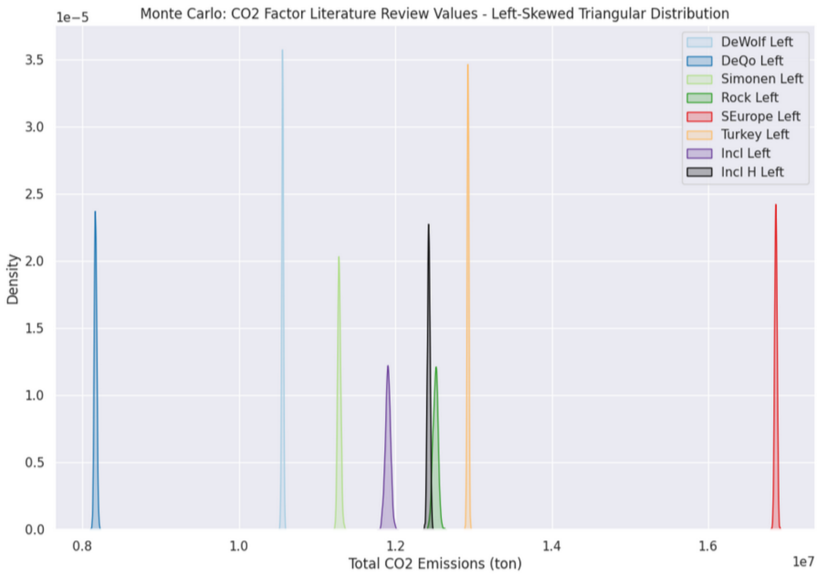

(c) Monte Carlo Triangular Left Skewed

Figure A.18: OAT variation of the CO_2 Factor Range

A.5.3. Mathematical explanation of narrow distributions

The characteristics of the resulting distributions that need to be explained, are:

- Why the distributions are narrow and do not overlap.
- Why they follow a bell-shaped curve.

Narrow distributions

To address the first question, a mathematical explanation was developed and subsequently validated through testing. Essentially, the narrow distribution of CO_2 emissions can be attributed to two main factors: the large number of buildings and the fact that each building's area is constant (or at least bounded - see Figure A.15). When you aggregate emissions from many buildings, the random fluctuations tend to cancel each other out, which means that the overall variability relative to the mean decreases (Coefficient of Variance). In other words, the more buildings you include, the closer the total emissions get to their expected value, resulting in a much narrower distribution.

Below, follows the mathematical explanation:

Assume that for each building i, the CO_2 emission is given by

$$X_i = A_i \cdot f_i, \tag{A.1}$$

where:

- A_i is the constant (deterministic) area of building i, and
- f_i is a random variable representing the CO_2 factor with mean μ and variance σ^2.

The total emission for n buildings is:

$$T_n = \sum_{i=1}^{n} X_i = \sum_{i=1}^{n} A_i f_i. \tag{A.2}$$

By the linearity of expectation, we have

$$\begin{aligned}
E[T_n] &= \sum_{i=1}^{n} E[X_i] && \text{(A.3)}\\
&= \sum_{i=1}^{n} A_i E[f_i] && \text{(A.4)}\\
&= \mu \sum_{i=1}^{n} A_i && \text{(A.5)}\\
&= \mu\, S_n, && \text{(A.6)}
\end{aligned}$$

where

$$S_n = \sum_{i=1}^{n} A_i.$$

Since the f_i are independent, the variance of the sum is the sum of the variances:

$$\begin{aligned}
\mathrm{Var}(T_n) &= \sum_{i=1}^{n} \mathrm{Var}(X_i) && \text{(A.7)}\\
&= \sum_{i=1}^{n} A_i^2\, \mathrm{Var}(f_i) && \text{(A.8)}\\
&= \sigma^2 \sum_{i=1}^{n} A_i^2 && \text{(A.9)}\\
&= \sigma^2\, Q_n, && \text{(A.10)}
\end{aligned}$$

where

$$Q_n = \sum_{i=1}^{n} A_i^2.$$

Thus, the standard deviation of T_n is

$$\sigma_{T_n} = \sqrt{\mathrm{Var}(T_n)} = \sigma\sqrt{Q_n}. \tag{A.11}$$

The coefficient of variance or -relative error is defined as the ratio of the standard deviation of T_n to its expected value:

$$\frac{\sigma_{T_n}}{E[T_n]} = \frac{\sigma\sqrt{Q_n}}{\mu\, S_n}. \tag{A.12}$$

For a large number of buildings:

$$\overline{A}_n = \frac{1}{n}\sum_{i=1}^{n} A_i \quad \text{and} \quad \overline{A^2}_n = \frac{1}{n}\sum_{i=1}^{n} A_i^2.$$

Then, we can approximate:

$$S_n \approx n\,\overline{A}_n \quad \text{and} \quad Q_n \approx n\,\overline{A^2}_n.$$

Substitute these into the expression for the relative error:

$$\frac{\sigma_{T_n}}{E[T_n]} \approx \frac{\sigma\sqrt{n\,\overline{A^2}_n}}{\mu\, n\,\overline{A}_n} \tag{A.13}$$

$$= \frac{\sigma}{\mu} \cdot \frac{\sqrt{\overline{A^2}_n}}{\overline{A}_n} \cdot \frac{1}{\sqrt{n}}. \tag{A.14}$$

- The term $\frac{\sigma}{\mu}$ is the coefficient of variation for the individual CO_2 factor f_i; it reflects the inherent variability of the CO_2 factor relative to its mean.
- The term $\frac{\sqrt{\overline{A^2}_n}}{\overline{A}_n}$ measures the dispersion of the building areas. If all buildings have the same area, then $\overline{A^2}_n = \overline{A}_n^2$ and this term is equal to 1. Here, even though the buildings do not have the same area, $\sqrt{\overline{A^2}_n and \overline{A}_n have the same order of magnitude The term \frac{1}{\sqrt{n}}}$ shows that as the number of buildings n increases, the relative error decreases proportionally to $1/\sqrt{n}$.

Thus, the final expression for the relative error is:

$$\boxed{\frac{\sigma_{T_n}}{E[T_n]} \approx \frac{\sigma}{\mu} \cdot \frac{\sqrt{\overline{A^2}_n}}{\overline{A}_n} \cdot \frac{1}{\sqrt{n}}.}$$

This shows that the relative error of the outcome (i.e., the spread of the distribution relative to the mean) decreases as $1/\sqrt{n}$, causing the distribution of the total emissions to become narrower as the number of buildings increases.

To check this theory, the results will be examined for consistency with the proposed explanation. This is achieved by analyzing three distributions of the CO_2 Factor that exhibit significant overlap:*De Wolf, Mix, and Broad* ranges (Figure A.21).

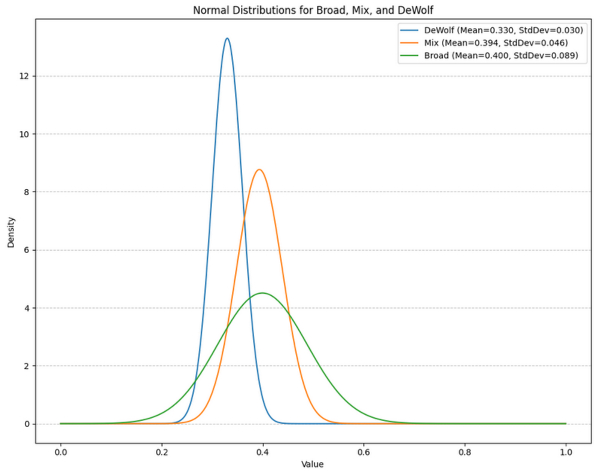

Figure A.19: Distribution of the CO_2 Factor for "Mix", "Broad" and "DeWolf" distribution.

For each distribution, 1,000 simulations are conducted with a limited number of buildings. The objective is to determine whether increasing the number of buildings leads to a progressively narrower distribution. To assess this, simulations are performed with sample sizes (i.e., number of buildings) of 10, 100, 1,000, 20,000, and 30,000 as seen in Figure A.20.

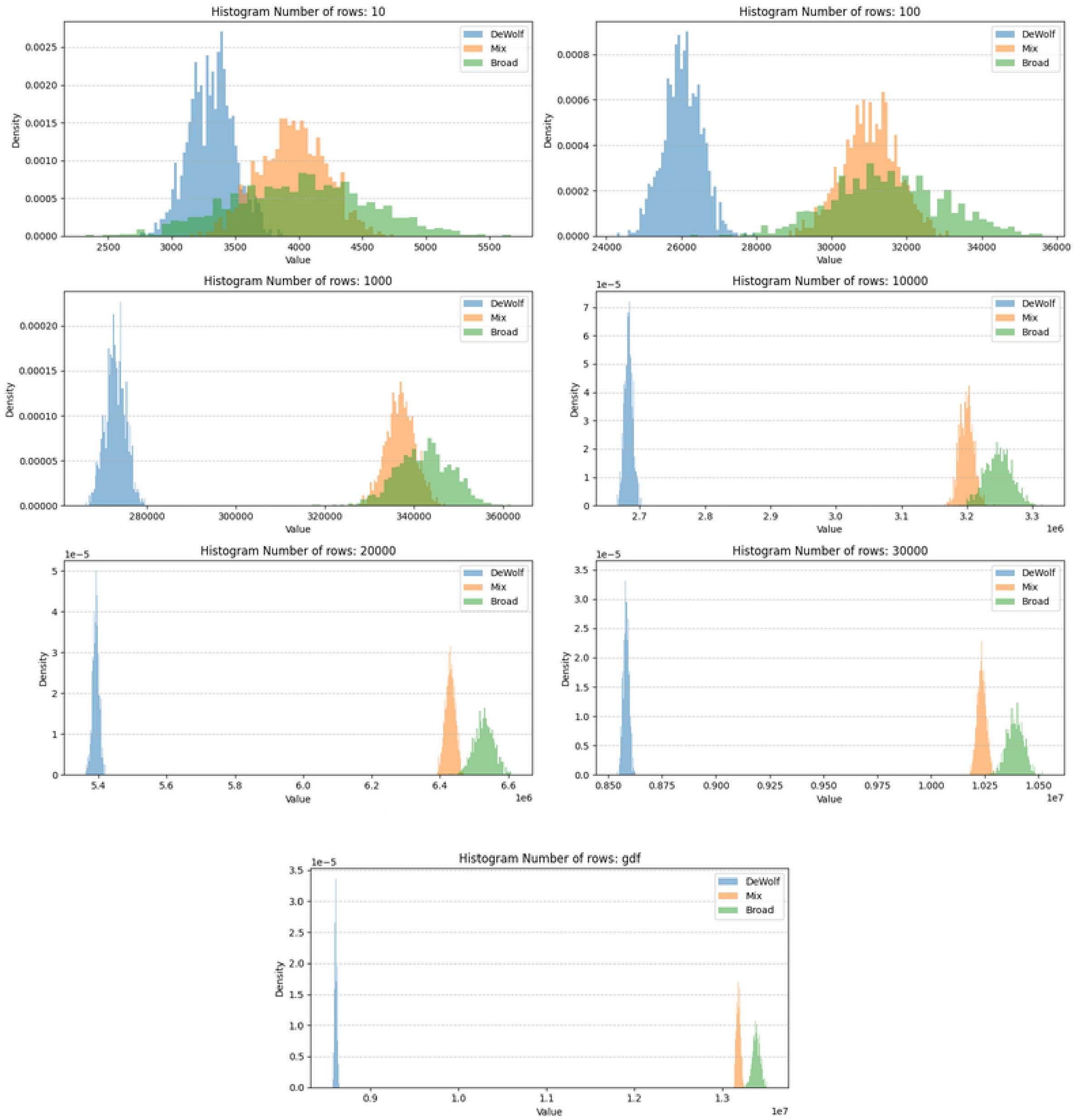

Figure A.20: Monte Carlo Simulations with an increasing sample of buildings

A similar trend can be observed by examining the behavior of the coefficient of variance (CV) percentage as the number of buildings increases. For the same three distributions, the CV is defined as the the standard deviation divided by the mean. Having a low CV shows that the relative variance is decreasing.

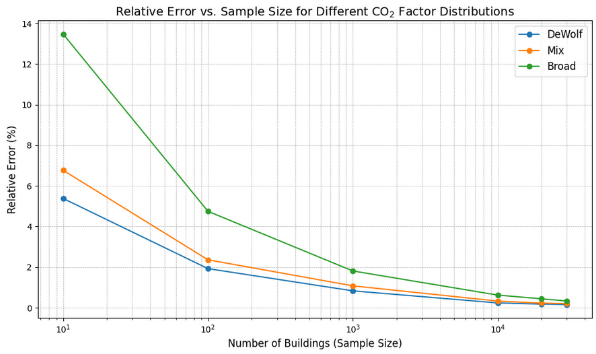

Figure A.21: Coefficient of Variance for three ranges of the CO_2 Factor

Both figures seems to have the expected behavior as the number of buildings increase.

Normal distributions

Central Limit Theorem appears to account for the observed normal distribution of results across various underlying distributions - normal, uniform, and triangular (see Figures A.18a, A.9, and A.10). More specifically, the theorem states that the probability distribution of the means of different samples (in this case the resulted mean from each simulation) drawn from the same population (same range of the CO_2 factor) tends to approximate a normal distribution (as visualized in Figure A.22). In this analysis, 1,000 simulations were performed, yielding a histogram of 1,000 sample means that demonstrates this tendency toward normality.

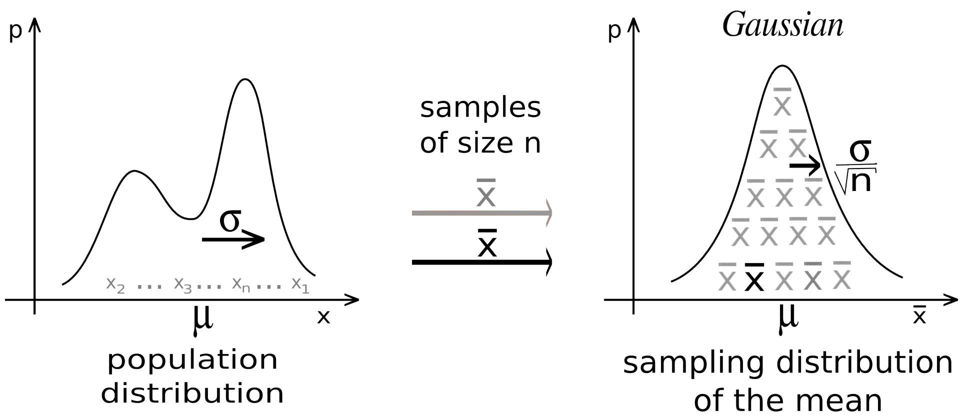

Figure A.22: Distribution of the CO_2 Factor for "Mix", "Broad" and "De Wolf" distribution.

A.5.4. Social Cost of Carbon Results - Alternative results

As explained in the methodology, the SCC distribution compiled by Tol 2023, can be translated into a distribution of the estimated cost (in US dollars), that society will carry. The resulting histogram, is shown in Figure A.23.

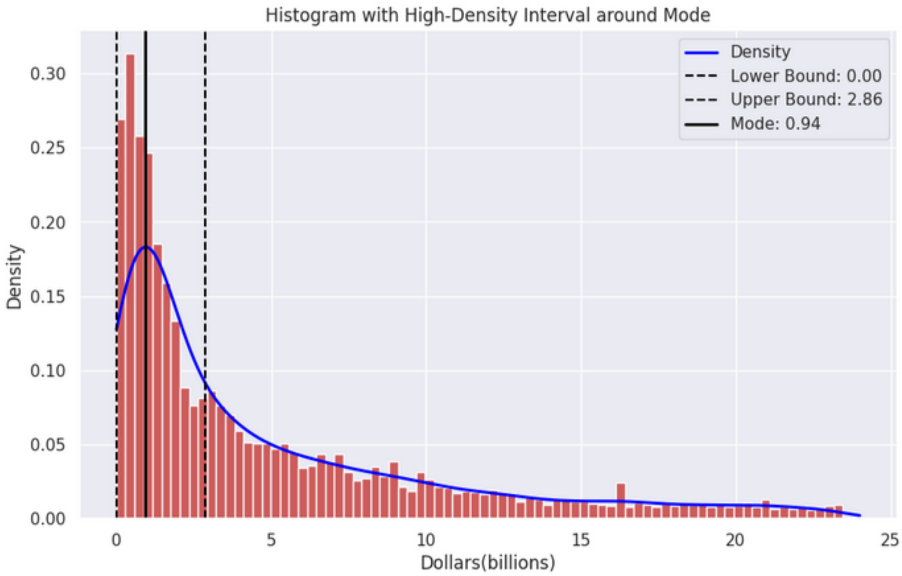

Figure A.23: Histogram of the social cost of carbon that the rebuilding of Antakya could potentially have

As the plot indicates, the high-density interval (HDI) around the mode of the distribution captures a cost range of $0.00 to $2.86 billion, with the mode at $0.94 billion. This interval represents the range within which the majority of the potential cost values are concentrated. In other words, the estimated economic damages that society pay over time, due to the release of 13.4 million tonnes of CO_2 emissions (mean value of main results) from the rebuilding process in Antakya will range between 0 to 2.86 $ billion dollars, with the highest probability to be around 0.94$ dollars (based on the SCC values).

A.5.5. Sustainable house

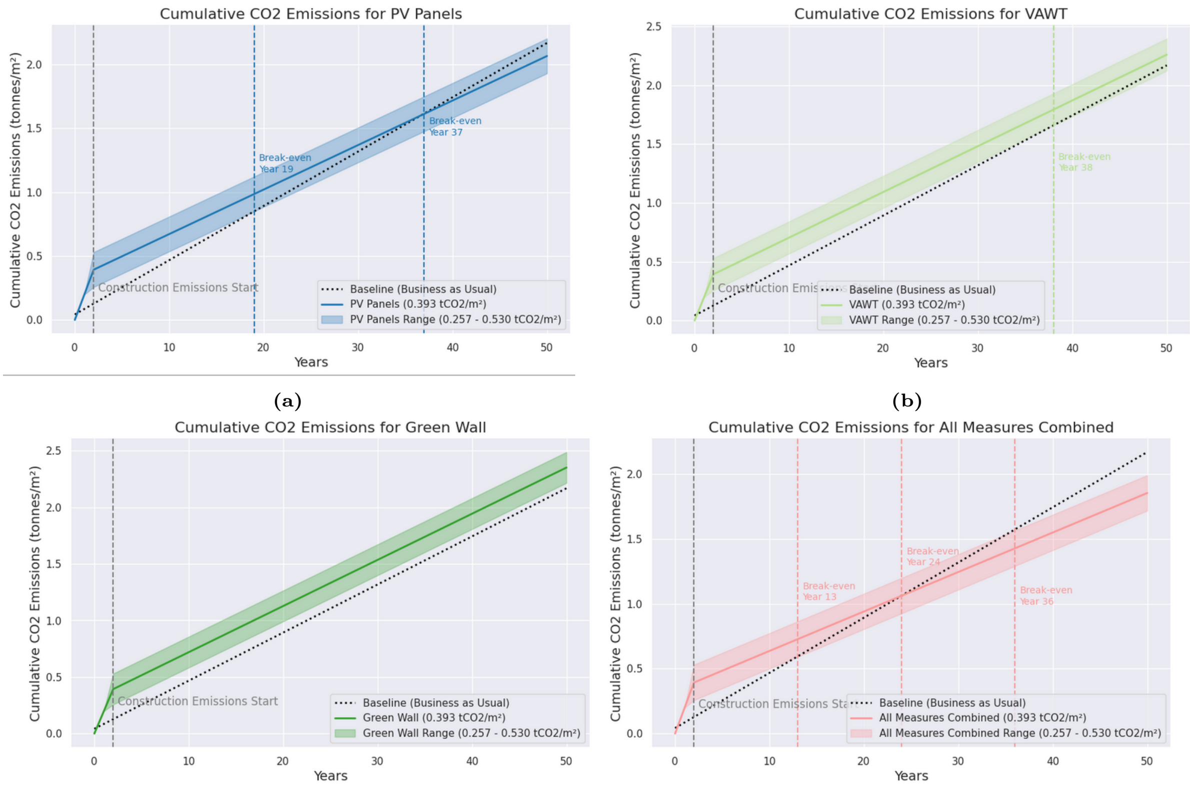

(a) (b)

(c) (d)

Figure A.24